THE STRUCTURE AND EVOLUTION OF CHAOS IN DYNAMICAL SYSTEMS

by

Paul L. Jenkins B.Sc. (Hons.)

A thesis submitted for the degree of
Doctor of Philosophy

Supervisor: Dr. D.M. Heffernan

School of Physical Sciences
Dublin City University
Glasnevin
Dublin 9

March 1993

DECLARATION

I hereby certify that this material, which I now submit for assessment on the programme of study leading to the award of Doctor of Philosophy is entirely my own work and has not been taken from the work of others save and to the extent that such work has been cited and acknowledged within the text of my work.

Signed: Paul Jenkins

Date: 2/2/1993

CONTENTS

CHAPTER 5 NON-HYPERBOLIC SYSTEMS AND INTERMITTENCY

CHAPTER 6 POINCARE MAPPINGS OF DIFFERENTIAL EQUATIONS

ABSTRACT

An in depth study of temporal chaotic systems, both discrete and continuous, is presented. The techniques for the characterization of chaotic attractors are: Lyapunov stability, dimension spectra and unstable periodic orbits. Comparison of numerical and analytical methods clarify some of the limitations of these techniques. A two dimensional hyperbolic baker map with a complete set of unstable orbits is examined. The evolution of structure and changes in the $f(\alpha)$ spectrum for this map are related to changes in an underlining Cantor set. Numerical calculation of unstable periodic orbits for a related baker map with an incomplete set of unstable orbits allow the investigation of the properties of a pruned Cantor set. The effects of the pruning on the associated $f(\alpha)$ spectrum are investigated. It is also shown that the unstable manifold of a hyperbolic toral map does not wind densely around the torus, but consists of an infinite number of line segments. This facilitates the efficient computation of the dimension spectrum through a rotation of this manifold. A new structure not previously observed in discrete systems is characterized. Intermittency theory previously applied to dissipative systems is applied to a variety of two dimensional non-dissipative systems. A new type of intermittency is found from a detailed comparison between existing theory and numerical experiments. The important and unresolved problem of the correspondence between continuous and discrete systems is investigated using analytical and numerical techniques. Properties of the chaotic attractors of infinite dimensional delayed differential equations are examined as a function of the time delay and nonlinearity parameters.

CHAPTER 1

INTRODUCTION TO CHAOTIC SYSTEMS

1.1 INTRODUCTION

The growth of research papers in the area of chaos has been spectacular in the last ten years. Some scientists have even placed chaos alongside the two other great revolutions of physical theory in the twentieth century- relativity and quantum mechanics. While these theories challenge the Newtonian system of dynamics, chaos questions the traditional beliefs from within the Newtonian framework A century ago, Poincaré showed that the motion of three bodies under gravity can be extremely complicated. His discovery was the first evidence of what is now called chaos: the ability of simple dynamical systems, without in built randomness, to generate highly irregular behaviour.

The progress in dynamical systems from which chaos is derived, is linked with the rapid development of powerful computers. The study of chaotic dynamics reflects in part the influence of computers on theoretical physics, for chaotic systems are "nonintegrable", and much of the work in the field involves numerical simulations.

Chaos is genuinely interdisciplinary as some of the following examples illustrate. In chemistry, sustained oscillations in chemically reacting systems, Hudson and Mankin (1981), In biology stimulated cardiac cells, Guevara (1981), Astronomy, the chaotic tumbling of Hyperion one of Saturn's satellites, Wisdom (1987); Economics, the pricing of treasury bills, Hsieh (1991). The important link between these disciplines it that they exhibit nonlinear behaviour and chaos theory is seen as a way of analyzing these

systems.

This introductory chapter will illustrate the basic principles of chaos in dynamical systems with a particular example, a nonlinear electronic oscillator. The application of chaos to turbulence in hydrodynamical systems is briefly discussed. The type of dynamical systems that form the basis of this thesis and of chaos will be presented in Sec. 1.2.

1.2 DYNAMICAL SYSTEMS

The mechanisms which underly the onset of chaotic motion are relatively well understood. Two generic routes have been discovered and thoroughly analysed, period doubling (Feigenbaum, 1978) and quasi-periodicity (Ruelle and Takens, 1977), in addition to the intermittent transition (Pomeau and Manneville, 1980). A complete description of developed chaos is, however, much more difficult to achieve This thesis is concerned with the structure and evolution of developed chaos in temporal chaotic systems.

Static fractals are introduced in chapter 3, these objects may be multi-dimensional and can have exact self similar properties The evolution of Cantor sets is examined from the point of view of their generalized dimensions and their spectrum of scaling indices. The relationship between one dimensional Cantor sets and dynamical systems is well known, this relationship is extended for higher dimensional Cantor sets.

All of the systems below are initial value problems. It is a common misconception that nonlinearity is required for chaos The first three systems are linear and display chaotic behaviour. The stronger condition is an infinite set of periodic orbits (Sec. 2.6). The one dimensional iterative map

$$X_{i+1} = A\ X_i \qquad \text{mod } 1 \qquad (1.1)$$

with A>1 for chaotic solutions is examined in chapter 3.

The fundamentals of chaos and the reasons for the existence of chaos is examined for this simple map. The orbits of this map can be arranged on complete and pruned trees. The properties of the dimension spectra and the associated $f(\alpha)$ spectra are examined for a range of parameter values A. The evolution of chaos in this map from the onset to complete randomized time series is investigated.

Hyperbolic systems are are studied in chapter 4. The following two dimensional system is called the baker map

$$\begin{pmatrix} X_{i+1} \\ Y_{i+1} \end{pmatrix} = \begin{cases} \begin{pmatrix} R_1 X_i \\ Y_i / S \end{pmatrix} & 0 \le Y \le S \\ \begin{pmatrix} 1/2 + R_2 X_i \\ (Y_i - S)/(1-S) \end{pmatrix} & S < Y \le 1 \end{cases} \tag{1.2}$$

the parameters satisfy the following conditions for chaotic behaviour, $0<R_1,R_2\le 1$ and $S\le 1/2$. This system is the product of a line and a Cantor set. The processes by which a strange attractor can be created and the evolution of structure in this hyperbolic map will be examined. An example of some strange attractors for Eq. (1.2) can be seen in Fig. 4.2. A modified form of this map is the product of a line and a pruned Cantor set. The effects of this pruning on the associated $f(\alpha)$ spectrum is investigated. The generalized dimension spectrum can be obtained analytically for this map. A comparison with numerically generated spectrums is presented in Sec. 2.5.4.

The third linear chaotic systems examined is defined on a torus. It is a higher dimensional version of Eq. (1.1) and is defined as $L_A : T \longrightarrow T$ where

$$A = \begin{pmatrix} a & b \\ c & d \end{pmatrix} \tag{1.3}$$

with a,b,c and d $\in \mathbb{R}$. To our knowledge this is the first study of chaos in this map for noninteger coefficients and determinant less than one. New results concerning the unstable manifold allows both efficient computation of dimension spectra and the analysis of a two dimensional

Cantor structure, not previously observed in dynamical systems.

The following nonlinear iterative map is an example of the type of nonhyperbolic system investigated in chapter 5.

$$\begin{aligned} X_{i+1} &= (A - X_i - B_1 Y_i) X_i \\ Y_{i+1} &= (A - Y_i - B_2 X_i) Y_i \end{aligned} \tag{1.4}$$

with the parameters A, B_1 and B_2. The dynamical behaviour of this map varies from simple to highly complex as the parameter space is explored. The two main themes of this chapter are intermittency and surface attractors (cf. Fig.'s 5.8 and 5 9 (a) respectively). Intermittent crisis describes sudden changes in a chaotic attractor as a system parameter is varied This is the first study of intermittent crises in non-hyperbolic systems like Eq. (1.4). Numerical calculations of the intermittent constant are compared with theoretical values, leading to the analysis of a new type of intermittency. The properties of chaos on a two dimensional unstable manifold are investigated.

The above discrete systems share many properties with continuous systems. For continuous systems three degrees of freedom and nonlinearity are necessary conditions for chaotic solutions. One example of three ordinary differential equations are given below

$$\begin{aligned} dX/dt &= Y(Z - 1 + X^2) + \gamma X \\ dY/dt &= X(3Z + 1 - X^2) + \gamma Y \\ dZ/dt &= -2Z(\alpha + XY) \end{aligned} \tag{1.5}$$

with constants α and γ. A similar set of differential equations formulated by Lorenz (1963) has occupied an important place in the history of chaos. Eq. (1.5) is used in chapter 6 to investigate the important and unresolved problem of the correspondence between continuous and discrete systems, using a variety of numerical and analytic techniques. The fact that very little of the behaviour of these equations can be proved with strict mathematical

rigour is a reminder of the subjects intrinsic mathematical difficulty.

First order delay differential equations are investigated in chapter 7 An example is given below

$$\frac{dX(t)}{dt}=AX(t-\tau)^2\,^4\exp(X(t-\tau)^2)-BX(t) \qquad (1.6)$$

Parameters are A, B and τ For delay parameter τ greater than zero, this equation is infinite dimensional. Using Poincaré section techniques the evolution of chaos is studied for this system. The concept of a strange attractor with an infinite dimension is examined.

None of the above temporal systems can exhibit the phenomenon of turbulence because they lack a spatial dimension. Partial differential equations are used to model turbulence and are not considered due to computational constraints. An example of an set of partial differential equations used to model a rf-biased Josephson junction (Guerrero and Octavio, 1989) are given in dimensionless form by

$$-\frac{\delta^2\phi}{\delta X^2}+\frac{\delta^2\phi}{\delta t^2}+\mathrm{Sin}\phi=-\frac{1}{\sqrt{\beta}}\frac{\delta\phi}{\delta t}+\rho\mathrm{Sin}\,(\Omega t) \qquad (1.7)$$

ρ is the rf amplitude, β is a measure of the damping and Ω the rf frequency. To take into account the presence of an external applied magnetic field, they use the following boundary conditions

$$\frac{\delta\phi(0,t)}{\delta X}=\frac{\delta\phi(L,t)}{\delta X}=\eta \qquad (1.8)$$

where η is a measure of the external field. The intermittency and the fractal attractors examined in this spatiotemporal system have remarkable similarity with the purely temporal systems investigated in this thesis. Low dimensional chaos has been observed in a hydrodynamical experiment (Stavans et al., 1985), the spatial coherence is maintained even after the loss of temporal coherence. This should be contrasted with weak turbulence where the systems spatial coherence breaks down and chaotic behaviour sets in. Stassinopoulos and Alstrom (1992) have used a set

of coupled maps (similar to Eq. (1.4) to examine spatiotemporal chaos The temporal discreteness of coupled maps allows for faster computation of the dynamics since no explicit integration is required as in the simulations of differential equations.

1.3 EXPERIMENTAL CHAOS

The following electronic experiment is used to highlight one possible evolution of a system as a control parameter is varied. The details are taken from Su et al. (1989). The circuit diagram for the experiment is shown in Fig. 1.1 It consists of a resistively coupled diode resonator system with modulation. Ashwim (1990) has examined similar systems of oscillators. The model that Su, Rollins and Hunt use is briefly described as follows. An ideal p-n junction diode is assumed with the additional three characteristics

(i) The diode will not conduct until the forward voltage drop reaches V_f.

(ii) When the voltage drop is less than V_f, the diode does not conduct but acts as a capacitor with fixed capacitance C

(iii) The diode does not shut off immediately, but continues to conduct for a time equal to the reverse recovery time τ_r, with τ_r depending on maximum forward currents

$$\tau_r = \sum_j \alpha_j \tau_m [1 - \exp(-I_j/I_c)] \qquad (1.9)$$

where I_j is the maximum forward current during the j^{th} conducting cycle. τ_m and I_c are diode parameters. Four cycles are used with α_j being the weights. The coupled diode resonator is described by the following set of differential equations

$$
\begin{aligned}
L\frac{di_1}{dt} &= V_o\cos\theta - V_1 - R(i_1+i_2) \\
L\frac{di_2}{dt} &= V_o\cos\theta - V_2 - R(i_1+i_2) \\
\frac{dV_1}{dt} &= \begin{cases} 0, & \text{when diode 1 is conducting} \\ i_1/C_1, & \text{when diode 1 in nonconducting} \end{cases} \\
\frac{dV_2}{dt} &= \begin{cases} 0, & \text{when diode 2 is conducting} \\ i_2/C_2, & \text{when diode 2 in nonconducting} \end{cases} \\
\frac{d\theta}{dt} &= \omega
\end{aligned}
\tag{1.10}
$$

where the drive voltage $E(t)=V_0\cos(\omega t)$, and i_1, V_1, C_1 and i_2, V_2, C_2 are currents through, voltage across and reverse capacitance of diodes 1 and 2, respectively. L and R are the inductance and resistance shown in Fig. 1.1. The method of solution together with typical parameters can be found in Su et al. (1989). Figure 1.2 shows several Poincaré sections formed by plotting peak forward currents $I_1(n)$ versus $I_2(n)$ at several values of the drive voltage; all other parameters kept fixed. The simulated diagrams are on the left with the experiment on the right. The resemblance of the Poincaré sections obtained from the simulation to those measured from the real system is striking, including much of the detailed structure.

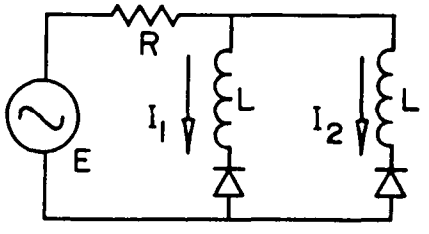

Fig. 1.1. Circuit diagram used to model the resistively coupled diode resonator system.

Some details of the evolution shown in Fig. 1.2 is given below. At a drive voltage lower than that used in

Fig. 1.2 (a), the Poincaré section is a single point. As the voltage increased the period doubles and the Poincaré section is two points Then a Hopf bifurcation occurs where the two points open into two circles. The ratio of the spontaneous frequency to the drive frequency is very close to a rational number. Figure 1.2 (b) is near the critical line for the quasiperiodic transition to chaos. Universal scaling has been shown to occur at this point (Su et al. (1987)) Figure 1.2 (c) has developed into a multiple piece chaotic attractor from a torus. A two piece attractor is shown in Fig. 1 2 (d), for increasing drive voltage This development could be similar to the system examined in Sec. 5.5 2 In Fig 1.2 (e) is a quasiperiodic state which occurs at high drive voltages. There is a sudden transition to this attractor, possibly due to intermittency (cf Sec. 5.4-5.6). Finally, Fig 1 2 (f) is for a different set of parameters, it shows a mode locked period-14 state which

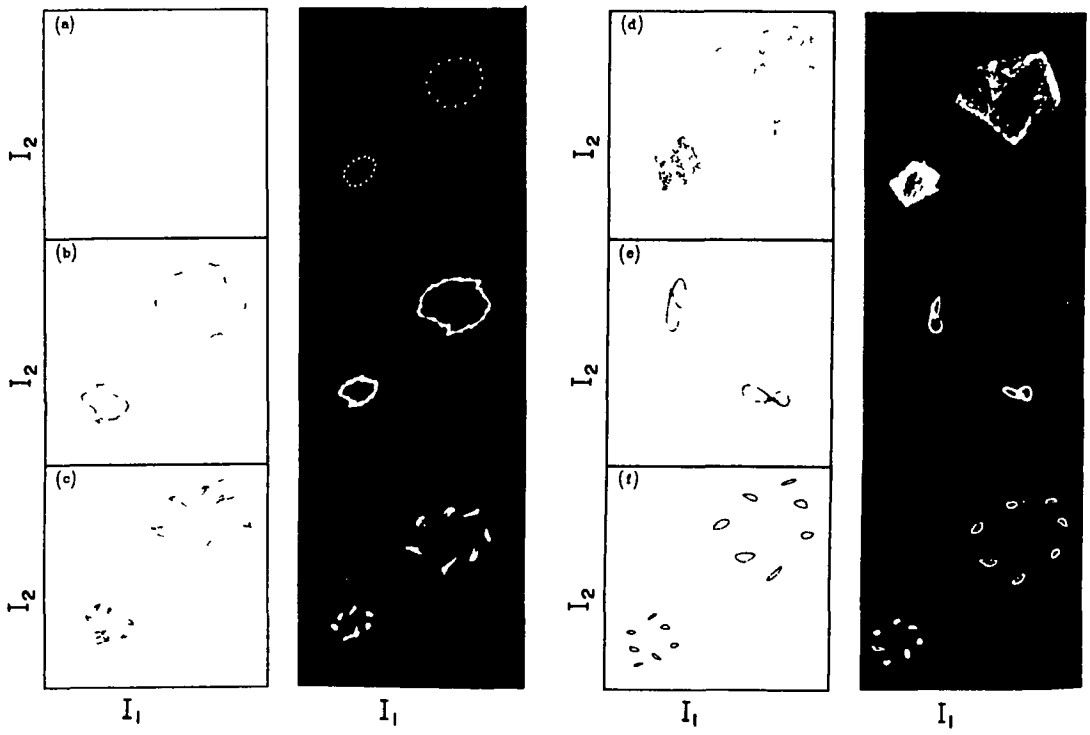

Fig. 1.2. Corresponding stimulated (left) and measured (oscilloscope photographs on the right) Poincaré sections formed by the peak forward currents I_2 vs I_1 for the coupled diode resonator system. (From Su et al., 1987).

has undergone a Hopf bifurcation. The size, shape, and the position of the small circles are in remarkable agreement.

There is excellent detailed global agreement between the model proposed and the experiment. The success of this model suggests that driven diode resonator systems exhibit chaotic behaviour because of a delay feedback effect related to slow diffusion and long lifetime of the excess minority carriers near the p-n junction of the diode. The importance of delay feedback effects will be examined in chapter 7 This is an example where the chaotic dynamics leads to a greater understanding of the physics of p-n junctions.

CHAPTER 2

TECHNIQUES FOR ANALYZING CHAOS

2.1 INTRODUCTION

Dynamical systems with only a few degrees of freedom can, despite the deterministic nature of its governing equations, exhibit random behaviour. The main tools for characterizing the properties of a chaotic regime are the spectrum of Lyapunov exponents λ_i, the fractal dimension D and the entropy K. Typical chaotic attractors are multifractal (Hentschel et al. 1983), that is, their dimension D_q and entropy K_q varies with the index q, ($q \in (-\infty, +\infty)$), thus providing a spectrum of dimension and entropy values for the attractor. After introducing the Lyapunov exponents in section 2.2 and their associated dimension and entropy we proceed to examine the dynamical quantities D_q and K_q in section 2.3. An alternative representation in terms of the $f(\alpha)$ spectrum and $g(\Lambda)$ spectrum is examined in section 2.4. An algorithm for the extraction of the dynamical quantities D_2 and K_2 from a single variable time series is discussed in section 2.5. Data requirements for efficient computation of these quantities are examined and recent applications to experimental chaos are also reviewed. Finally in section 2.6 chaotic orbits are explored using the well known set of periodic orbits. The relationship between the unstable periodic orbits and the dimensions and entropies can be determined. Analytic dimension spectra D_q are compared with numerically generated spectra. This comparison highlights some of the difficulties in computing dimension spectra from single variable time series.

2.2 LYAPUNOV STABILITY

The spectrum of Lyapunov exponents provides a summary of the local stability properties of an attractor. Positive Lyapunov exponents measure exponential spreading of nearby trajectories, while negative Lyapunov exponents measure convergence of trajectories onto the attractor.

2.2.1 LYAPUNOV EXPONENTS

The calculation of a Lyapunov exponent for a one dimensional system will considered first. Consider the logistic map in the following form

$$X_{i+1} = f(X_i) = 1 - AX_i^2 \tag{2.1}$$

A linerization about X_i gives

$$\varepsilon_{i+1} = Df(X_i)\varepsilon_i \tag{2.2}$$

where $Df(X_i) = -2AX_i$ The single Lyapunov exponent is defined as

$$\lambda = \lim_{N\to\infty} \frac{1}{N} \sum_{i=1}^{N} \log |Df(X_0)| \tag{2.3}$$

with initial condition X_0 For a single basin of attraction λ is independent of the initial value X_0. For $\lambda > 0$, we have a chaotic orbit, for $\lambda < 0$ a stable (attracting) orbit. For A = 2 the Lyapunov exponent has a value λ = 0.534.

For a n-dimensional system the Lyapunov exponents are calculated as follows. Consider the $C^r(r\geq 1)$ vector field

$$X_{i+1} = f(X_i), \qquad X \in \mathbb{R}^n \tag{2.4}$$

and a linerization about X_i gives

$$\varepsilon_{i+1} = Df(X_i)\varepsilon_i \qquad \varepsilon \in \mathbb{R}^n \tag{2.5}$$

Let $\{\varepsilon^1,\ldots,\varepsilon^n\}$ be any orthonormal basis in $\mathbb{R}^n$. Then the Lyapunov exponents λ_j along the direction ε^j are defined as

$$\lambda = \lim_{i\to\infty} \frac{1}{i} \sum_{i=1}^{\infty} \log \frac{|| \varepsilon_{i+1}^j ||}{|| \varepsilon_i^j ||} \tag{2.6}$$

where $|| \quad || = \sqrt{\langle .,. \rangle}$ with $\langle .,. \rangle$ denoting the standard scalar product on $\mathbb{R}^n$. This expression gives us information concerning the contraction and expansion of phase space but

nothing about twisting and folding. The Lyapunov exponents are similarly defined for a continuous system. This method of computing the Lyapunov exponents is based on a knowledge of the system. Algorithms have been successfully used for computing Lyapunov exponents from a time series Zeng et al. (1991). These algorithms have also been applied to experiments (Eckmann et al , 1986).

The Lyapunov exponents are arranged in decreasing order. The qualitative stability properties of an attractor can be conveniently summarized by indicating +,0,-,..- according to the sign of each exponent. Thus [+,0,-] would indicate a chaotic attractor in three dimensional phase space. A positive Lyapunov exponent is numerical evidence for the existence of chaos. A Lyapunov exponent of magnitude zero implies a continuous system since the exponent in the direction of the flow can neither separate nor merge.

2.2.2 Lyapunov Dimension and Entropy

Kaplan and York (1979) have put forward a conjecture to relate the spectrum of exponents to a dimension. They define a quantity called the Lyapunov dimension D_L given by

$$D_L = j + \frac{\sum_{i=1}^{j} \lambda_i}{|\lambda_{j+1}|} \tag{2.7}$$

where j is the largest integer for which $\lambda_1+....+\lambda_j \geq 0$. Another conjecture put forward by Mori (1980) applies in limited situations (Farmer 1980).

When the sum of the Lyapunov exponents, often called the divergence, is greater than zero, Eq. (2.7) does not apply. In this case

$$D_L = j \tag{2.8}$$

where j is an integer representing the total number of Lyapunov exponents in the system. A one dimensional map, with $\lambda_1>0$, has Lyapunov dimension $D_L=1$ 0 while a two dimensional system with $\lambda_1+\lambda_2>0$ has dimension $D_L=2$.

The Lyapunov entropy K_L is defined by, Pesin (1977).

$$K = \sum_{i=1}^{k} \lambda_i^+ \qquad (2.9)$$

where the sum is over the positive Lyapunov exponents. The entropy is a measure of information loss in a system with units of inverse time. It is a measure of how chaotic a system is, $K_L=0$ for an ordered system while $K_L=\infty$ for a random system. Although a positive Lyapunov exponent implies chaos we will see in later chapters that this should be interpreted with caution.

2.3 GENERALIZED DIMENSIONS AND ENTROPIES

Suppose that there is an attractor in phase space and the trajectory X(t) is in the basin of attraction. The state of the system is measured at intervals of time t. Most definitions of dimension use the notion of partitioning phase space into boxes of size ε. We define probabilities $P(i_1,i_2, \ldots ,i_d)$ to be joint probabilities such that $X(t=t)$ is in box i_1, $X(t=2t)$ is in box i_2, ,....., and $X(t=d\tau)$ is in box i_d. Using these probabilities, a generalized information of order q ($q \in \mathbb{R}$) is defined as,

$$I_q(\varepsilon) = \frac{1}{1-q} \ln \sum_{i_1, \ldots ,i_d} P^q (i_1,i_2, \ldots ,i_d) \qquad (2.10)$$

The concept of a fractal (non-integer) dimension D<d of an attractor in d dimensional phase space can be derived from information considerations, where the dimension describes how the information $I(\varepsilon)$ scales with varying spatial resolution ε, according to:

$$D = - \lim_{\varepsilon \to 0} \frac{I(\varepsilon)}{\ln \varepsilon} \qquad (2.11)$$

On the basis of $I_q(\varepsilon)$ a continuous spectrum of dimensions of order q (Hentschel et al. 1983) is introduced by substituting $I_q(\varepsilon)$ into Eq. (2.11):

$$D_q = \frac{1}{q-1} \lim_{\varepsilon \to 0} \frac{\ln \sum_{i_1, \ldots, i_d} P^q (i_1, i_2, \ldots, i_d)}{\ln \varepsilon} \qquad (2.12)$$

The most frequently used dimensions are the Hausdorff (or fractal) dimension D_0, the information dimension D_1 and the correlation dimension D_2. D_0 and D_1 are obtained in the limit $q \to 0$ and $q \to 1$ respectively. For the set of generalized dimensions it can be shown that $D_q \leq D_{q'}$, if $q' < q$. The dimensions of different order measure different distributions of points occurring on the attractor.

Using the information $I(\varepsilon)$ we can define the entropy K_1:

$$K = \lim_{\tau \to 0} I(\varepsilon) \qquad (2.13)$$

Substituting for $I_q(\varepsilon)$, we can also define a continuous spectrum of entropies of order q (Renyi 1970):

$$K_q = \frac{1}{q-1} \lim_{\varepsilon \to 0} \lim_{t \to 0} \lim_{d \to \infty} \frac{1}{d\tau} \frac{\ln \sum_{i_1, \ldots, i_d} P^q (i_1, i_2, \ldots, i_d)}{\ln \varepsilon} \qquad (2.14)$$

The limit $q > 0$, yields the so called topological entropy, whereas the limit $q > 1^+$ is the metric or Kolmogorov entropy. The q^{th} order dimensions of an attractor are static invariant, since they do not depend on any time scale. However the entropy is a dynamic invariant property, it has to be specified per unit time.

Table 2.1.

Dimension and entropy values, for different types of attractors. $(1 < n < \infty)$.

Attractor Type	D_q	K_q	
Period n fixed point	0.0	0.0	for all q
Period n limit cycle	1.0	0.0	for all q
2-Torus	2.0	0.0	for all q
Strange Attracctor	$D_q \leq D_{q'}$	$K_q \leq K_{q'}$	$q' < q$

For strange attractors the set D_q contains information on the appearance and statistical properties of the chaotic time series. Table 2.1 gives a summary of this dimension

set and entropy set for number of well known attractors. Homogeneous attractors are defined by $D_q = D_{q'}$ and $K_q = K_{q'}$ for $q \neq q'$. Quantitatively, the dimension set D_q and the entropy set K_q permit regular systems (fixed point and limit cycles) to be distinguished from irregular (chaotic) systems.

2.4 LEGENDRE TRANSFORMATIONS

The spectrum of dimensions D_q introduced in the previous section is used to characterize a multifractal. A similar characterization is obtained by the spectrum of scaling indices, the $f(\alpha)$ spectrum, introduced by Halsey et al. (1986). Suppose there is a set embedded in a finite portion of d-dimensional Euclidean space. We divide the set into N disjoint pieces S_i, i=1,2,...,N with measure P_i and size ε_i in order to construct a partition function:

$$\Gamma(\tau,q,\{S_i\}_N) = \sum_{i=1}^{N} \frac{p_i^q}{\varepsilon_i^\tau} \qquad (2.15)$$

As $\varepsilon \longrightarrow \infty$, the partition sum diverges if $\tau>\tau(q)$, becomes zero if $\tau<\tau(q)$, and may approach a finite nonzero value if $\tau=\tau(q)$. Thus, by requiring $\Gamma(\tau,q)$=constant, it is possible to define a relation between τ and q

$$\tau(q) = (q-1)\, D_q \qquad (2.16)$$

A scaling exponent α is defined by saying that

$$P^q = \varepsilon^{q\alpha_i} \qquad (2.17)$$

α can take on a range of values between α_{max} and α_{min}, corresponding to different regions of the measure. The number of times α takes on values between α' and $\alpha'+d\alpha'$ will be of the form

$$d\alpha' p(\alpha') \varepsilon^{-f(\alpha')} \qquad (2.18)$$

where $f(\alpha')$ is a continuous function. The exponent $f(\alpha')$ reflects the different dimensions of the sets upon which the singularities of strength α' may lie. If we now divide the system into pieces of size ε and express the partition sum (2.15) as an integral over α,

$$\Gamma(\tau,q) = \varepsilon^{-\tau} \int d\alpha' p(\alpha') \varepsilon^{q\alpha' - f(\alpha')} \qquad (2.19)$$

In the limit $\varepsilon \longrightarrow 0$, the dominant contribution to the integral is received when the exponent $q\alpha'-f(\alpha')$ is close to its minimum value, a saddle-point approximation is performed

$$\frac{d}{d\alpha'} [\alpha' q - f(\alpha')] \Big|_{\alpha'=\alpha(q)} = 0 \qquad (2.20)$$

so that

$$\frac{d f}{d \alpha} = q \quad \text{and} \quad \frac{d^2 f}{d \alpha^2} < 0 \qquad (2.21)$$

from which it follows: $D_0 = f_{max}$, $D_{-\infty} = \alpha_{max}$ and $D_{+\infty} = \alpha_{min}$. Thus for any attractor the curve $f(\alpha)$ will be convex with a single maximum at $q=0$ and with infinite slopes at $q= \pm\infty$. This leads to the following Legendre transformation (Halsey et al., 1986) which is used to determine $f(\alpha)$:

$$\alpha(q) = \frac{d}{dq} \left((q-1) D_q \right)$$
$$f(\alpha) = q\, \alpha(q) - (q-1) D_q \qquad (2.22)$$

A similar transformation can be obtained for the spectrum K_q.

$$K_q = \frac{1}{q-1} \lim_{\varepsilon \to 0} \lim_{t \to 0} \lim_{d \to \infty} \frac{1}{d\tau} \frac{\ln \sum_{i_1', \ldots, i_d} P^q (i_1, i_2, \ldots, i_d)}{\ln \varepsilon} \qquad (2.23)$$

Define $\Lambda(i_1, \ldots, i_d)$ by (Eckmann and Procaccia 1986)

$$P^q (i_1, \ldots, i_d) = \exp(-dt\Lambda(i_1, \ldots, i_d)) \qquad (2.24)$$

For ε sufficiently small and fixed d, the number of times one finds a Λ between Λ' and $\Lambda'+d\Lambda'$ is

$$\exp(t\, d\, g(\Lambda'))\, d\Lambda' \qquad (2.25)$$

Substituting Eq. (2.24) and (2.25) into Eq. (2.23), one sees that in the limit as ε goes to 0,

$$K_q = \frac{1}{q-1} (q\, \Lambda(q) - g(\Lambda)) \qquad (2.26)$$

and therefore a knowledge of K_q yields both Λ and $g(\Lambda)$ according to

$$\Lambda(q) = \frac{d}{dq}\left[(q-1)K_q \right]$$
$$g(\Lambda) = q.\Lambda(q) - (q-1)K_q \qquad (2.27)$$

2.5 CORRELATION INTEGRALS

In this section algorithms are examined for computing the dimensions D_q. Data requirements and experimental applications will be discussed.

2.5.1 CORRELATION DIMENSION

Grassberger and Procaccia (1983)[a] introduced an algorithm for extracting the dimension D_2 from a single variable time series. It is based on the correlation between points on the attractor. Consider a set (X_i, i=1....N) of points obtained from a time series $X_i = X(t+i\tau)$, with a fixed increment τ between successive measurements. N is the total number of data points on the attractor. The time series can be experimental or obtained numerically from a computer experiment.

Due to the exponential divergence of trajectories on a chaotic attractor, most pairs of points (X_i, X_j) with $i \neq j$ will be uncorrelated. Some points will be spatially correlated and this spatial correlation is measured with the correlation integral $C_2(\varepsilon)$:

$$C_2(\varepsilon) = \lim_{\varepsilon \to 0} \frac{1}{N^2} \sum_{i,j=1}^{N} \Theta(\varepsilon - |X_i - X_j|) \qquad (2.28)$$

The Heavside function $\Theta(\varepsilon - |X_i - X_j|)$ serves to count the number of pairs (X_i, X_j) whose distance $|X_i - X_j|$ is less than ε. It has been shown previously (Grassbeger and Procaccia, 1983[b]) that $C_2(\varepsilon)$ scales like:

$$C_2(\varepsilon) \approx \varepsilon^{D2} \qquad (2.29)$$

D_2 is called the correlation dimension, by plotting ln $C_2(\varepsilon)$ against ln ε the dimension D_2 can be obtained from the slope of the graph,

$$D_2 = \frac{d \ln C_2(\varepsilon)}{d \ln \varepsilon} \qquad (2.30)$$

The above correlation integral has to be modified in order to measure dimensions greater than two. The modification consists of embedding the time series in d dimensional phase space, i.e. the construction of d dimensional vectors $(X_{i+1}, X_{i+2}, \ldots, X_{i+d})$ Instead of calculating the separation between pairs of points we calculate the separation between pairs of d dimensional vectors i.e. we count the number of pairs (i,j) with:

$$\left[(X_{i+1}-X_{j+1})^2+(X_{i+2}-X_{j+2})^2+\ldots+(X_{i+d}-X_{j+d})^2 \right]^{1/2} \qquad (2.31)$$

Hence the modified correlation integral is:

$$C_2^d(\varepsilon) = \lim_{\varepsilon\to 0} \frac{1}{N^2} \sum_{i,j=1}^{N} \Theta \left(\varepsilon - \left[\sum_{n=1}^{d} |X_{i+n}-X_{j+n}|^2 \right]^{1/2} \right) \qquad (2.32)$$

This correlation integral $C_2^d(\varepsilon)$ is related to the probability defined in Eq (2.1) by,

$$C_2^d(\varepsilon) \approx \sum_{i_1, \ldots, i_d} P^2(i_1, i_2, \ldots, i_d) \qquad (2.33)$$

Consequently, combing Eq 's (2.23) and (2.32) leads to an equation which involves K_2, (Grassberger and Procaccia, 1983[a]),

$$C_2^d(\varepsilon) \approx \lim_{d\to\infty} \lim_{\varepsilon\to 0} \varepsilon^{D2} \exp(-d\tau K2) \qquad (2.34)$$

By calculating:

$$K_2^d(\varepsilon) = \frac{1}{\tau} \ln \left[\frac{C^d(\varepsilon)}{C^{d+1}(\varepsilon)} \right] \qquad (2.35)$$

we should find

$$\lim_{d\to\infty} \lim_{\varepsilon\to 0} K_2^d(\varepsilon) \approx K_2 \qquad (2.36)$$

Cohen and Procaccia (1985), has developed a similar algorithm for the extraction of the dimension D_1 and the metric entropy K_1 and applied it to a number of well known chaotic maps Using the two dimensional Henon map $(X,Y) \longrightarrow (1-AX^2+Y, BX)$ (Henon, 1976) with A=1.4 and B=0.3, a time series is generated with N=15000 data point. Shown in Fig. 2.1 (a) is a plot of ln $C_d^2(\varepsilon)$ against lnε for a series of increasing values of d, the series of straight lines

with slope D_2 are displaced from each other by the factor $\exp(-d\tau K_2)$. The dimension obtained from the slope of these lines is $D_2=1.46\pm0.02$. The error represents the statistical variation in the least square fit.

For each value of embedding dimension the Kolmogorov entropy is estimated over an appropriate scaling region in ε. The extrapolated value is $K_2=0.32\pm0.02$ as shown in Fig. 2.1 (b). D_2 and K_2 are lower bounds on the Lyapunov dimension ($D_L=1.26$) and the Lyapunov entropy ($K_L=0.42$) respectively.

Cutler (1991) has done an indepth study of errors and provides confidence intervals for the dimension D_2 and D_1. Fractal dimensions and Lyapunov exponents can be estimated faster and more efficiently with the knowledge of the optimal embedding dimension and delay time. Buzug and Pfister (1992) have proposed two methods to obtain this optimal embedding dimension.

2.5.2 Data Requirements

Estimate of the number of data points N required to calculate a dimension D_2 and a entropy K_2 are considered. To do this we will choose a one dimensional system of known dimension and entropy. The system is defined by

$$X_{i+1} = AX_i \quad \mod 1 \tag{2.37}$$

and will be considered in more detail in chapter 3. For $A > 1$ the system is chaotic with $D_2 \approx 1.0$ and $K_2 \approx \log(A)$. Boundary effects are negligible for this system. Using Eq. (2.28)

$$C_2^d(\varepsilon) \approx \lim_{d\to\infty} \lim_{\varepsilon\to 0} \varepsilon^{D2} \exp(-d\tau K_2) \tag{2.38}$$

where $C_2^d(\varepsilon)$ is defined by

$$C_2^d(\varepsilon) = \lim_{N\to\infty} \frac{M}{N^2} \tag{2.39}$$

where M is the number of pairs (i,j) with

$$\left[\sum_{n=1}^{d} |X_{i+n}-X_{j+n}|^2\right]^{1/2} < \varepsilon \tag{2.40}$$

Combining Eq. (2.38) and Eq. (2.39),

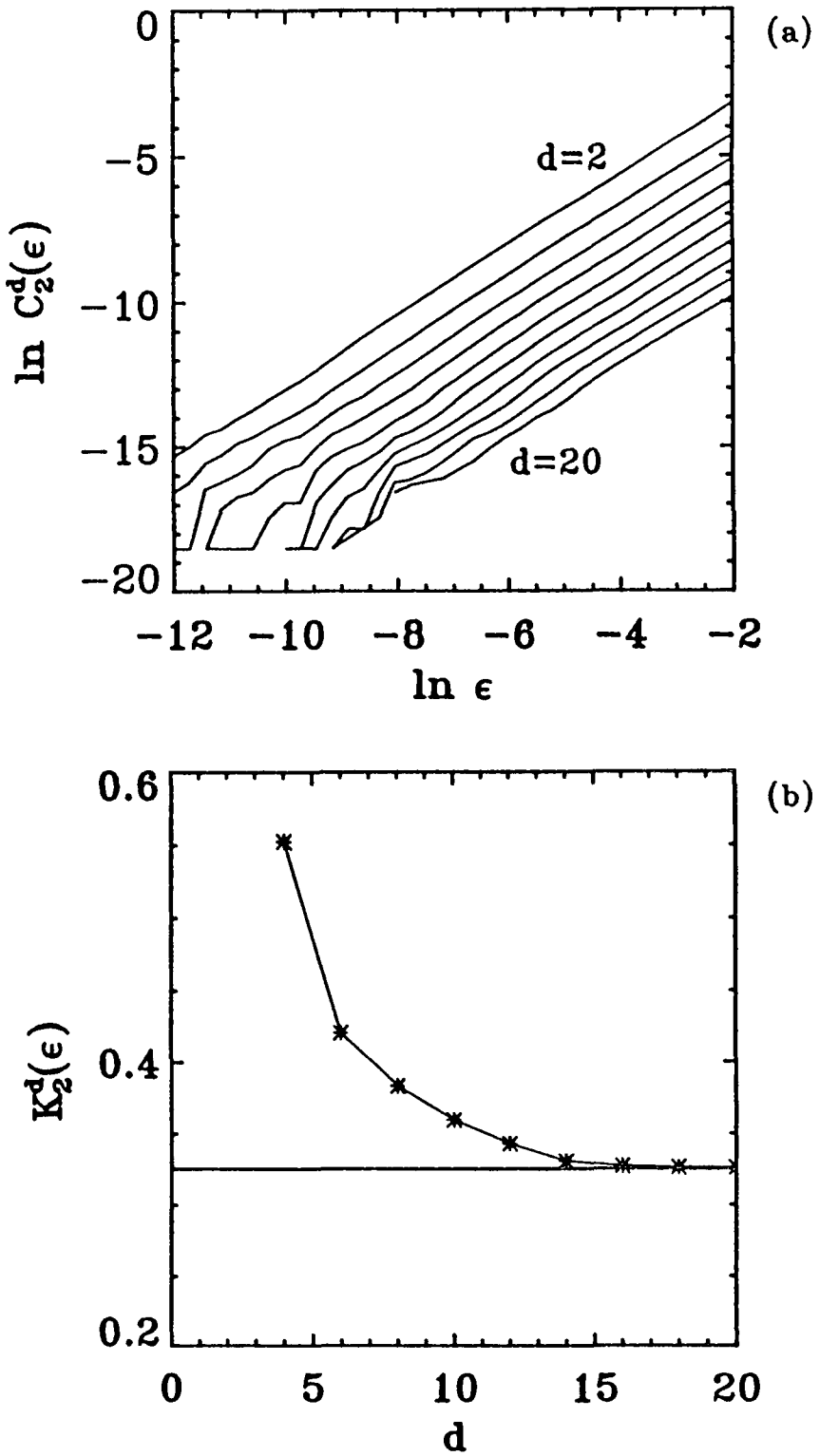

FIG. 2.1. (a) Correlation integral ln $C^2(\varepsilon)$ verse ln ε for Henon map, computed with N=15000 data points. The values of embedding dimension d are d=2 (top curve),4,6,...,18,20 (bottom curve). (b) Values of $K^2(\varepsilon)$ for the Henon map averaged over the scaling region in ε. The extrapolated ($d \longrightarrow \infty$) value is K_2=0.32±0.02.

$$N \approx \left(\frac{M}{\varepsilon^{D2} \exp(-d\tau K_2)} \right)^{1/2} \qquad (2.41)$$

The variables are defined as follows $\tau=1$, $d=8$, $D_2=1.0$, $\varepsilon=10^{-6}$ and $M_{min}=1$. For $K_2=\log(2)$ the number of points required is $N \approx 5000$, while for $K_2=\log(4)$ the number of points required is approx $N \approx 8*10^4$. Smith (1988) has suggested that 42^{D2} points are the minimum number of data points. Nerenberg and Christopher (1990) has also made estimates of data requirements with the inclusion of boundary effects The importance of these two estimates is that neither include the entropy in their calculations. As can be seen from the previous example no estimate of data requirements is correct which does not take into account the entropy

2.5.3 Experimental Applications

The correlation dimension and entropy have been computed for a range of experimental systems Carroll et al. (1989). Experimental applications of the correlation dimension to a modulated semiconductor laser diode in a cavity were carried out. The laser output was detected with a Si APD and captured with a digitizing camera system (Tektronicx DCS 01) O'Gorman (1989). Power spectrum analysis indicated that the waveforms might be chaotic, O'Gorman et al. (1991). Time series were limited to 500 data points. It is possible to obtain a dimension $D_2 \approx 1.0$ for a numerically generated periodic waveform consisting of 500 data points. Noise, filtering, drift and the limited number of data have made the determination of $D_2 \approx 1.0$ impossible. Due to this difficulty the analysis was not extended to chaotic waveforms Studies have been carried out by Badii and Politi (1988) and Mitschke et al. (1988) to examine the effects of filtering. These studies have indicated that filtering increase the measured dimension, but the entropy is unaffected by filtering.

2.5 4 Spectrum of Dimensions

The correlation integral Eq (2.28) can be modified to calculate the spectrum of dimension D_q, (Pawelzi and Schuster, 1987, Atmanspacher et al., 1987).

$$C_q^d(\varepsilon) = \lim_{\varepsilon \to 0} \left[\frac{1}{N} \sum_{i=1}^{N} \left[\frac{1}{N} \sum_{j=1}^{N} \Theta\left(\varepsilon - \left[\sum_{n=1}^{d} |X_{i+d} - X_{j+d}|^2 \right]^{1/2} \right) \right]^{q-1} \right]^{\frac{1}{q-1}} \quad (2.42)$$

Badii and Politi (1984) have developed a similar algorithm for computing the generalized dimensions and the metric entropies, they have used this algorithm to calculate the Hausdorff dimension D_0 for a number of well known strange attractors. Kostelich and Swinney (1987) have compared Eq. (2.42) for calculating D_2 with the algorithm of Badii and Politi for calculating D_1, they have concluded that the later is more efficient for high dimensional systems.

Two examples will illustrate the difficulties of estimating the generalized fractal dimensions D_q by the spatial correlation method Eq. (2 42). For both of these examples analytic expressions are available for the D_q spectrum. The first of these examples is the baker map Eq. (4.1), this system will be examined in greater detail in Sec. 4.2. The probability distribution of this map is shown in Fig. 2.1 (a) A time series of $1.4*10^5$ data points is obtained, with embedded dimension d=4. An estimate of D_q requires a suitable region in the ln-ln plot. The range of scale used in Fig. 2.2 (b) is $6*10^{-6}<\varepsilon<5*10^{-2}$. Eq. (2.42) was implemented for the following values of q -10 to 0 and 2 to 12 increments 0 25, which corresponds to 82 different values of q. Several curves are shown in Fig. 2.2 (b); they correspond to the values of q=10 (top curve), 6,2,0,-4,-8 (bottom curve).

The exact D_q spectrum is shown by the continuous line in Fig. 2.3 (a). Two approximations are obtained from the slopes of the graph in Fig. 2 1 (b), corresponding to different range of scale ε The dashed line (– – –) is for the interval $-3.9< \ln \varepsilon <-8.2$ and the dashed dotted line (— —) is for the interval $-4.4<\ln \varepsilon<-9.1$. By a

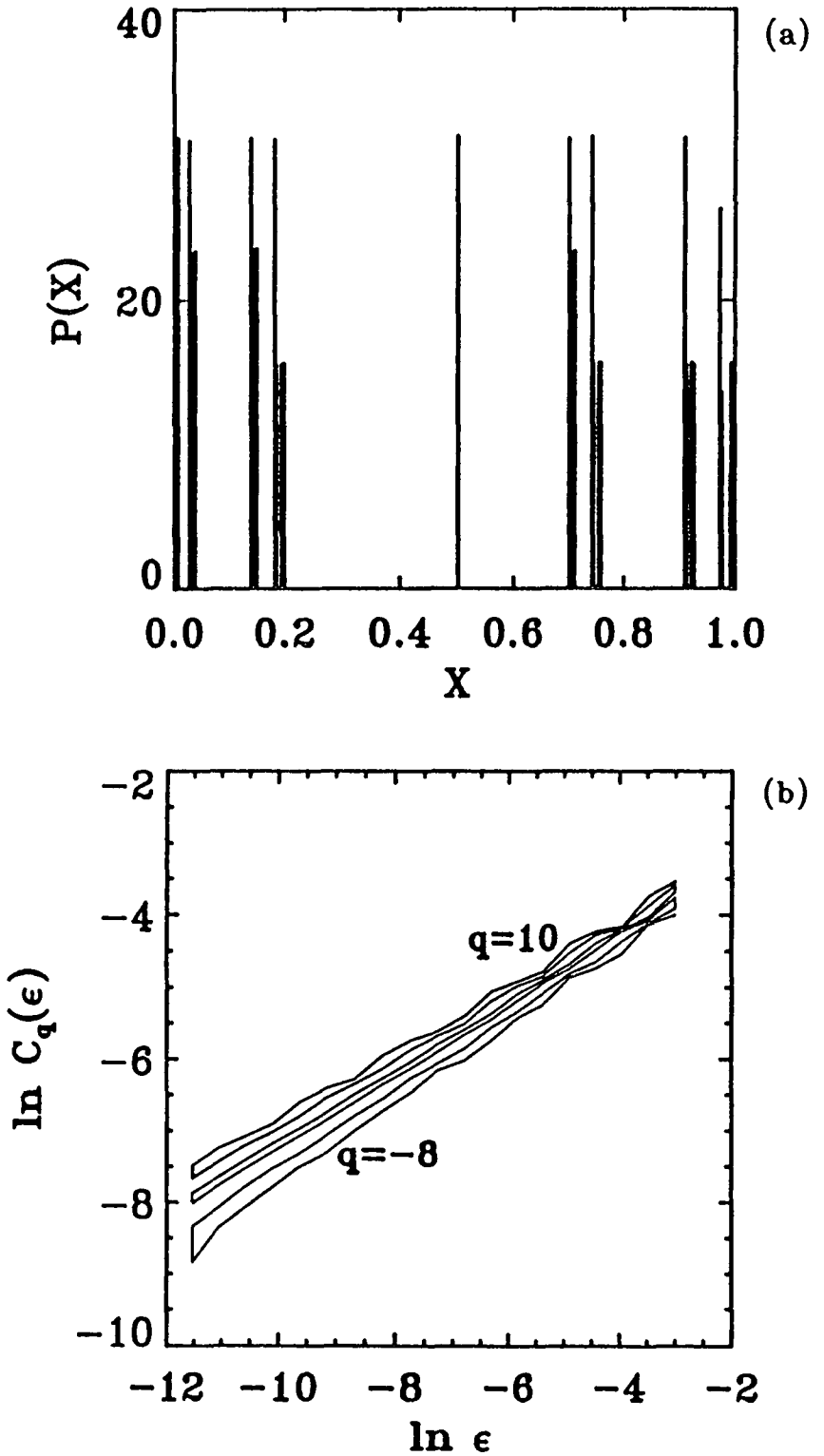

FIG. 2.2. (a) Multifractal distribution computed with $4*10^6$ iterations of Eq. (4.1). (b) Correlation integral $C_q(\varepsilon)$ for a time series consisting of $N=1.4*10^5$ data points, embedded in dimension d=4. Points pertaining to the same value of q are connected by lines. The values of q are q=10 (top curve),6,2,0,−4,−8 (bottom curve).

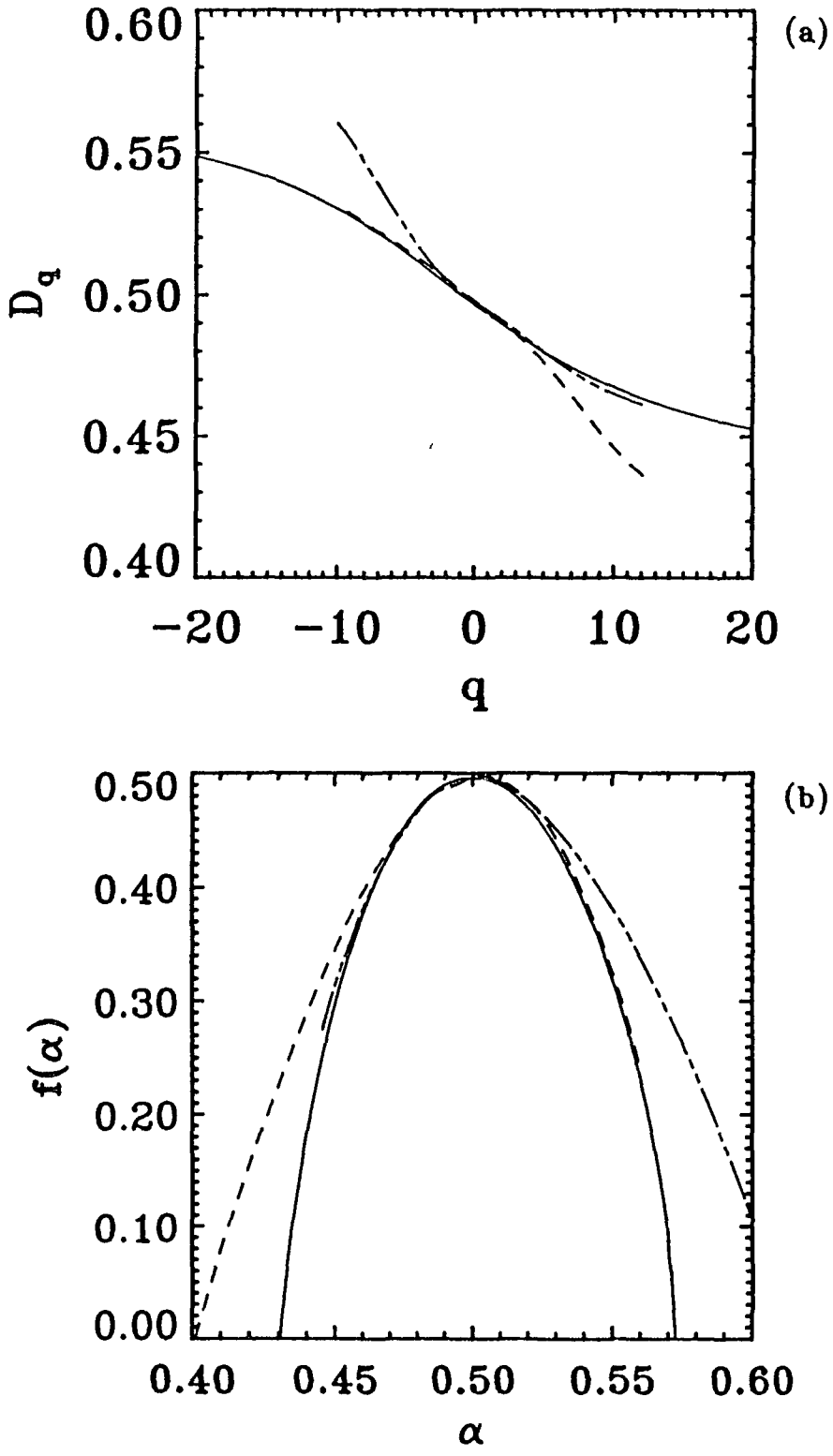

FIG. 2.3. (a) The dimension spectrum D_q computed with $N=1.4*10^5$ data points and an embedding dimension of d=4. The solid curve is the exact D_q spectrum, (see section 4.2 for derivation). Two approximations are shown, corresponding to different range of scale ε. The dashed line (– – –) is for the interval $-3.9 < \ln \varepsilon < -8.2$ and the dashed dotted line (— —) is for the interval $-4.4 < \ln \varepsilon < -9.1$. (b) The corresponding f(α) spectrum.

combination of these two curves, a good fit is obtained for D_q. The $f(\alpha)$ spectrum of singularities is shown in Fig. 2.3 (b). It was obtained from the two approximate D_q spectra in Fig. 2.3 (a). via the, Legender transformation Eq. (2.22).

The results of Fig. 2.2 and 2.3 deserves several comments. The number of iterations used and the chosen embedding dimension is sufficient for an accurate estimate of D_q for $-10 \leq q < 12$. The deviation from the true value is less than 1%. For this particular fractal their is an unique D_q for each value of q. There are oscillations in the ln-ln plot used to estimate D_q. These oscillations are a fundamental limitation of the algorithm and are due to the local nature of the measurement. As the $|q|$ increases the magnitude of the oscillations increases. The oscillations are due to inaccurate estimates of the multifractal measure shown in Fig. 2.6. The dimension D_q is independent of the length scale ε for this fractal. Similar periodic oscillations (called lacunarity) have been shown by Mandelbrot (1977) to reflect the fractal properties of self similar strange attractors

The range q =-10 to 12 is insufficient to obtain convergence in the $f(\alpha)$ spectrum Fig. 2.3 (b). The absolute value of q required to obtain the extremities α_{max} and α_{min} approaches infinity. For the $f(\alpha)$ spectrum shown in Fig. 2.3 (b) it was checked that $df/d\alpha \approx q$ to within a couple of percent. As the magnitude of D_q increases it becomes increasingly difficult to determine D_q for negative q (Meisel et al., 1992, Arneodo et al., 1987 and Pawelzik and Schuster, 1987).

The second example is the one dimensional circle map Eq. (2.37) with A=2. The total number of data points is $N=2*10^5$, with embedding dimension d=4. The exact D_q spectrum is $D_q=1$ for all q. The ln-ln plot is shown in Fig. 2.4 (a), for several values of q. Note the absence of any oscillations in this ln-ln plot. The map has a uniform probability distributing for this value of A (cf. Sec 3.2). The D_q spectrum is shown in Fig. 2.4 (b). The exact D_q

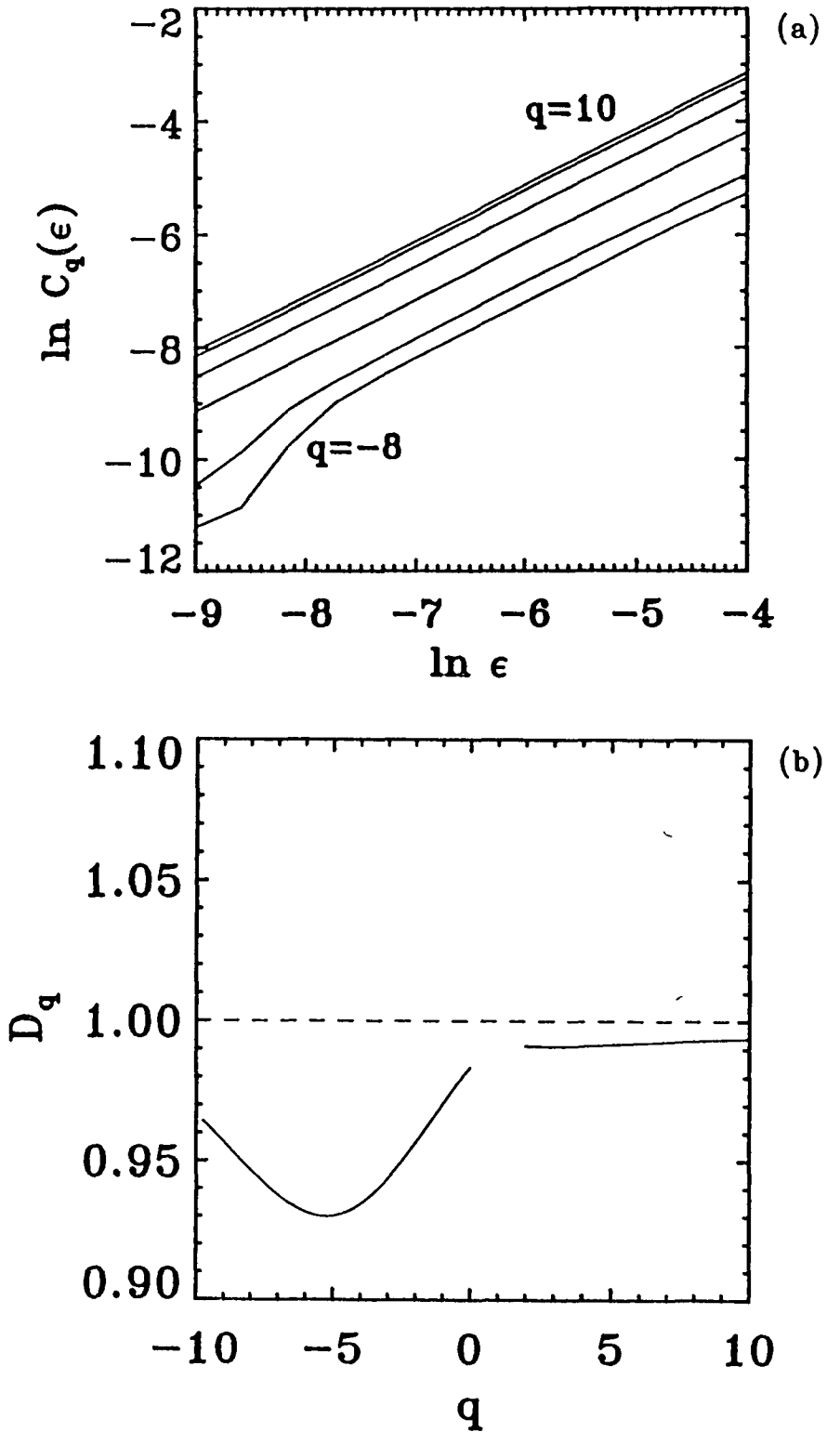

FIG. 2.4. (a) Correlation integral $C_q(\varepsilon)$ for the one dimensional map Eq. (2.1). The time series consisting of $N=2*10^5$ data points, embedded in dimension d=4. The values of q are q=10 (top curve),6,2,0,-4,-8 (bottom curve). (b) The exact D_q spectrum is shown by the dashed line and is equal to one for all values of q. The solid line is the estimated value from the generalized correlation integral.

spectrum is shown by the dashed line and is equal to one for all values of q. The solid line is the estimated value from the slope of the graph in Fig. 2.4 (a). For positive q the answer is within 1% of the true value, while for negative q there is a 7% difference. The $f(\alpha)$ spectrum for this value of A is a point spectrum. It is apparent from this figure that D_q does not increase with negative q, this does lead to inaccuracies when computing the differential of the D_q function so as to obtain the $f(\alpha)$ spectrum.

Successful applications of these ideas to experimental systems have been reported, Su et al. (1989). These applications are concerned with the $f(\alpha)$ spectrum at the onset to chaos for both the period doubling transition and the quasiperiodic transition to chaos.

2.6 UNSTABLE PERIODIC ORBITS

In this section unstable periodic orbits (UPO's) are reviewed. The method of extracting these orbits from a chaotic attractor is discussed and the relationship of the stability of these orbits to dimensions and entropies is examined.

2.6 1 DEFINITION OF UPO'S

Chaotic attractors are dense with unstable periodic orbits. A periodic orbit is defined as follows.

Definition 2.1. A periodic point P for $F:\mathbb{R}^n \longrightarrow \mathbb{R}^n$ is periodic of period m if $F^m(P)=P$.

Periodic orbits can be hyperbolic or elliptic.

Definition 2.2. A fixed point P for $F:\mathbb{R}^n \longrightarrow \mathbb{R}^n$ is called hyperbolic if DF(P) has no eigenvalues on the units circle, DF(P) is the Jacobian matrix at P. If P is periodic of period n, then P is hyperbolic if $DF^n(P)$ has no eigenvalues on the unit circle.

There are three types of hyperbolic periodic orbits, attracting, repelling and saddles.

Definition 2 3. Let $F^n(P)=P$

1. P is an attracting periodic point if all of the eigenvalues of $DF^n(P)$ are less than one in absolute value.

2. P is a repelling periodic point if all of the eigenvalues are greater than one in absolute value.

3. P is a saddle periodic point otherwise, i.e. some of the eigenvalues of $DF^n(P)$ are larger and some are less than one in absolute value.

Case 3 distinguishes higher dimensional systems from one dimensional systems. Case 1 corresponds to a stable periodic orbit while case 2 and 3 correspond to an unstable periodic orbit. For elliptic fixed points, it is the modulus of the eigenvalue that determines whether it is attracting, repelling or saddle fixed point.

2.6.2 Computing UPO's

When calculating the orbits, one first lays a grid of points over the attractor. Typically the number of grid points is at least 5 times larger than the number of periodic points that one expects to find. Then starting at each point, one solves for a periodic orbit of period n using the map and a Newton-Raphson iteration scheme. Until the condition $F^n(P)=P$ is true to a preassigned accuracy. The different periodic orbits are recorded and then the number of grid points is increased by a factor 2 or 3 to check that no new orbits appear. Since the map is known, the Lyapunov exponents can be calculated exactly and hence, we can classify the type of hyperbolic orbit. It is also possible to extract these orbits from a time series Auerbach et al. (1987) and Pawelzik and Schuster (1991).

Water and Hoppenbrouwers (1991) analyzed chaotic motion in an experiment on a parametrically excited pendulum in terms of unstable periodic orbits. These orbits provide a useful quantitative comparison with the results of a numerical simulation.

To demonstrate this procedure the unstable periodic orbits are calculated for the Henon map $(X,Y)\longrightarrow(1-AX^2+Y,BX)$ with A=1.4 and B=0.3. With the following results.

Table 2.2

The total number of unstable periodic orbits m of period n and the total number of cycle points.

Per n	1	2	3	4	5	6	7	8	9	10
N_n	1	3	1	7	1	15	29	63	55	103
m	1	1	0	1	0	2	4	7	6	10

N_n is the total number of cycle points of order n, and m is the total number of orbits of period n. The Lyapunov number of these cycles where calculated, and hence, the dimensions using $D=1+\lambda_+/|\lambda_-|$ The orbits of period 8 have dimension between 1.26-1 31

A knowledge of the number of period orbits of order n allows an estimate of the topological entropy K_0. The topological entropy of a dynamical system can be defined as

$$K_0 = \lim_{n\to\infty} \frac{1}{n}\log N_n \qquad (2.43)$$

the n^{th}-order approximation is defined by

$$K_0^{(n)} = \frac{1}{n} \log N_n \qquad (2.44)$$

for the Henon map $K_0^{(n)}$=0 46 in excellent agreement with the positive results.

2.6.3 Relation to Dimension and Entropy

In this section we discuss the relation of the unstable periodic orbits on chaotic attractors to the ergodic properties of these attractors. Consider a d-dimensional twice differentiable map $X_{m+1}=F(X_m)$. The

magnitude of the eigenvalues of the Jacobian matrix of the n times iterated map F^n at the j^{th} fixed point are denoted $\varepsilon_{1j}, \varepsilon_{2j}, \quad \varepsilon_{uj}, \quad \varepsilon_{(u+1)}, \quad \varepsilon_{dj}$, where we order the eigenvalues as follows: $\varepsilon_{1j} \geq \varepsilon_{2j} \geq \quad \geq \varepsilon_{uj} > 1 \geq \varepsilon_{(u+1)} \geq \quad \geq \varepsilon_{dj}$ The number of unstable eigenvalues is u. Let L_j be the product of the unstable eigenvalues at the j^{th} fixed point of F^n

$$L_j = \varepsilon_{1j}\varepsilon_{2j} \quad \varepsilon_{uj} \tag{2.45}$$

Let $D=\Delta+\delta$ where Δ is the integer part of D and δ is the fractional part of D In addition, let

$$S_j(D) = \varepsilon_{1j}\varepsilon_{2j} \quad \varepsilon_{\Delta j}(\varepsilon_{(\Delta+1)j})^{\delta} \tag{2.46}$$

The partition function in terms of L_j and S_j is, Grebogi et al. (1988).

$$\Gamma(q,D,n) = \sum_j L_j^{-1}[S_j(D)]^{-(q-1)} \tag{2.47}$$

In two-dimensional case with $\varepsilon_{1j} > 1 > \varepsilon_{2j}$ this reduces to

$$\Gamma(q,D,n) = \sum_j \varepsilon_{1j}^{-q}\, \varepsilon_{2j}^{-(q-1)} \tag{2.48}$$

Taking the limit $n \longrightarrow \infty$ is analogous to taking the limit $l \longrightarrow 0$ in Eq. (2.15),

$$\Gamma(q,D) = \lim_{n\longrightarrow\infty} \Gamma(q,D,n) \tag{2.49}$$

Setting q=1 we can compare D_1 and D_L. We have $\Gamma(q,D)=1$. Formally expanding Eq. (2.47) around q=1 we obtain

$$\Gamma(q,D,n) = 1 - (q-1)\sum_j L_j^{-1}\log(S_j(D)) + O[(q-1)^2] \tag{2.50}$$

Letting $n \longrightarrow \infty$ the coefficient of the (q-1) term is

$$\sum_j L_j^{-1}\log(S_j(D)) = 0 \tag{2.51}$$

Inserting S_j

$$\lim_{n\longrightarrow\infty}\Big[\sum_j L_j^{-1}\log(\varepsilon_{1j}\varepsilon_{2j} \quad \varepsilon_{\Delta j}) + \delta \sum_j L_j^{-1}\log(\varepsilon_{(\Delta+1)j}) \Big] = 0 \tag{2.52}$$

Solving for δ and adding to Δ we have D_1 equal

$$D_1 = \Delta - \lim_{n\to\infty} \frac{\sum_j L_j^{-1}\log(\varepsilon_{1j}\varepsilon_{2j}..\varepsilon_{\Delta j})}{\sum_j L_j^{-1}\log(\varepsilon_{(\Delta+1)j})} \qquad (2.53)$$

The Kaplan-York formula states that for a typical system,

$$D_L = \Delta - \frac{\log(\varepsilon_1\varepsilon_2..\varepsilon_\Delta)}{\log(\varepsilon_{\Delta+1})} \qquad (2.54)$$

with Δ being the largest integer such that $\log(\varepsilon_1\varepsilon_2..\varepsilon_\Delta) > 1$. Comparing (2.53) and (2.54) we see that these equation are the same if all orbits have the same stability or $D_1 \approx D_L$ if the orbits have approximately the same stability. Dynamical systems will be encountered in chapter 3 and 4 where $D_1 = D_L$.

2.7 CONCLUSION

In this chapter the major techniques for analyzing chaotic dynamical systems have been introduced. They include Lyapunov stability, generalized dimensions, $f(\alpha)$ spectra and unstable periodic orbits. These techniques will form the bases of the following chapters. The concept of maximum Lyapunov dimension has been introduced when the divergence of the system is greater than zero. Data requirements for a system with negligible boundary effects have been investigated and compared with previous studies. A relationship has been established between the number of data points required for the computation of D_2 and K_2. Experimental applications of D_2 and K_2 have been extensively reported in the literature. Our own application to an experimental system has shown that noise, filtering, drift and the limited number of data points are determental to obtaining $D_2=1$ for an experimental sine wave.

A comparison of numerically generated $f(\alpha)$ spectra with analytic results has highlighted some of the limitations of the generalized correlation integral. The oscillations in the ln-ln plot are a fundamental limitation of the multifractal measure. Inaccuracies in the

numerically generated D_q spectrum violate the inequality $D_q > D_{q'}$, for $q<q'$ leading to inaccuracies when computing the $f(\alpha)$ spectrum.

Unstable periodic orbits are of fundamental importance in the analysis of chaos and its evolution as will be apparent from the proceeding chapters. The method of extraction has been reviewed together with their relationship to Lyapunov exponents and dimensions for uniform hyperbolic systems

CHAPTER 3

INTERVAL MAPS AND CANTOR SETS

3.1 INTRODUCTION

This chapter is mainly concerned with one dimensional dynamical systems, in particular interval maps and Cantor sets. In Sec. 3.2 a hyperbolic map which is defined on a circle is investigated using periodic orbits and $f(\alpha)$ spectrums Numerical errors are examined in terms of these orbits. In contrast the well known logistic map which is nonhyperbolic is reviewed in Sec 3.3. There are many objects in physics and mathematics that exhibit self similar properties. Mandelbrot (1977) introduced the term fractal to described these self similar properties and applied it to a variety of natural phenomena. Some of the simplest fractals are Cantor sets and they are examined in Sec. 3 4 and 3 5, in terms of the generalized dimension and the scaling indices The results of this chapter will be used in the proceeding chapters to examine higher dimensional dynamical systems.

3 2 CIRCLE MAP

The simplest chaotic one dimensional map is the map of the circle given by,

$$X_{i+1} = A\, X_i \mod 1 \qquad (3.1)$$

This is hyperbolic for all values of A excluding A=±1. For A=1 and an additional constant term this map can be considered as a rotation of the circle (Cornfeld et al., 1982). For $A < |1|$ there are periodic solutions, while for $A > |1|$ there are chaotic solutions (cf. Sec 3.2.2). This

map is not a homeomorphism since it is not one-to-one and therefore its inverse is not defined. For A=2 this map is two-to-one. Since this map is defined on a circle X=0 is equivalent to X=1. The Lyapunov exponent λ is given by

$$\lambda = \ln |A| \qquad (3.2)$$

and is positive for $A > |1|$. The possibility of divergence and bounded trajectories causes the map to stretch an interval and fold a portion of the interval back on itself. Since folding cannot take place for one-dimensional invertible maps, such maps do not display chaotic behaviour. The chaotic behaviour of this map is examined for $A \in [1,\infty]$. The correlation dimension D_2 is $D_2 \approx 1.0$ for all values of $A > 1$ (cf. Sec 2.5.2 & 2.5.4).

3.2.1 Periodic Orbits

The n^{th} return map $f^n(X) = A^nX$ so that X is periodic of period n if and only if $A^nX = X+k$ for some integer k, i.e. if $x = k/(A^n-1)$ where $0 \le k < A^n$. Hence the periodic points of period n for f are the $(A^n-1)^{th}$ root of unity. It follows that periodic points are dense on the unit interval. In Table 3.1 the periodic orbits for n=3 and A=2 are listed.

Table 3.1

Period 3 orbits and their associated symbolic dynamics for the parameter A=2.

k	Period 3 orbits			Binary Seq.
0	0/7	0/7	0/7	0 0 0
1	1/7	2/7	4/7	0 0 1
2	2/7	4/7	1/7	0 1 0
3	3/7	6/7	5/7	0 1 1
4	4/7	1/7	2/7	1 0 0
5	5/7	3/7	6/7	1 0 1
6	6/7	5/7	3/7	1 1 0
7	7/7	7/7	7/7	1 1 1

It can be seen from this table that there are two

orbits of length three and two orbits of length one, corresponding to a total of 2^3. Each of these orbits are represented by a binary sequence. The sequence 001, 010 and 100 are equivalent. It can be seen form this table that the orbits lie on rational points on the interval. To describe the dynamics of Eq. (3.1) via symbolic dynamics we need to modify the binary sequence somewhat since there is an ambiguity in the sequence associated to any rational number of the form $p/2^k$ where p is an integer. For example, 1/2 may be described by either 1 or 0. To remedy this, we identify any two sequences of this form with an *, where * = 0 or 1.

Eventually periodic points of period n are defined by the following definition.

Definition 3.1 A point X is eventually periodic of period n if there exists $m > 0$ such that $f^{n+i}(X)=f^i(X)$ for all $i \geq m$. That is $f^i(X)$ is periodic for $i \geq m$.

If $X=k/A^n$ then $f^n(x)=k$ so that x is eventually fixed. If the map is a homeomorphism then eventually fixed point can not occur.

3.2.2 Numerical Errors

In all nonlinear systems computers are used to study the dynamics of the system, by iterating the systems equations over millions of mappings periods. In what sense do computations using finite precision and round off errors effect the dynamics of the system?

For $A>|1|$ in Eq. (3.1) all periodic orbits are repelling. For A equal to an odd integer there is chaotic behaviour for all irrational initial conditions. While for A equal to an even integer there is no chaotic behaviour, regardless of initial conditions used because some of the eventually periodic points can be represented accurately with the finite precision. When Eq. (3.1) is iterated the solution tends to the fixed point zero through an

eventually periodic point of period n. While for A approximately an integer, (e g. A=*.0000000000000001 where * is an even integer), eventually periodic point can not be represented accurately hence the chaotic solutions.

The orbits of Eq (3.1) with A=2 are rational numbers for all orbits of period n (Table 3.1). Inserting one component of a periodic orbit into Eq. (3.1), consecutive iterations will cycle around this orbit. If a computer is used for the same experiment finite precision results in the trajectory escaping from this repelling orbit after a couple of iterations The escape rate from this periodic orbit is $\delta X_{i+1}=\delta X_i 2$, where δX_0 is the initial separation from the orbit The smaller δX_0 the longer the duration of time spent in the vicinity of that orbit. It is this finite value of δX_0 that is responsible for chaotic behaviour in these dynamical systems. Greater numerical precision puts a lower bound on the magnitude of δX_0. Rannou (1974) explored this question using an integer map and concluded that chaotic motion is intrinsic to systems described by exact dynamics, independent of computer noise or roundoff errors.

3.2 3 Probability Density

The probability density has been computed numerically for A=1.1, 2 0 & 2.5 and is shown in Fig 3.1. For A=2.0 the probability density is uniform This uniform distribution can be explained in terms of the uniform distribution of periodic orbits along the unit interval While for A=1.1 and 2 5 the distribution is nonuniform. Peaks in the probability distribution can be related to the concentration of periodic orbits at that position along the interval. As A tends towards infinity there is a uniform probability density, this is because the time series is completely random. A small entropy corresponds to a deterministic system, while large entropy corresponds to a completely random system, the entropy is lnA.

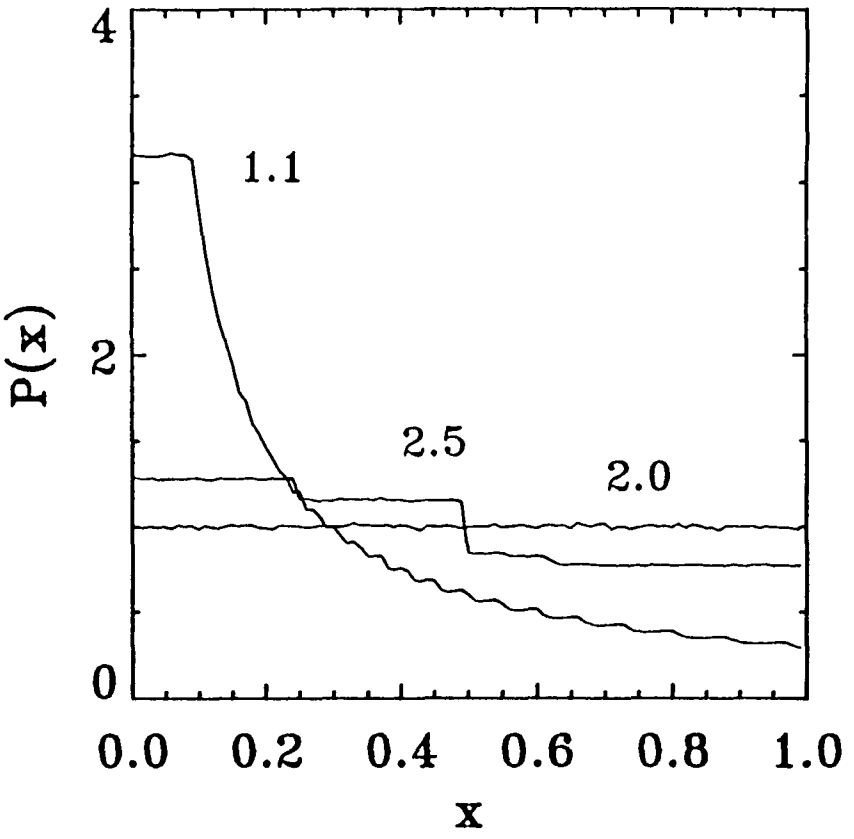

FIG. 3.1. Probability density P(X) vs X for the circle map. Three values of A are shown 1.1, 2.0 and 2.5.

3.2.4 F(α) SPECTRUM

Using the probability density calculated in the previous section it is possible to calculate an approximate D_q spectrum and the corresponding f(α) spectrum (Duong-vav 1987). For A=2.5 the probability density can be approximated by,

$$p(X) = \begin{cases} 1.28 & 0.00 < X \leq 0.25 \\ 1.15 & 0.25 < X \leq 0.50 \\ 0.84 & 0.50 < X \leq 0.60 \\ 0.77 & 0.60 < X \leq 1.00 \end{cases} \qquad (3.3)$$

Starting with this probability density the interval [0,1] is subdivided into n segments of size l_i, each with a constant probability $P_i = a$, where a is now the area chosen in the calculation,

$$a = \int_{X_{i-1}}^{X_i} p(X)dx \qquad \text{with } p(x) \text{ normalized to 1} \qquad (3.4)$$

Given a chosen a, X_i can be calculated. The segment $l_i = X_i - X_{i-1}$ with the corresponding $P_i = a$ are used in the relation

$$\sum_{i=1}^{1/a} \frac{P_i^q}{l_i^{(q-1)Dq}} = 1 \qquad (3.5)$$

to solve for D_q. The numerical results are presented in Fig. 3.2 (a), for D_q as a function q. The Legendre transformation Eq. (2 22) give the corresponding $f(\alpha)$ spectrum as shown in Fig. 3.2 (b). To verify that this D_q spectrum is correct a calculation of the spectrum using Eq. (2 42) was implemented with $N=2*10^5$ and d=4. The results are shown by the dashed dotted line in Fig. 3.2, for q=2 to 12. There is close agreement between the two dimension sets For negative q the dimensions could not be obtained. The spread in dimensions for $q \in (-20,20)$ is 0.97-1.03. For A=1.1, Eq (2 42) indicate that the dimensions for q>0 are indistinguishable from 1.0.

A similar calculation for A=2 gives $D_q = 1 \ \forall \ q \in \{-\infty,\infty\}$. At this value of A=2 we have an example of uniform hyperbolic attractors. A=1 1 and 2.5 are example of non-uniform hyperbolic attractors. The probability density is related to the concentration of periodic orbits at a particular point along the interval. For q=0 we simply obtain $f=D_0=1$ 0, where D_0 is the Hausdorff dimension of the set. The Hausdorff dimension of a one dimensional unstable manifold is always $D_0=1$ 0.

3.3 LOGISTIC MAP

In this section, the extensively studied quadratic or logistic map is reviewed.

$$X_{i+1} = F(X_i) = u\, X_i(1-X_i) \qquad (3.6)$$

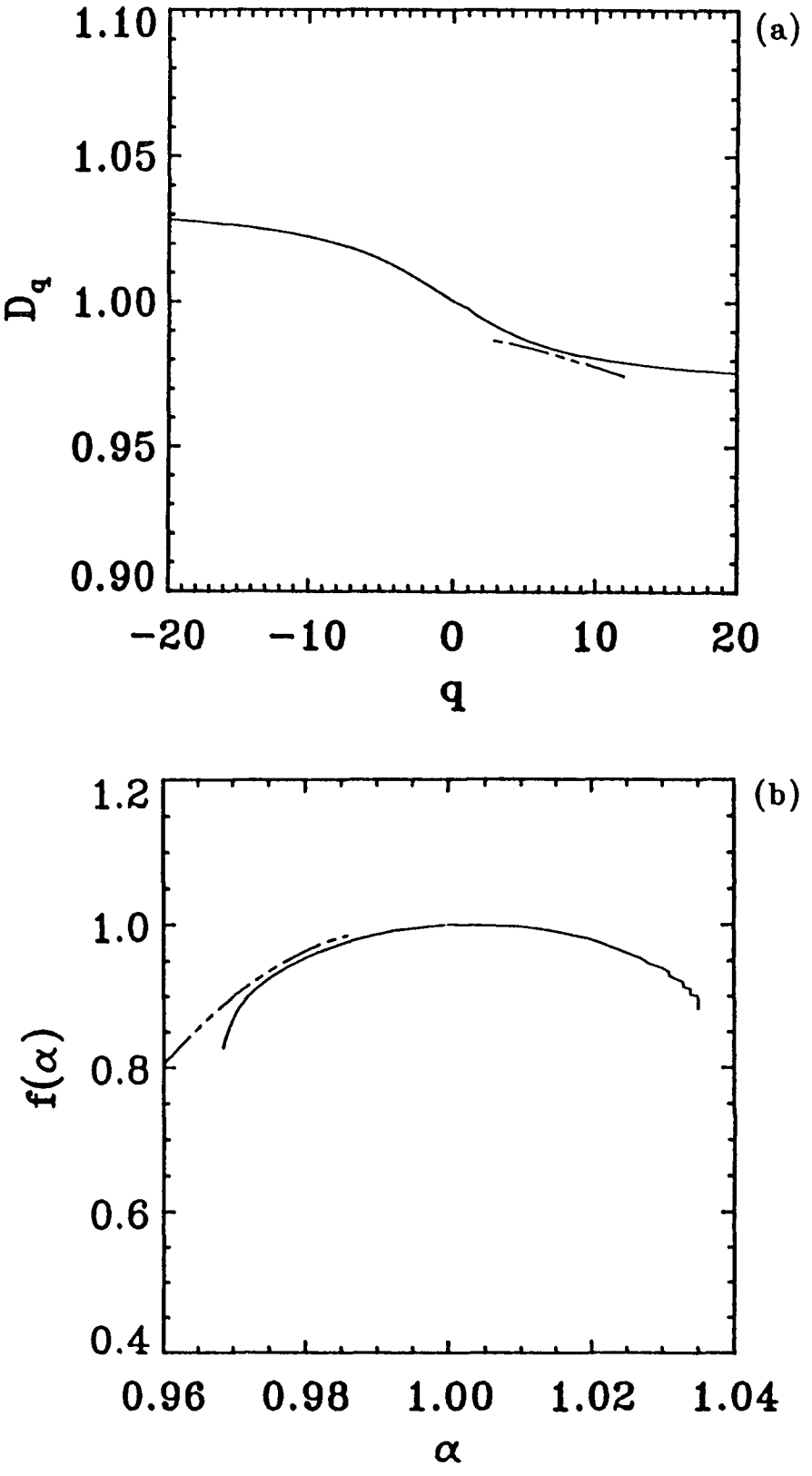

FIG. 3.2. (a) D_q spectrum for the circle map with A=2.5. The continuous line is the D_q spectrum from Eq. (3.5) and the dashed dotted line is from Eq. (2.42). (b) The corresponding $f(\alpha)$ spectrums of (a).

The dynamics of this map are related to the infinite dimensional delay differential equations in chapter 7. Of specific interest is the period doubling route and the $f(\alpha)$ spectra.

3.3.1 Periodic Attractors

For $u>1$ F_u has two fixed points one at 0 and the other at $X_u = (u-1)/u$. Note that $dF_u(0)/dX = u$ and $dF_u(X_u)/dX = 2-u$. Hence u is a repelling fixed point for $u>1$ and X_u is attracting for $1<u<3$. When $u=3$ $dF_u(X_u)/dX = -1$. As u passes through 3 the dynamics of F_u become increasingly complicated A new period 2 is born, then a period 4 etc.. This period doubling involves

1. A change from an attracting to a repelling orbit, together with
2 The birth of a new periodic orbit of twice the period.

The Schwarzian derivative of a function F at X is defined as

$$SF(x) = \frac{F'''(X)}{F'(X)} - \frac{3}{2}\left(\frac{F''(X)}{F'(X)}\right)^2 \qquad (3.7)$$

The Schwarzian derivative allows us to define an upper bound on the number of attracting periodic orbits that a map like the quadratic map may have. It also allows us to examine why a map makes a transition from simple to chaotic dynamics Let us quote a number of properties for the Schwarzian derivative, (the proofs can be found in Deveany (1986)).

1. Suppose $SF<0$ and F has n critical points. Then F has at most n+2 attracting periodic orbits.
2. If $SF<0$, the $SF^n<0$ for all $n>1$
3 If F(X) has infinitely many critical points, then so does $F^n(X)$.

The quadratic map $F_u(X)$ has one critical point (X=1/2). Hence, for each u there exits at most three attracting periodic orbits Of course there may be no attracting

periodic point. In actual fact it can be proven that there exists at most one periodic orbit for each u. As the parameter u is increased towards u_∞=3.5699... F_u has an attracting periodic orbit of period 2^n with n tending to infinity as u tends to the accumulation point u_∞. The attractor at u_∞ is called the Feigenbaum attractor, and the dimension D_2 is 0.500±0.005. This is a very special attractor. There is no sensitive dependence on initial conditions and the attractor u_∞ is not chaotic.

3.3.2 Chaotic Attractors: F(α) Spectrum

For the logistic map with u=4 the probability distribution converges rapidly to

$$P(X) = \frac{1}{\pi}\,[X(1-X)]^{-1/2} \tag{3.8}$$

By the use of this, one can calculate explicitly D_q and find (Ott et al., 1984)

$$D_q = \begin{cases} 1 \quad \text{for} \quad q \le 2, \\ q/[2(q-1)] \ \text{for} \ q \ge 2. \end{cases} \tag{3.9}$$

The D_q spectrum is nonanalytic at q=2. The f(α) spectrum consists of the isolated points f(1)=1 and f(0)=1/2. Badii (1989) evaluated the f(α) spectrum from a histogram of the probability distribution Linear behaviour was found between these points. At the intervening values of u between u_∞ and u=4 there are highly singular probability distributions along the unstable manifold (Collet and Eckmann, 1980). The are no published f(α) spectrums for these intervening values. For u>4 all points eventually escape to infinity along a Cantor set. Details about the orbits and their symbolic dynamics can be found in Grassberger (1988).

3.4 CANTOR SETS

In this section Cantor sets are examined from the point of view of their generalized dimensions and their spectrum of scaling indices. Cantor sets are of fundamental

importance to the understanding of chaos.

If a measure is constructed from an exact recursive rule, one can easily determine the D_q and the $f(\alpha)$ spectra. Suppose that the measure is generated by the following process. Start with the original region which has a measure one and length one. Divide the region in to pieces S_i, i=1,2,...,N with measure P_i and l_i. Then at the first stage a partition function is constructed,

$$\Gamma_1(\tau,q) = \sum_{i=1}^{N} \frac{P_i^q}{l_i^\tau} \tag{3.10}$$

Continue the cantor construction. At the next stage each piece of the set is further divided into N pieces, each with a measure reduced by a factor P_i and size by a factor l_i. At this stage the partition function is

$$\Gamma_2(\tau,q) = \Gamma_1^2(\tau,q) \tag{3.11}$$

the first partition function will generate all the other $\Gamma_n = \Gamma_1^n$. For this reason Γ_1 is called a generator for the set.

3.4.1 Uniform Cantor Set

A simple example is the classical Cantor set obtained by dividing the interval [0,1]. Start with the unit interval but remove the open middle third i.e. the interval [1/3, 2/3]. Each of these intervals receive the same measure P=1/2. Next, remove from what remains the two middle thirds again, i.e. (1/9,2/9) and (7/9,8/9). Note that 2^n open intervals are removed at the n^{th} stage of this process. Thus for this measure we require

$$2\left\{ \frac{(\frac{1}{2})^q}{(\frac{1}{3})^\tau} \right\} = 1 \tag{3.12}$$

which yields $\tau = (q-1)\ln 2/\ln 3$, $D_q = \ln 2/\ln 3$. In this example $\alpha=f=D_q$. This uniform Cantor set is an example of a fractal. Intuitively, a fractal is a set which is self similar under magnification. By varying the interval size l_i we can vary the dimension $D_q = \ln P/\ln l$ of the Cantor set in the range [0,1]. For $D_q = 1$ we no longer have a Cantor

set but a line segment of uniform probability. A Cantor set is defined by the following definition.

Definition 3.2 A set Λ is a Cantor set if it is a closed, totally disconnected and a perfect subset of I. A set is totally disconnected if it contains no intervals; a set is perfect if every point in it is an accumulation point or a limit point of the other points in the set.

The length of the components of Λ_n tend to zero with increasing n, $\Lambda=\bigcap_{n\geq 0}\Lambda_n$ is a Cantor set. Although this example was trivial we shall see in section (4.2) the importance of uniform Cantor set when we examine two dimensional chaotic attractors. A more general example of a Cantor set is the two scale Cantor set.

3.4.2 Two Scale Recursive Sets

Let n_1 denote the number of pieces of length l_1 and n_2 the number of length l_2. Further, let the respective probabilities be P_1 and P_2. The probabilities are normalized such that $n_1P_1+n_2P_2=1$. The generator is given by

$$\Gamma^n(\tau,q) = \left[n_1\frac{P_1^q}{l_1} + n_2\frac{P_2^q}{l_2} \right]^n = 1 \qquad (3.13)$$

as $n \longrightarrow \infty$ Γ dose not depend on n. In Fig. 3.3 (a) we show $D_q = \tau(q)/(q-1)$ as a function of q obtained numerically by solving Eq. (3.13) with measure $P_1=0.6$ and $P_2=0.4$ and rescaling $l_2=0.1$. Three different values of l_1 are used 0.1, 0.3 and 0.7. Using a binomial expansion Eq. (3.13) can be written as

$$\Gamma(q,\tau) = \sum_{m=0}^{n} \binom{n}{m} n_1^m\, n_2^{(n-m)} P_1^{mq}\, P_2^{(n-m)q}\, (l_1^m l_2^{(n-m)})^{-\tau(q)} = 1 \qquad (3.14)$$

Using the analytic methods of Halsey et al. (1986) analytic expressions for the $f(\alpha)$ spectra can be obtained. In the limit $n\longrightarrow\infty$ the largest term in the sum of Eq. (3.14) should dominate. To find this term we compute

$$\frac{\delta \ln\Gamma(q,\tau)}{\delta m} = 0 \qquad (3.15)$$

Using Stirling approximation, we find that Eq. (3.15) is equivalent to

$$\tau = \frac{\ln(n/m-1)+q\ln(P_1/P_2)}{\ln(l_1/l_2)} \qquad (3.16)$$

Since we expect the maximum term to dominate the sum, we have the second equation

$$\binom{n}{m} P_1^{mq} P_2^{(n-m)q} (l_1^m l_2^{(n-m)})^{-\tau(q)} = 1 \qquad (3.17)$$

inserting Eq. (3.16) into Eq. (3.17) leads to an equation for n/m. After manipulation, one finds

$$\ln(n/m)\ln(l_1/l_2) - \ln(n/m-1)\ln(l_1) = q(\ln(P_1)\ln(l_2) - \ln(P_2)\ln(l_1)) \qquad (3.18)$$

For a given q there will be a value of n/m which solves Eq. (3.18) and, in turn , determine τ from Eq. (3.16). The density exponent f is determined by

$$\binom{n}{m} (l_1^m l_2^{(n-m)})^f = 1 \qquad (3.19)$$

using Stirling approximation, we find

$$f = \frac{(n/m-1)\ln(n/m-1) - (n/m)\ln(n/m)}{\ln(l_1) - (n/m-1)\ln(l_2)} \qquad (3.20)$$

The exponent determining the singularity in the measure, α is determined by

$$P_1^m P_2^{(n-m)} = (l_1^m l_2^{(n-m)})^\alpha \qquad (3.21)$$

or

$$\alpha = \frac{\ln(P_1) + (n/m-1)\ln(P_2)}{\ln(l_1) - (n/m-1)\ln(l_2)} \qquad (3.22)$$

Thus, for any chosen q, the measure scales as $\alpha(q)$ on a set of segments which converge to a set of dimension f(q). As q is varied different regions of the set determine

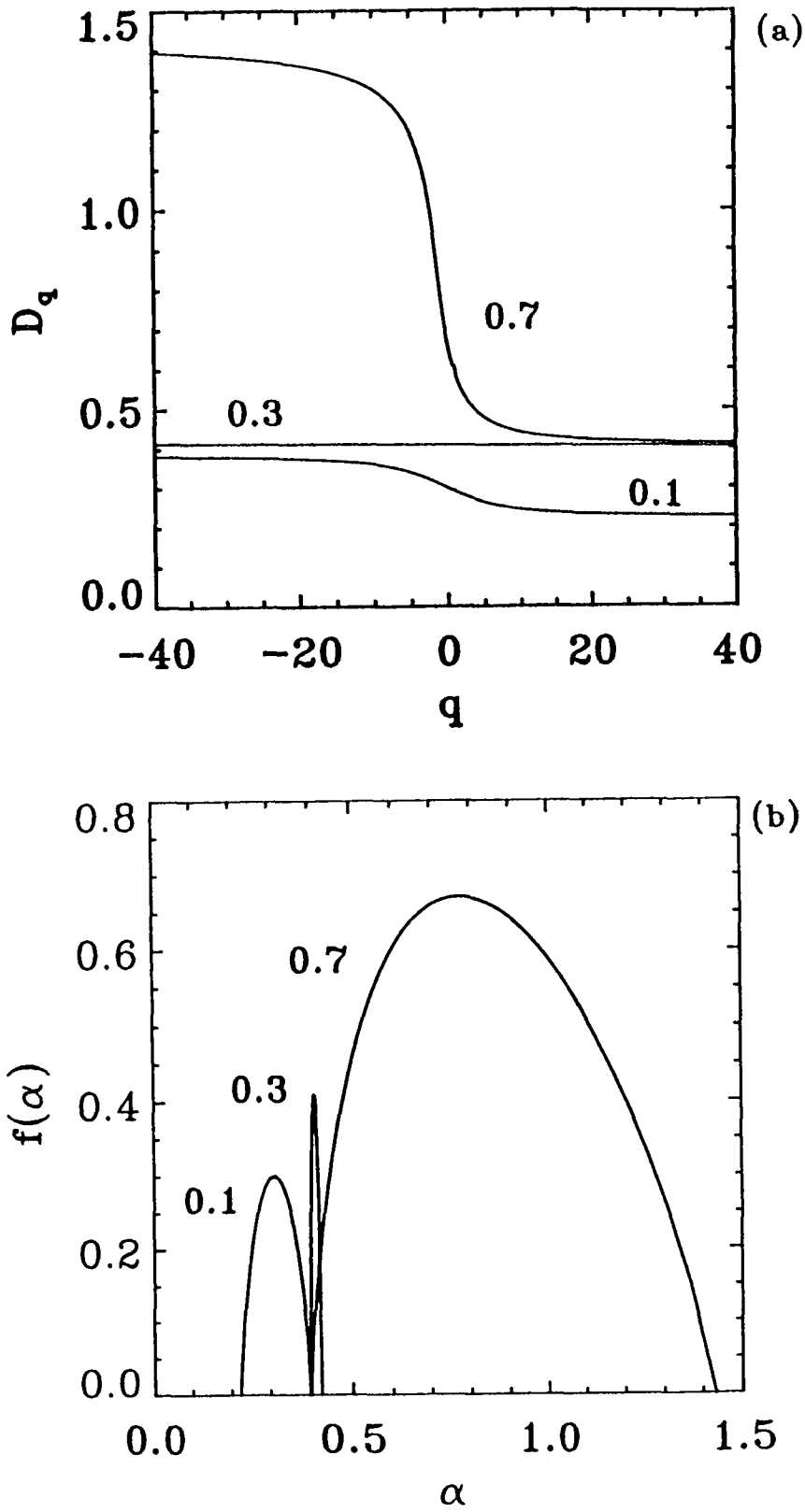

FIG. 3.3. (a) D_q plotted vs q for the two scale Cantor set, with measure P_1=0.6 and P_2=0.4 and rescaling l_2=0.1. Three different values of l_1 are used 0.1, 0.3 and 0.7. (b) the corresponding f(α) spectrums.

D_q. The extreme α vales are,

$$D_{-\infty} = \alpha_{max} = \ln P_2/\ln l_2 \quad \text{and} \quad D_{\infty} = \alpha_{min} = \ln P_1/\ln l_1 \qquad (3.23)$$

In Fig 3.3 (b) the $f(\alpha)$ curve obtained from Eq.'s (3.20) and (3.22) is display with n=400 and the other parameter values are as given in Fig. 3.3 (a). For q=0 we simply obtain $f=D_0$ where D_0 is the Hausdorff dimension of the set. From Eq. (3 13) D_0, is defined by the transcendental equation

$$l_1^{D_0} + l_2^{D_0} = 1 \qquad (3.24)$$

With increasing l_1, D_0 tends to its maximum value of 1.

3.4.4 Three Scale Cantor Set

Some of the most interesting problems lie on supports of continuous measure, including the circle map strange attractor and ordinary differential equations. Supports of continuous measure have a Hausdorff dimension D_o=1. (Tél, 1988)

Consider the following example: l_1=0.2 l_2=0.4, P_1=0.1, P_2=0.45, n_1=1 and n_2=2 Note that $P_2/l_2 > P_1/l_1$ and $l_2 > l_1$. Although the measure on the line segment is rearranged at each step of the recursive process, the support for the measure remains at each step the original line segment. Thus as we would expect, D_0=1. The $f(\alpha)$ spectrum for these parameters is shown in Fig. 3.4. The densest region on the line segment contract not to one point, but to a set of points of finite dimension. The lowest value of α and D_∞ is $D_\infty = \alpha = \log(0.45)/\log(0.4)=0.87$, with a corresponding nonzero value of f=0.756. Note that there is always only one segment at the lowest values of the density, so that we still expect $D_{-\infty}$ to correspond to a value of f=0. It is also possible to construct a Cantor set for which the most rarefied region corresponds to a set of finite dimension. Alternative processes that cause truncation of the $f(\alpha)$ spectrum are examined in Sec 4.3.2.

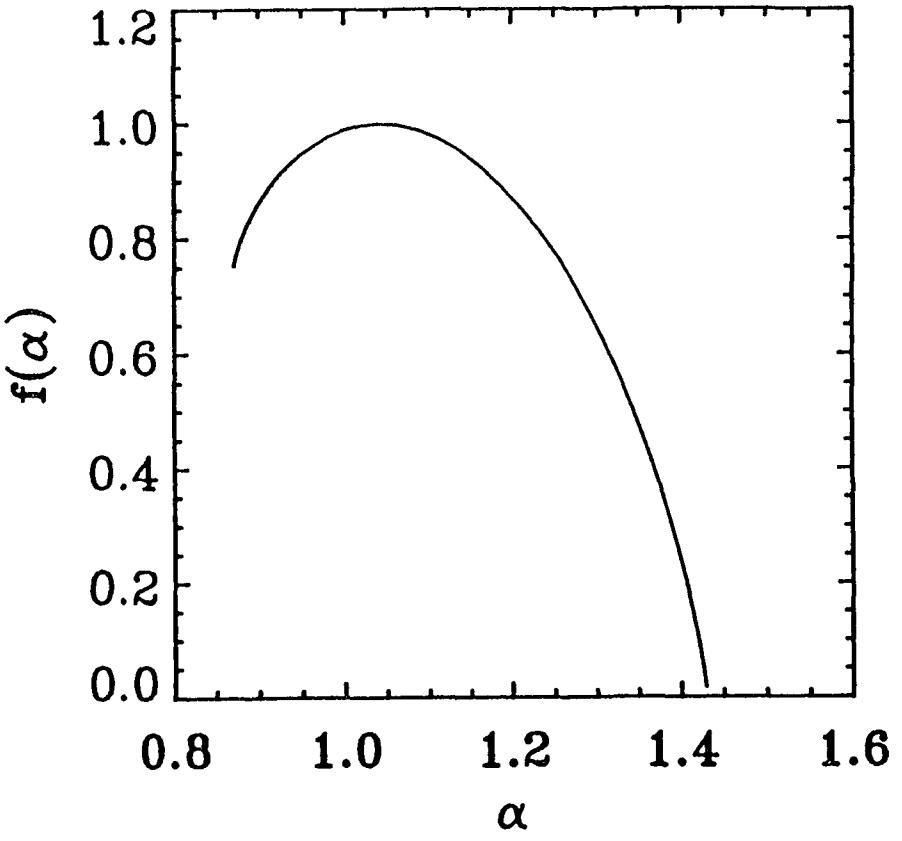

FIG. 3.4. The function f(α) for a Cantor set, with measure P_1=0.1 and P_2=0.45 and rescaling l_1=0.2 and l_2=0.4 with n_1=1 and n_2=2. Note that D_∞ corresponds to an nonzero value of f=0.756...

3.4.4 Two Dimensional Cantor Sets

A two dimensional multifractal is shown in Fig. 3.5 (a). This set could be constructed by the following rule. Start with a square and divide it into 16 pieces. Remove all pieces except the four in the middle, which now form a large square, and the four squares in the corners. Then continue the procedure and divide each of the five squares into five new ones, and so on. A each stage of the process half of the original area is removed. As in the one dimensional Cantor set there is still points left in the region. These points which exist in an area of magnitude zero are separate, forming a two dimensional Cantor dust. A similar process can be used to generate other types of structures in both two and three dimensions Jones (1991).

The fractal object in Fig. 3.5 (a) was generated using a three dimensional map similar to the two dimensional map

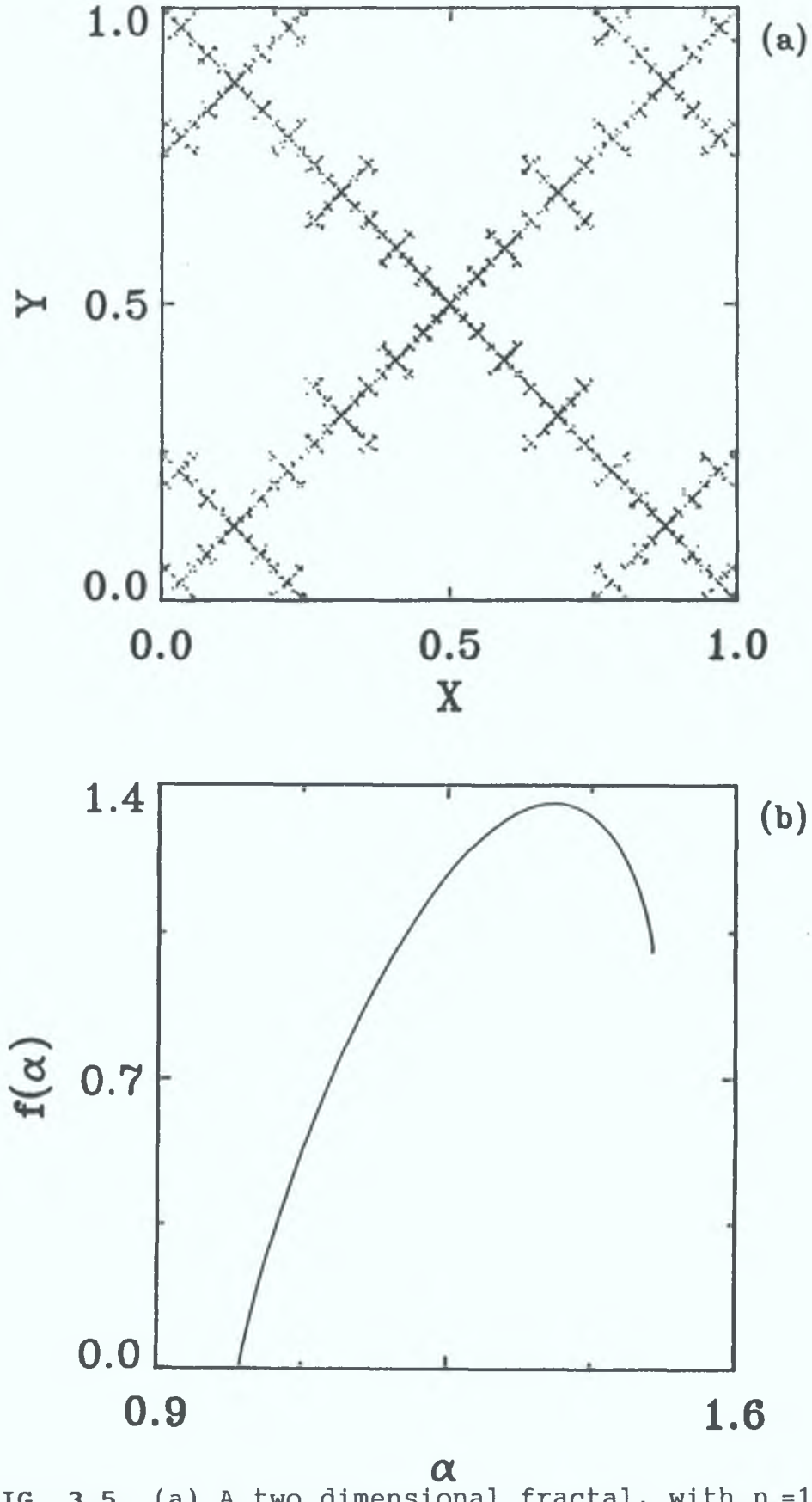

FIG. 3.5. (a) A two dimensional fractal, with n_1=1, n_2=4, P_1=1/2, P_2=1/8, l_1=1/2 and l_2=1/4. (b) the f(α) spectrum of the fractal object in (a).

defined by Eq (4.1). The generator for this object is given by Eq. (4.11) with $n_1=1$, $n_2=4$, $l_1=1/2$, $l_2=1/4$, $P_1=1/2$, and $P_2=1/8$. The $f(\alpha)$ spectrum can be completely determined in terms of these parameters Hakansson and Russberg (1990), and is given in Fig. 3.5 (b). The Hausdorff dimension for this fractal is given by $D_o=1.3570....$ Note the similarities of this $f(\alpha)$ spectrum with the three scale Cantor set. Two important questions concerning these structures will be answered in Sec. 4.4.3, firstly do these structures exist in dynamical systems and secondly under what conditions can they be found.

3 5 SCALING PROPERTIES

An alternative classification of a multifractal is in terms of scaling functions. Feigenbaum et al. (1989) considered the case of an equimeasure partition where P_i is a constant A matrix approach is considered here for non constant P_i or l_i, Chhabra et al. (1989). Recently this matrix has been formulated into an eigenvalue equation (Kovacs and Tél, 1992). The starting point for obtaining the transfer matrix is the partition function

$$\Gamma(\tau,q) = \sum_i \frac{P_i^q}{l_i^\tau} \tag{3.25}$$

the index i is written as a sequence of binary, ternary numbers $(\varepsilon_1,...,\varepsilon_n)$ Eq (3.25) then reads

$$\Gamma(\tau,q) = \sum_{\varepsilon_n,...,\varepsilon_1} \frac{P(\varepsilon_n,...,\varepsilon_1)^q}{l(\varepsilon_n,...,\varepsilon_1)^\tau} \tag{3.26}$$

The microscopic information is carried by the so called scaling function (Feigenbaum et al., 1986). Two scaling functions are defined one for the probabilities and the other for the lengths. In each case the scaling function is the ratio of the daughter-to-mother

$$\begin{aligned} \sigma_p(\varepsilon_{n+1}, .,\varepsilon_1) &= P(\varepsilon_{n+1},...,\varepsilon_1)/P(\varepsilon_n,. .,\varepsilon_1) \\ \sigma_l(\varepsilon_{n+1}, .,\varepsilon_1) &= l(\varepsilon_{n+1},...,\varepsilon_1)/l(\varepsilon_n,...,\varepsilon_1) \end{aligned} \tag{3.27}$$

The probabilities and the lengths can be thus expressed as a product of σ's which can be inserted into the partition sum (3.26) to yield

$$\Gamma(\tau,q) = \sum_{\varepsilon_{n+1},\ldots,\varepsilon_1} \frac{\sigma_P(\varepsilon_{n+1},\ldots,\varepsilon_1)^q \;\; \sigma_P(\varepsilon_n,\ldots,\varepsilon_1)^q}{\sigma_1(\varepsilon_{n+1},\ldots,\varepsilon_1)^\tau \;\; \sigma_1(\varepsilon_n,\ldots,\varepsilon_1)^\tau}$$

$$* \frac{\sigma_P(\varepsilon_{n-1},\ldots,\varepsilon_1)^q \;,\; \ldots\ldots,\; \sigma_P(\varepsilon_1)^q}{\sigma_1(\varepsilon_{n-1},\ldots,\varepsilon_1)^\tau \;,\; \ldots\ldots\ldots,\; \sigma_1(\varepsilon_1)^\tau} \tag{3.28}$$

Summations on $\varepsilon'_n,\ldots,\varepsilon'_2$ are added these are immediately compensated by Kronecker δ functions·

$$\Gamma(\tau,q) = \sum_{\substack{\varepsilon_{n+1},\ldots,\varepsilon_1 \\ \varepsilon'_n,\ldots,\varepsilon'_2}} \frac{\sigma_P(\varepsilon_{n+1},\ldots,\varepsilon_1)^q \;\; \sigma_P(\varepsilon'_n,\ldots,\varepsilon'_2,\varepsilon_1)^q}{\sigma_1(\varepsilon_{n+1},\ldots,\varepsilon_1)^\tau \;\; \sigma_1(\varepsilon'_n,\ldots,\varepsilon'_2,\varepsilon_1)^\tau}$$

$$* \frac{\sigma_P(\varepsilon'_{n-1},\ldots,\varepsilon'_2,\varepsilon_1)^q \;,\; \ldots\ldots,\; \sigma_P(\varepsilon_1)^q}{\sigma_1(\varepsilon'_{n-1},\ldots,\varepsilon'_2,\varepsilon_1)^\tau \;,\; \ldots\ldots,\; \sigma_1(\varepsilon_1)^\tau} \delta_{\varepsilon_n\varepsilon'_n,\ldots,\varepsilon_2\varepsilon'_2} \tag{3.29}$$

A transfer matrix T is defined by

$$\langle \varepsilon_{n+1},\ldots,\varepsilon_2 \mid T \mid \varepsilon'_n,\ldots,\varepsilon'_2,\varepsilon_1 \rangle$$

$$= \delta_{\varepsilon_n\varepsilon'_n,\ldots,\varepsilon_2\varepsilon'_2} \;\; \frac{\sigma_P(\varepsilon_{n+1},\ldots,\varepsilon_1)^q}{\sigma_1(\varepsilon_{n+1},\ldots,\varepsilon_1)^\tau} \tag{3.30}$$

Then it follows that one is the largest eigenvalue of the matrix T. For large n, Eq. (3.30) can be considered as an eigenvalue equation. The lowest order nontrivial approximation of the transfer matrix reads

$$T^{(1)} = \begin{pmatrix} \sigma_P^q(0,0)/\sigma_1^\tau(0,0) & \sigma_P^q(0,1)/\sigma_1^\tau(0,1) \\ \sigma_P^q(1,0)/\sigma_1^\tau(1,0) & \sigma_P^q(1,1)/\sigma_1^\tau(1,1) \end{pmatrix} \tag{3.31}$$

Writing the general characteristic polynomial

$$\lambda^2 - \lambda\left(\frac{\sigma_P^{q}(0,0)}{\sigma_1^{\tau}(0,0)} + \frac{\sigma_P^{q}(1,1)}{\sigma_1^{\tau}(1,1)}\right) + \frac{\sigma_P^{q}(0,0)\,\sigma_P^{q}(1,1)}{\sigma_1^{\tau}(0,0)\,\sigma_1^{\tau}(1,1)} - \frac{\sigma_P^{q}(0,1)\,\sigma_P^{q}(1,0)}{\sigma_1^{\tau}(0,1)\,\sigma_1^{\tau}(1,0)} = 0 \qquad (3.32)$$

Such an equation is solved by a multidimensional Newton-Raphson technique. The $\tau(q)$ values can are obtained from Eq. (3.13). As expected the scaling exponents are related to the measures and lengths of the Cantor set, $\sigma_P(0,0) = \sigma_P(1,0) = P_1$, $\sigma_P(1,1) = \sigma_P(0,1) = P_2$, $\sigma_1(0,0) = \sigma_1(1,0) = l_1$ and $\sigma_1(1,1) = \sigma_1(0,1) = l_2$ with $\lambda=1$. For a particular set of scaling functions there is a nonunique D_q spectrum.

3 6 CONCLUSION

The periodic orbits of the hyperbolic circle map with integer coefficient all lie on rational points on the interval. The fundamentals of chaotic behaviour in this map have been explained in terms of these orbits and the associated numerical error which determines the accuracy of the orbit With non integer coefficient the probability density is nonuniform and the D_q spectrum is not unity for all q

The theory of Cantor sets which is pertinent to the characterization of chaos in higher dimensional systems has been reviewed Specifically the concept of evolution has been introduced to described the changes in a uniform and a two scale Cantor set as one of the parameters of the set is change

The termination of the $f(\alpha)$ spectrum at a non zero value of f has been examined using a three scale Cantor set A two dimensional Cantor set structure has been reviewed. The importance of this type of structure to dynamical systems will be apparent in Sec. 4.4.3.

CHAPTER 4

DEVELOPMENT OF CHAOS IN TWO AND THREE DIMENSIONAL DISCRETE HYPERBOLIC SYSTEMS

4.1 INTRODUCTION

Chaos in two and three dimensional discrete hyperbolic systems is examined in this chapter. In Sec. 4.2 the theory that establishes the connection between the baker map and a Cantor set is reviewed. Analytic expressions for the generalized entropies are obtained. The connection between generalized dimensions, entropies and Lyapunov exponents is considered The processes by which a strange attractor can be created and the evolution of the structure in these attractors will be examined. In Sec. 4.3 a pruned baker map with an incomplete set of periodic orbits is examined. Numerical methods are used to extract these orbits. The effect of pruning on the Cantor set and the associated $f(\alpha)$ spectrum is investigated. Sec. 4.4 is based on a hyperbolic toral map in two and three dimensional space. A understanding of the properties of the unstable manifold allow efficient computation of the dimension spectra. A new type of structure not previously observed in dynamical systems is analyzed. Conclusions are given in Sec. 4.5.

4.2 BAKER MAP

The generalized baker map is defined (Balatoni and Renji, 1956 and Farmer et al., 1983) by the recursion relations on the unit square

$$\begin{pmatrix} X_{i+1} \\ Y_{i+1} \end{pmatrix} = \begin{cases} \begin{pmatrix} R_1 X_i \\ Y_i / S \end{pmatrix} & 0 \leq Y \leq S \\ \begin{pmatrix} 1/2 + R_2 X_i \\ (Y_i - S)/(1-S) \end{pmatrix} & S < Y \leq 1 \end{cases} \tag{4.1}$$

with R_1, $R_2 < 1/2$, $S < 1$. The strange attractor is the closure of the unstable manifolds of the periodic points. The attractor lies along the unstable manifold in the Y direction with the Cantor set in the X direction. This manifold originating from the periodic orbits consists of an infinite number of line segments. This a uniformly hyperbolic system, by uniform we mean the probability density is constant along the unstable manifold. Because of hyperbolicity stable and unstable directions are defined everywhere. Hyperbolic systems are defined through the following definition, we will confine our attention to the plane.

Definition 4.1. Let $F:\mathbb{R}^2 \longrightarrow \mathbb{R}^2$ be continuous and C^r. A set Λ is called a hyperbolic set for F if

1. For each point $p \in \Lambda$, there are a pair of lines $E^s(p)$ and $E^u(p)$ in the tangent plane at p which are preserved by DF(p).
2. $E^s(p)$ and $E^u(p)$ vary continuously with p.
3. There is a constant $\lambda > 1$ such that $|DF(p)(v)| \geq \lambda|v|$ for all $v \in E^u(p)$ and $|DF^{-1}(p)(v)| \geq \lambda|v|$ for all $v \in E^s(p)$.

Roughly speaking the term hyperbolic means that at each point in the domain of the map there is a splitting of the domain into a part which is strongly contracting (the horizontal direction) and a part which is strongly expanding (the vertical direction). This results in an invariant set called a strange attractor.

4.2.1 Relationship of Baker Map to Cantor Set

Using symbolic dynamics Procaccia (1987) with X(X,Y)

=1 for Y>S and X(X,Y)=0 for Y<S, every sequence of 1's and 0's is allowed, and in particular there are 2^n orbits belonging to an unstable orbit of period n. The eigenvalues of the n-cycle depend only on the number of 1's and 0's in the sequence Denoting the number of 0's by m, we have

$$\varepsilon_1^{(n)} = S^{-m}(1-S)^{-(n-m)} , \qquad \varepsilon_2^{(n)} = R_1^m R_2^{(n-m)} \tag{4.2}$$

Using Eq (2.48), which relates the partition function to the stability of the unstable orbits (Grbogi et al., 1987),

$$\Gamma(q,D) = \sum \varepsilon_1^{-q} \varepsilon_2^{-\tau(q)} \tag{4.3}$$

where the sum is over all allowed unstable orbits of period n $\tau(q)$ is defined such that it takes into account the dimension along the unstable manifold

$$\tau(q) = (D_q - 1)(q-1) \tag{4.4}$$

Eq (4 3) can only be used when the probability density is uniform along the unstable manifold. Inserting Eq. (4.2) into Eq. (4 3), gives

$$\Gamma(q,D) = \sum_{m=0}^{n} N_{nm} S^{mq}(1-S)^{(n-m)q} (R_1^m R_2^{(n-m)})^{-\tau(q)} \tag{4.5}$$

where N_{nm} is the number of fixed points of the n times iterated map which belong to periodic orbit with m 0's in its sequence. It can be shown that N_{nm} is the number of ways of arranging m zeros and n-m ones,

$$N_{nm} = \left(\begin{array}{c} n \\ m \end{array} \right) \tag{4.6}$$

Apart from the power $(D_q - 1)$ Eq. (4.5) is equivalent to Eq. (3.14) which was obtained for the two scale cantor set. The parameters S, (1-S), R_1, and R_2 are equivalent to P_1, P_2, l_1, and l_2 of the two scale Cantor set. Three different D_q spectra are shown in Fig. 3.3 (a). Paoli et al. (1989) have observed phase transitions in the D_q spectrum for a hyperbolic baker map with dimension ≥3.

4.2 2 Generalized Entropy Spectrum

The generalized entropies and their Legendre transform

can be defined through the following relationship (Eckmann and Procaccia, 1986),

$$\sum_{m=0}^{n} \binom{n}{m} S^{mq} (1-S)^{(n-m)q} = \exp(-n\,\vartheta(q)) \qquad (4.7)$$

Where $\vartheta(q) = (q-1)K_q = \Lambda q - g(\Lambda)$. In the limit $n \longrightarrow \infty$ the largest term in the sum of the right hand side of Eq. (4.7) should dominate. To find this term it is necessary to solve

$$\frac{\delta}{\delta m} \ln \binom{n}{m} S^{mq} (1-S)^{(n-m)q} = 0 \qquad (4.8)$$

Using Stirling approximation, it is possible to express q as a function of n/m

$$q = \frac{\ln(n/m-1)}{\ln(1-S)-\ln(S)} \qquad (4.9)$$

The density exponent $g(\Lambda)$is determined by

$$\binom{n}{m} = \exp(\, n\, g(\Lambda)\,) \qquad (4.10)$$

where again using Stirling approximation, we find

$$g = \ln(n/m) - (1-m/n)\ln(n/m-1) \qquad (4.11)$$

The exponent determining the singularity in the measure, Λ is determined by

$$S^{mq}(1-S)^{(n-m)q} = \exp(-n\Lambda q) \qquad (4.12)$$

or, alternatively,

$$\Lambda = \frac{m\ln(S) + (n-m)\ln(1-S)}{-n} \qquad (4.13)$$

Thus, for any chosen q, the measure scales as $\Lambda(q)$ on a set of segments which converge to a set of entropy $g(q)$. As q is varied, different regions of the set determine K_q. Fig 4 1 shows $g(\Lambda)$ against Λ for three values of S, namely S=0.2, 0.3 and 0.4. Phase transitions associated with the spectrum of generalized entropies have been studied by Sato and Honda (1990) for some one dimensional systems.

The following relationships can be established between K_q and the generalized partial dimensions $d^{(i)}$, (Eckmann and Rulle, 1985 and Badii and Politi, 1987).

$$K_q = \ln \varepsilon_q^+ d_q^{(1)} = -\ln \varepsilon_q^- d_q^{(2)} \qquad (4.14)$$

where $d^{(1)}$ & $d^{(2)}$ are the partial dimensions of the unstable and stable manifolds respectively, and ε_q^+ & ε_q^- are the generalized eigenvalues of the unstable and stable manifolds respectively. Eq (4.14) can be generalized to more than two dimensions. For the baker map $d_q^{(1)}=1$ for all q, while $d_q^{(2)}$ is the fractional part of D_q.

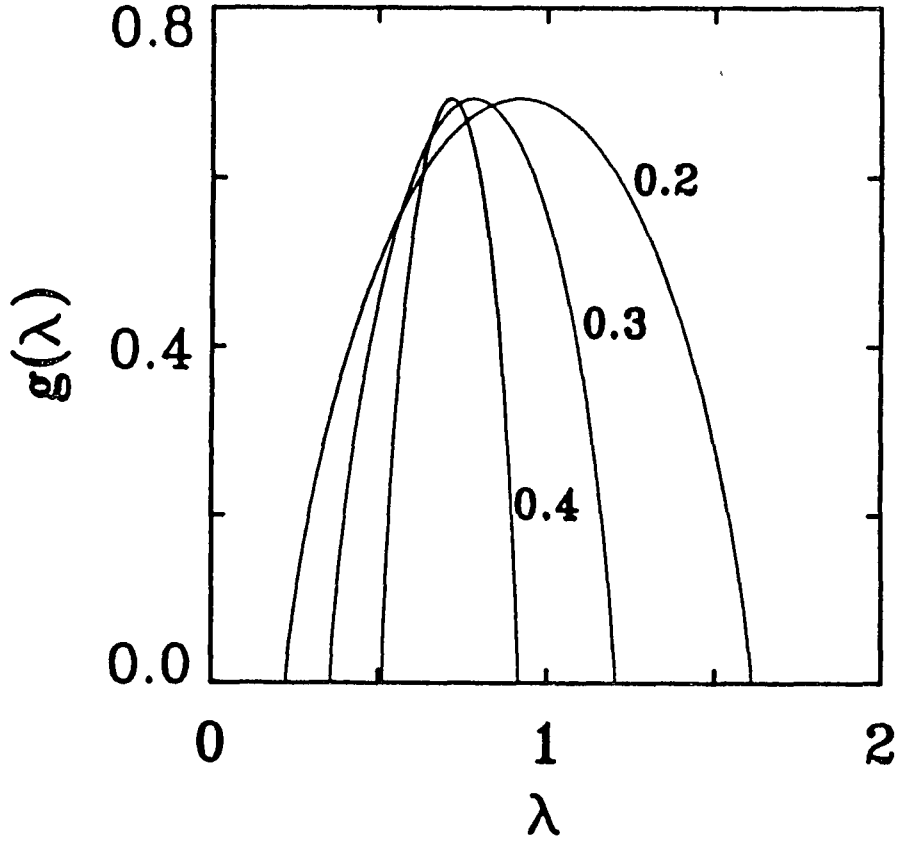

FIG. 4.1. g(ε) for three different values of S=0.2, 0.3 and 0.4. The range of ε extends for fixed S, from -ln(1-S) to -ln(S).

4.2.2 Development of Strange Attractors

The following definition is used to define a strange attractor.

Definition 4.2. Suppose $A \subset \mathbb{R}^n$ is an attractor. Then A is called a strange attractor if

1. There is a trapping region, M, in the phase space $\mathbb{R}^n$.

2. M contains a chaotic invariant Cantor set Λ on which the dynamics are topologically conjugate to a full shift of N symbols
3. The sensitive dependence on initial conditions on Λ extends to A
4. A is topologically transitive on Λ.
5. The periodic orbits are dense in A.

This definition excludes the following from being strange attractors: all one dimensional mappings, conservative systems and non-dissipative systems. The can be proved only for the simplest of systems due to the difficultly of showing that Λ is topologically transitive. A non integer Hausdorff dimension, (greater than one for discrete systems and greater than two for continuous systems), a positive entropy and a Cantor set would be numerical evidence to suggest the existence of a strange attractor.

For S=1/2 and $R=R_1=R_2$ the Lyapunov stability of the n-cycle of Eq (4.1) is denoted by,

$$\lambda_1^{(n)} = \log S^n , \quad \lambda_2^{(n)} = \log |R|^n \tag{4.15}$$

For $R \leq 1/2$ the dimension spectrum D_q is

$$D_q = 1 + \log(S)/\log(|R|) \tag{4.16}$$

The global dimension of the system is equal the dimension of the individual orbits This form of the baker map is equivalent to the uniform Cantor set, examined in section 3.4.2, with a point $f(\alpha)$ spectrum. Four attractors belonging to this map are shown in Fig. 4.2 (a)-(d) for S=1/2 and R= 0.1, 0.3, 0.4, 0.5 respectively. The dimensions D_q are 1 3, 1 58, 1.75 and 2.0 respectively. The first three are examples of strange attractors and are self similar under all scales of magnification.

For all values of R the Grassberger dimension D_2 of the Y time series is $D_2 \approx 1.0$, with entropy $K_2 = \log 2 = 0.7$. In the X direction D_2 is approximately the fractional part D_q, with the same entropy As R is increased from 0 to 0.5

the dimension of the attractor changes from 1.0 to 2.0, while the dimension of the underlining Cantor set changes from 0 to 1.0. The total number of orbits is fixed at 2^n. Let us examine the underline process that is responsible for this increase in dimension.

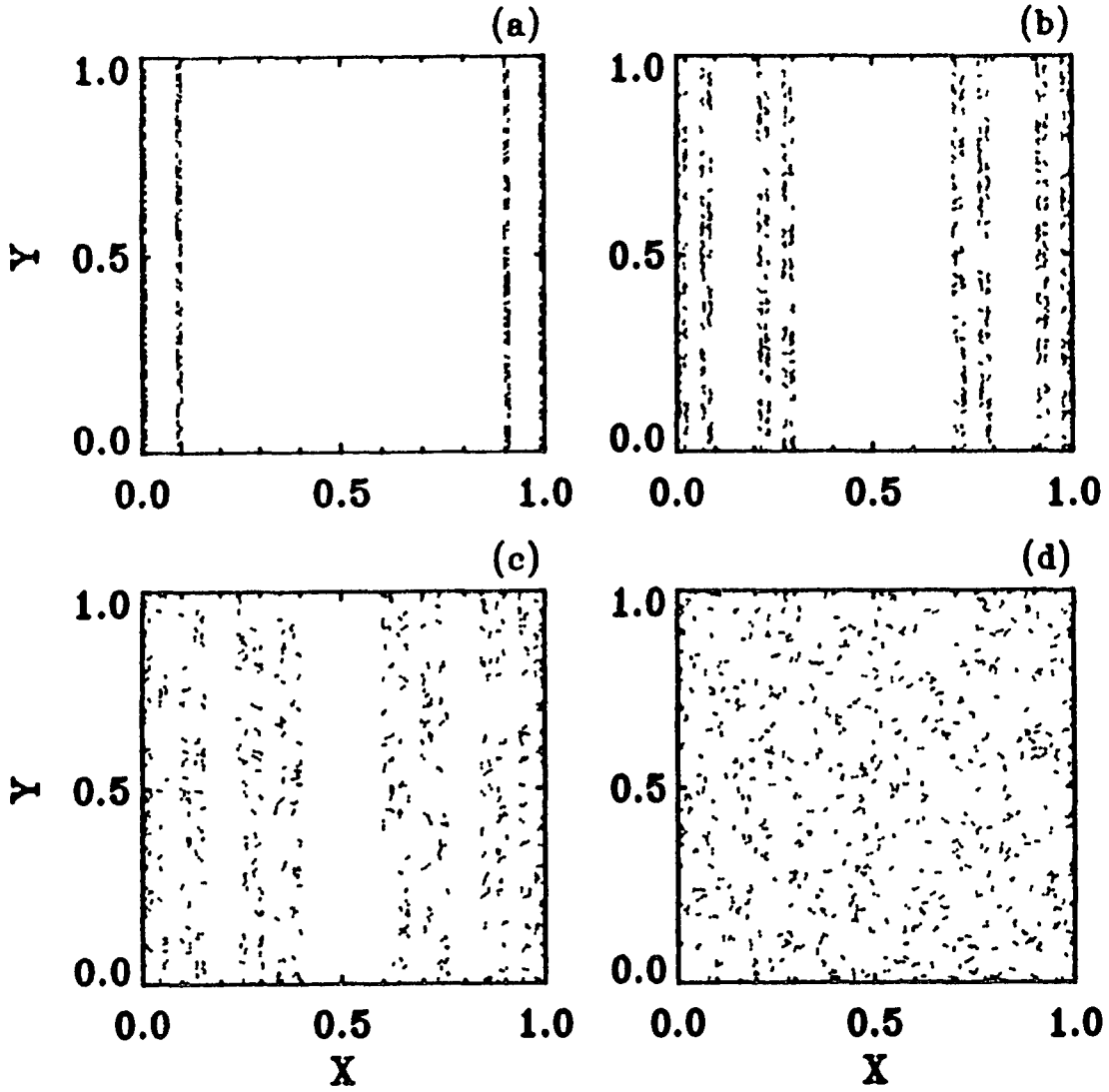

FIG. 4.2. Attractors for the Baker map with S=1/2, (a) R=0.1, (b) R=0.3, (c) R=0.4 and (d) R=0.5. The structure of these attractors is related to the middle third Cantor set.

It is noted from Fig 4.2 that there is a movement of the attractor towards X=0.5. As R is increased the unstable orbits are redistributed causing changes in the structure of the attractor. Since the dimension D_q in the Y direction is constant the increase in dimension and the corresponding

change in structure is related to changes in the Cantor set. The Hausdorff dimension D_0 of a one dimensional unstable manifold is one, therefore the increase in Hausdorff dimension for a two dimensional system is due to changes in the dimension of the Cantor set. This result is true for systems like the non-uniform toral map (Sec. 4.4) and the nonhyperbolic Henon map (Sec. 5.3).

4.3 PRUNED BAKER MAP

Consider the baker map in the following form (Graham and Hamm, 1991),

$$\begin{pmatrix} X_{i+1} \\ Y_{i+1} \end{pmatrix} = \begin{cases} \begin{pmatrix} R_1 X_i \\ T\ Y_i \end{pmatrix} & 0 \leq Y \leq 1/2 \\ \begin{pmatrix} 1-R_2(1-X_i) \\ 1-T\ (1-Y_i) \end{pmatrix} & 1/2 < Y \leq 1 \end{cases} \tag{4.17}$$

with $R_1=0.4$ and $R_2=0.6$ Strange attractors are obtained for $1<T\leq 2$. Strange repellers appear for $T>2$. In this form the number of periodic orbits of period n is dependent on the parameter T. In this section the allowed orbits are extracted and used to determine the $f(\alpha)$ spectrum.

4.3.1 Symbolic Dynamics

Numerical methods are used to obtain the unstable periodic orbits. These orbits are pruned in a systematic way. To display the effects of this pruning the orbits are represented in the symbolic plane where missing blocks correspond to pruned orbits. The symbolic dynamics of Eq. (4.17) are determined from the Y co-ordinate of the map. N_n denotes the total number of orbits of period n obtained numerically, using the techniques described in Sec. (2.6.2). The theoretical number of periodic orbits of period n expected from the universal grammar is T^n. The number of periodic points belonging to periodic orbits of length n in the map are presented in Table 4.1 for four values of T, namely T=1.2, 1.48, 1.8 and 2.0. The smaller

the value of T the slower the convergence of N_n to the theoretical value T^n. An n^{th} order approximate to the topological entropy, K_0, can be calculated from Eq. (2.44) and is given in Table 4.1.

Table 4.1.

The number of periodic points belonging to periodic orbits of length n in the baker map. The third column is the theoretical value expected from the universal grammar. The fourth column is the number of orbits obtained. The last column is the n^{th} order approximate of the topological entropy.

T	Period n	T^n	N_n	$K_0^{(n)}$
1.2	24	80	268	0.2329
	28	164	450	0.2182
	32	341	1020	0.2165
	⋮	⋮	⋮	⋮
	∞	...	...	0.1823
1.48	24	12197	12654	0.3935
	26	26718	27510	0.3932
	27	39542	38736	0.3913
	⋮	⋮	⋮	⋮
	∞	...	...	0.3920
1.8	12	1156	1152	0.5874
	14	3748	3782	0.5884
	18	39346	39314	0.5877
	⋮	⋮	⋮	⋮
	∞	...	...	0.5878
2.0	13	8192	8192	0.6931
	14	16384	16384	0.6931
	15	32768	32768	0.6931
	⋮	⋮	⋮	⋮
	∞	...	...	0.6931

Each orbit has a unique binary label and the periodic points lie on a binary tree. The symbolic sequence of a periodic point of period n has the form $(a_1, a_2, \ldots, a_n)$. The partition is at Y=0.5. The partition defines a_i=0 for a Y less than 0.5 and a_i=1 for Y greater than 0.5. Numerically periodic points have been calculated for periods up to

period 32. Any orbit on the attractor can be represented by a pair of numbers γ and δ called the symbolic plane (Cvitanovic et al., 1988). δ and γ are defined as

$$\delta = 1 - \sum_{k=1}^{\infty} d_k 2^{-k} \quad \text{where } d_k = \sum_{i=1}^{k} (1-a_{-i}) \bmod 2$$

$$\gamma = \sum_{k=1}^{\infty} c_k 2^{-k} \quad \text{where } c_k = \sum_{i=1}^{k} a_i \bmod 2 \tag{4.18}$$

The symbol plane for T=1.48 is shown in Fig. 4.3 (a). Points belonging to periodic orbits of length 26 are plotted. Allowed orbits are represented by blocks in the symbolic plane. In contrast the symbolic plane for T=1.8 is shown in Fig. 4.3 (b), using periodic points belonging to periodic orbits of length 16. A comparison of (a) and (b) shows that the forbidden orbits are represented by cut out rectangles in the symbolic plane. In Table 4.2 the grammar for the forbidden words is given for two values of T=1.2 and 1.4.

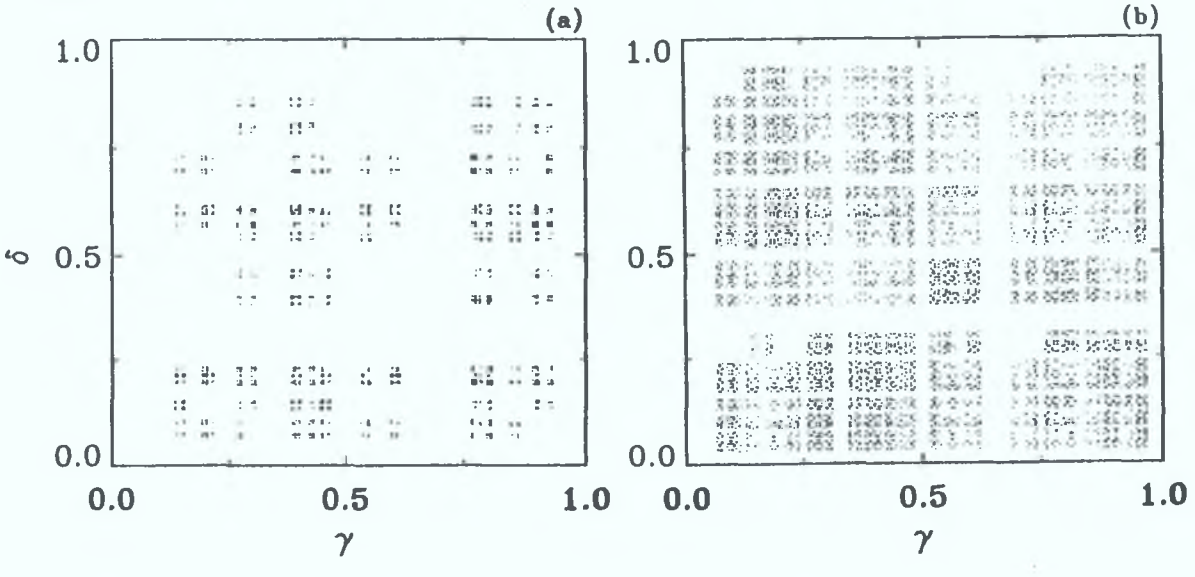

FIG. 4.3. The symbolic plane of the baker map (a) T=1.48, (b) T=1.8.

Shown in Fig. 4.4 is the strange attractor for T=1.48 and T=1.8. The attractor has a uniform probability in the Y direction and in the X direction the stable manifold lies on a pruned Cantor set. In Fig 4.4 we can observe the

effects of an increase in entropy, when the parameter T is increased the number of orbits of period n increases resulting new structure that was not previously present.

Table 4.2.

List of forbidden words in the baker map for T=1.2 and 1.4.

T=1.2		T=1.4	
Period	Forbidden Word	Period	Forbidden Word
3	000	3	000
3	111	3	111
6	100100	6	100100
6	110110	6	110110
7	1010100	9	110010100
7	1101010	10	1010010100
9	110010100	10	1101011010
10	1010010100	12	101010101100
10	1101011010	12	110101010100
10	1011001100	14	101010010101000
12	110100110100	14	110101011010
12	101100101100		

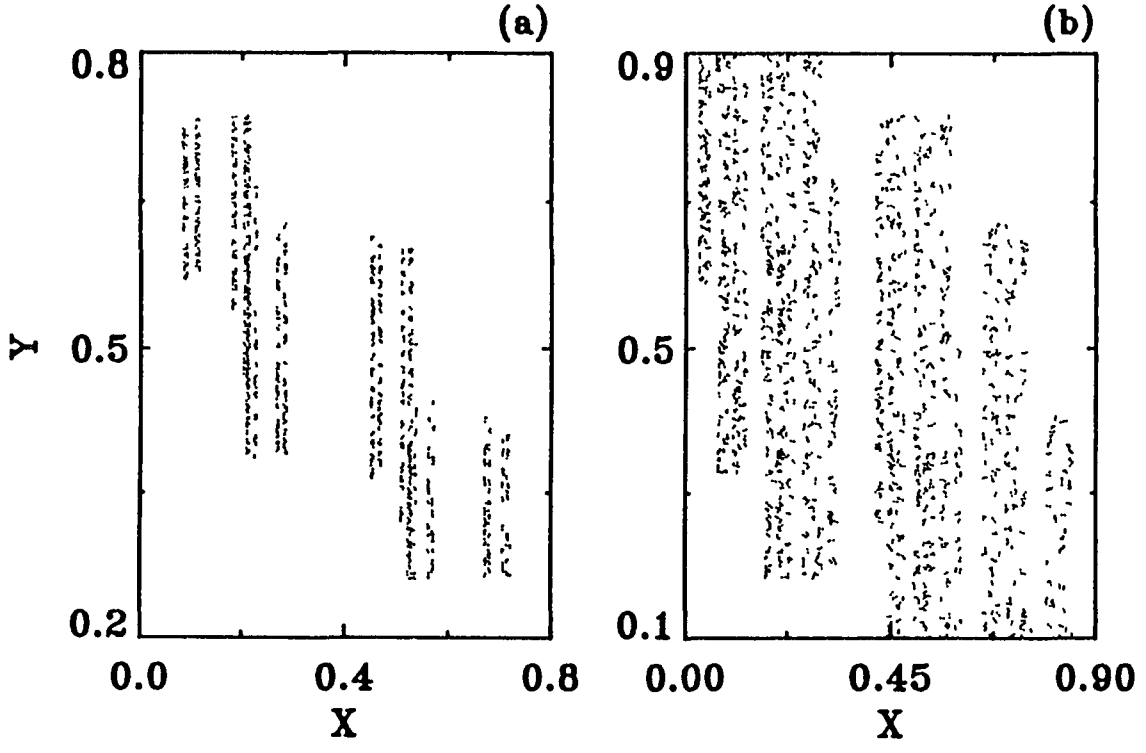

FIG. 4.4. Attractors for the Baker map, (a) T=1.48 and (b) T=1.8.

4.3.2 Pruned Cantor Sets: F(α) Spectrum

The properties of the f(α) spectrum for this pruned Cantor set are investigated for three values of T, namely, T=1.48, 1.8 and 2.0. Two techniques are adopted to calculate the f(α) spectrum. The first uses the analytic equations of Auerbach et al. (1988), however this technique has the draw back that the solution only converges for n large. The second method is to implement Eq. (4.3) numerically In both cases the allowed orbits are numerically calculated.

Auerbach et al (1988) proposed the following equation which relates the stability of the periodic orbits to the scaling exponents,

$$\lambda_1^{(n)}\alpha_1+\lambda_2^{(n)}\alpha_2=0 \qquad (4.19)$$

where α_1 & α_2 are the scaling exponents in the expanding and contracting direction respectively and $\lambda_1^{(n)}$ & $\lambda_2^{(n)}$ are the expanding and contracting Lyapunov exponents of period n. As we have already observed, for uniform hyperbolic attractors the measure is absolutely continuous in the expanding direction, $\alpha_1=1$. Therefore

$$\alpha = \alpha_1+ \alpha_2 = 1 - \lambda_1^{(n)}/ \lambda_2^{(n)} \qquad (4.20)$$

All that remains therefore is to locate the periodic orbits, calculate their stabilities and count how many times the value α falls in an interval of size Δα. The total number is denoted by N(α). The value of f is calculated as follows: The typical length scale $l(\alpha)$ associated with a cycle of order n is $l(\alpha)=\exp(\lambda_2^{(n)})$. If only contribution from lower-order cycles are found, say k<n then $l(\alpha)=\exp(\lambda_2^{(n)}n/k)$. Finally $f(\alpha)=\log N(\alpha)/\log l(\alpha)$, where $f(\alpha)=f(1+\alpha_2)=1+f_2(\alpha_2)$.

The Lyapunov exponents for Eq. (4.17) are

$$\lambda_1^{(n)} = n\ \ln(T)$$
$$\lambda_2^{(n)} = m\ \ln(R_1) + (n-m)\ \ln(R_2) \qquad (4.21)$$

from Eq. (4.20) α is therefore

$$\alpha = 1 - \frac{n\ \ln(T)}{m\ \ln(R_1) + (n-m)\ \ln(R_2)} \qquad (4.22)$$

with $f(\alpha)$ given by

$$f(\alpha) = 1 + \frac{\ln(N_{nm})}{m\ln(R_1) + (n-m)\ln(R_2)} \qquad (4.23)$$

where N_{nm} is the number of orbits of period n with m 0's. For $T<2$, N_{nm} may be zero, whereas for $T=2$ N_{nm} is simply $\binom{n}{m}$. The convergence of the $f(\alpha)$ spectrum (Eq. (4.22) and Eq. (4.23)) can be illustrated for T=2, and n=15, with m=0 to n, as shown in Fig. 4.5. It consists of 16 points represented by diamonds. The converged spectrum is shown by the continuous line. Convergence is obtained in the limit n going to infinity.

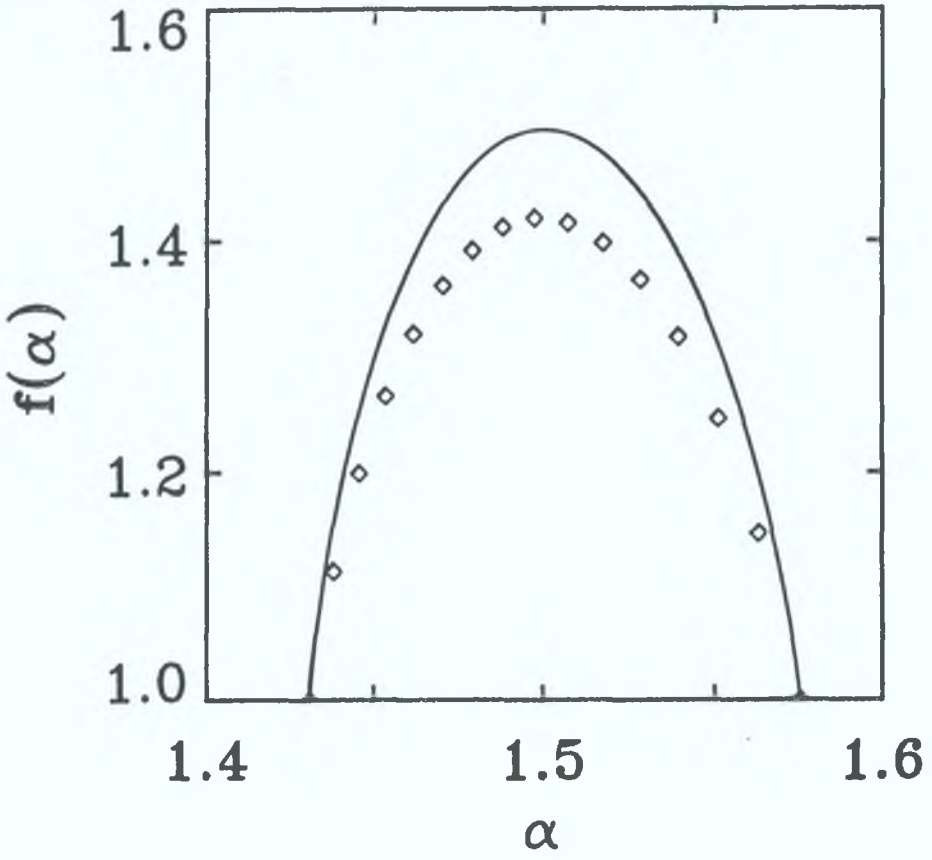

FIG. 4.5. The continuous line is the $f(\alpha)$ function for the baker map Eq. (4.17) for T=2.0. The diamonds correspond to the $f(\alpha)$ function obtained from all unstable orbits of period 15, the spectrum has clearly not converged.

The second method converges for small values of n (Jenkins et al., 1992). Inserting the eigenvalues of Eq. (4.17) into Eq. (4.3) yields

$$\Gamma(q,\tau) = T^{-nq} \sum_{m=0}^{n} N_{nm} \left(R_1^m R_2^{(n-m)}\right)^{-\tau(q)} \qquad (4.24)$$

where the sum includes only the allowed orbits. The number of allowed orbits of period n with m 0's are specified by N_{nm}. The sum over all values of N_{nm} gives the total number of orbits N_n. For T<2 the total number of orbits, N_{nm}, is determined using the procedure in Sec. 2.6.2. For T=1.48 and n=27 the following coefficients were obtained $N_{27,12}$=306, $N_{27,13}$=19062, $N_{27,14}$=19062, $N_{27,15}$=306. For 0≤m<12 and 15<m≤27 the coefficients are zero. The symmetry of this map is reflected in these coefficients. After calculating N_{nm} for a chosen n, $\tau(q)$ is calculated from Eq. (4.24) and then the $f(\alpha)$ spectrum is obtained via the Legendre transform Eq. (2.22). The calculated $f(\alpha)$ spectrum is shown in Fig. 4.6. The calculations converge well, in fact similar results were obtained for orbits of period less than 27. For T=1.8 orbits of period 18 give the

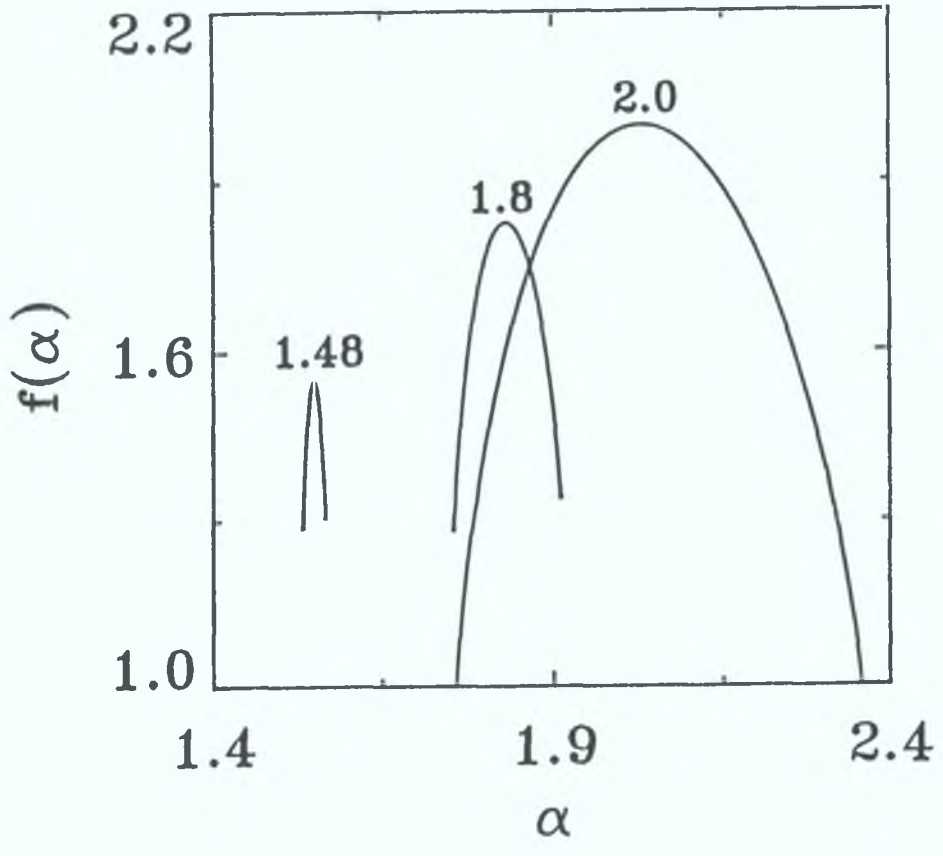

FIG. 4.6. $f(\alpha)$ spectrum of the baker map for the parameters T=1.48, 1.8 and 2.0 and were obtained from unstable orbits of period 27, 18 and 15 respectively.

following coefficients $N_{18,6}=54$, $N_{18,7}=1980$, $N_{18,8}=9720$, $N_{18,9}=15806$, $N_{18,10}=9720$, $N_{18,11}=1980$, $N_{18,12}=54$. For $0\leq m<6$ and $12<m\leq 18$ the coefficients are zero The resulting $f(\alpha)$ spectrum is also shown in Fig. 4 6

For $T\leq 1$ 4 all allowed orbits contribute the same α value to the spectrum which results in a point spectrum. For T=1.48 and 1 8, because of the nature of the pruning, α_{max} and α_{min} correspond to values of f with dimension greater than one The value T=2 corresponds to the $f(\alpha)$ spectrum of the two scale Cantor set. From Eq. (4.24), the Hausdorff dimension D_0 depends indirectly on T through the coefficients N_{nm}, increasing to its maximum value of 2 at T=2. The entropy spectrum is $K_q=\ln T$ for all q.

4 4 HYPERBOLIC TORAL MAP

In this section a completely different class of dynamical system is introduced, the hyperbolic toral maps. One difference between these maps and those that are discussed elsewhere in this thesis, is that these maps are defined on a torus rather than on Euclidean space. Even though the maps are induced by linear maps on Euclidean space the maps on the torus have extremely rich dynamical structure.

Consider the hyperbolic toral map $L_A:T\longrightarrow T$ where

$$A = \begin{pmatrix} a & b \\ c & d \end{pmatrix} \tag{4.25}$$

with a,b,c and d $\in \mathbb{R}$. L_A is clearly differentiable since its Jacobian matrix is simply the matrix A, with det(A)= ad-bc For non-integer coefficients L_A is not a diffeomorphism of T since the inverse is not unique. The eigenvalues are given by

$$\varepsilon_{\pm} = \frac{1}{2}\left[(a+d) \pm \sqrt{(a+d)^2+4bc-4ad} \right] \tag{4.26}$$

and the slope of the eigenvectors is

$$\frac{c}{\varepsilon_{\pm} - d} \tag{4.27}$$

Only real eigenvectors will be considered. When both of the

eigenvalues satisfy $|\varepsilon| < 1$ there is periodic solutions. The transition from periodic to chaotic behaviour corresponds to one of the eigenvalues crossing the unit circle. A periodic orbit of period n has eigenvalue ε^n.

The transformation with integer entries, and determinant 1 has been the subject of many studies (Vavaldi, 1987, Isola, 1990 and Keating, 1991). A typical example is the Arnold cat map, whose matrix A is

$$A = \begin{pmatrix} 2 & 1 \\ 1 & 1 \end{pmatrix} \tag{4.28}$$

This map is an area preserving diffeomorphism with eigenvalues $\varepsilon_{\pm}=\alpha^{\pm 2}$, where $\alpha=(1+\sqrt{5})/2$ is the golden number. Periodic points are dense in T. Let P be any point in T with rational coordinates. P is of the form $[\beta/k,\gamma/k]$, where β, γ and k are integers. Such points are dense in T, for we may take k arbitrarily large. P is periodic with period less than or equal to k^2. For integer coefficients the orbits are positioned on a lattice. Other studies (Amadasi and Casartelli, 1991 and Brambilla and Casartelli, 1985) of Eq (4.25) with non-integer coefficients and determinant 1 have concentrated on the elliptic orbits and the conservative chaos.

This hyperbolic toral system provides an ideal testing ground for some of the theories of chaos because of its simplicity To our knowledge this is the first study of chaotic behaviour in this system for non-integer coefficients and determinant less than one. The analysis of Eq (4.25) will proceed along the following lines: studies of the unstable manifold will illustrate the mechanism for chaos in this system, the development of strange attractors and their dimension spectra and finally the type of structures in a three dimensional toral map are analyzed.

4.4.1 Manifolds

One of the eigenvalues ε_s satisfies $|\varepsilon_s|<1$ and the other ε_u satisfies $|\varepsilon_u|>1$ The stable and unstable subspace W^s and W^u are lines parallel to the eigenvectors corresponding to the eigenvalues ε_s and ε_u. The stable and

unstable subspace W^s and W^u are dense in T for each [x,y] ϵ T. In the previous studies of Eq (4.25) with integer coefficients and with determinant one, it has been suggested that the reason W^s and W^u are dense is because they have irrational slope and hence, these curves wind densely around the torus (Devany, 1986 and Guckenheimer, and Holmes 1983).

In the dissipative case where the determinant is <1, there are strange attractors ($|\varepsilon_u|>1$) and the manifolds have rational slope (Jenkins and Heffernan, 1992). For example the following parameters a=1, b=7/5, c=2/5 and d=0 the unstable subspace has slope 2/7. Therefore, W^s and W^u dose not wind densely around the torus, chaotic behaviour is still present since $|\varepsilon_u|>1$. The subspace are dense in this case because the stable and unstable manifolds emanate from the infinite number of periodic orbits. Each orbit of period n has its own subspace W^s and W^u, which may be degenerate with other orbits of different period. Since the number of orbits is infinite the subspace is dense. The manifold for this system is not continuous but consists of an infinite number of line segments. The parameters a=4/3, b=2, c=1/3 and d=1 also give a strange attractor with subspace of rational slope The eigenvalues are ε_-=1/3 and ε_+=2. The stable subspace has slope -1/2 and the unstable subspace has slope 1/3.

For those attractors where the eigenvector is of rational slope, there is only a finite number of intersections of the stable and the unstable manifolds of distinct fixed points (heteroclinic intersections) or of the same fixed point (homoclinic intersections). As a system parameter evolves the consequences of a finite or a infinite number of homoclinic or heteroclinic intersections is not apparent from the structure or from the dimension. Badii (1989) has indicated that they are the main source of complex behaviour in dynamical systems, the above results do not substantiate this.

This same result concerning the nature of the unstable

manifold could have been determined from the two dimensional baker map Like the baker map the toral map is an another system where the evolution of strange attractors can be investigated without the usual problems of coexisting attractors and periodic windows within the chaotic regime

4.4 2 Development of Strange Attractors

The parameters of the toral map are arbitrary chosen to be A=1.0, B=7/5, D=0 0 with C in the range [0,1/B]. By varying C in this range the Lyapunov dimension of the attractor changes from one to two. Shown in Fig. 4.7 (a)-(d) is the attractor for C=1/5, 2/5, 1/2, 1/B=5/7 respectively. The Lyapunov dimensions of these attractors are 1.14, 1 37, 1.52 and 2.0. Negative initial conditions give rise to a mirror image attractor in the third quadrant. Some orbits of low periodicity are shown in Table 4.3. Note that orbits appear and disappear as the parameter C is increased Except for the fixed point zero the attractor is the closure of these orbits. The total number of orbits of period n for the values C under study is less than 2^n. The dimension of each orbit being equivalent to the Lyapunov dimension of the attractor. The toral map has no homoclinic tangencies so there is no obvious method for constructing a partition that allows identification of the allowed and disallowed orbits.

Table 4.3.

The number of orbits of period n for three different values of the parameter C

C \ n	3	4	5	8	9	10
0 2	–	–	–	1	1	–
0.3	–	1	1	1	2	1
0.4	1	1	–	3	1	3

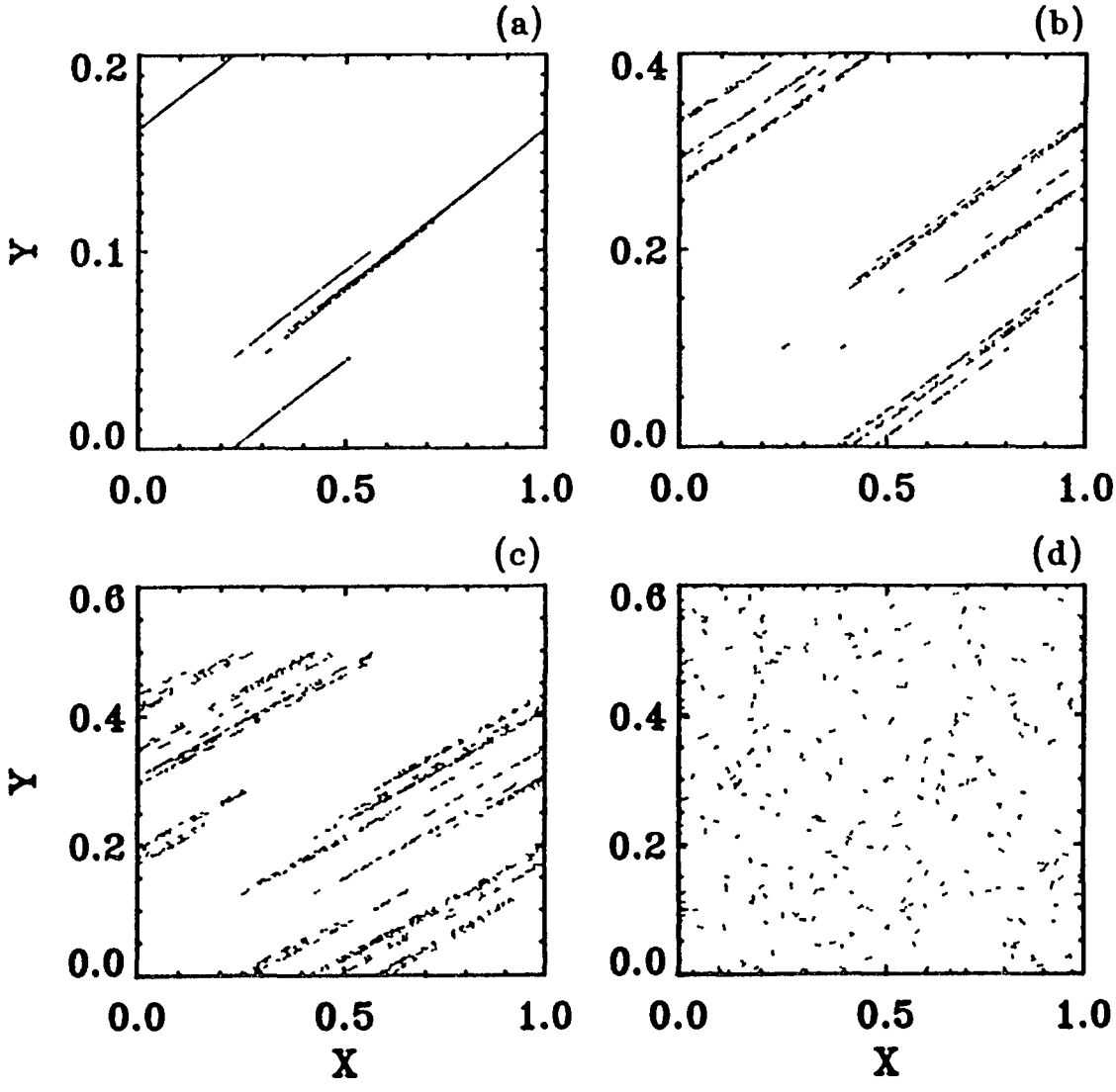

FIG. 4.7. Chaotic attractors for the toral map (a) C=1/5, (b) C=2/5, (c) C=1/2, (d) C=1/B=5/7.

For a hyperbolic attractor, when the measure is uniform in the expanding direction Eq. (4.18)

$$\lambda_1^{(n)}\alpha_1 + \lambda_2^{(n)}\alpha_2 = 0 \qquad (4.29)$$

is sufficient for the calculation of the f(α) spectrum. For the toral map it is incorrect to take $\alpha_1=1$ because the measure does exhibit complicated singularities in the expanding direction as illustrated in Fig. 4.8 for C=2/5. Thus a second equation relating α_1 and α_2 is needed. This relationship has been obtained by Gunaratne and Procaccia (1987) and the validity of it will be checked by applying it to the toral map. This second equation is given as

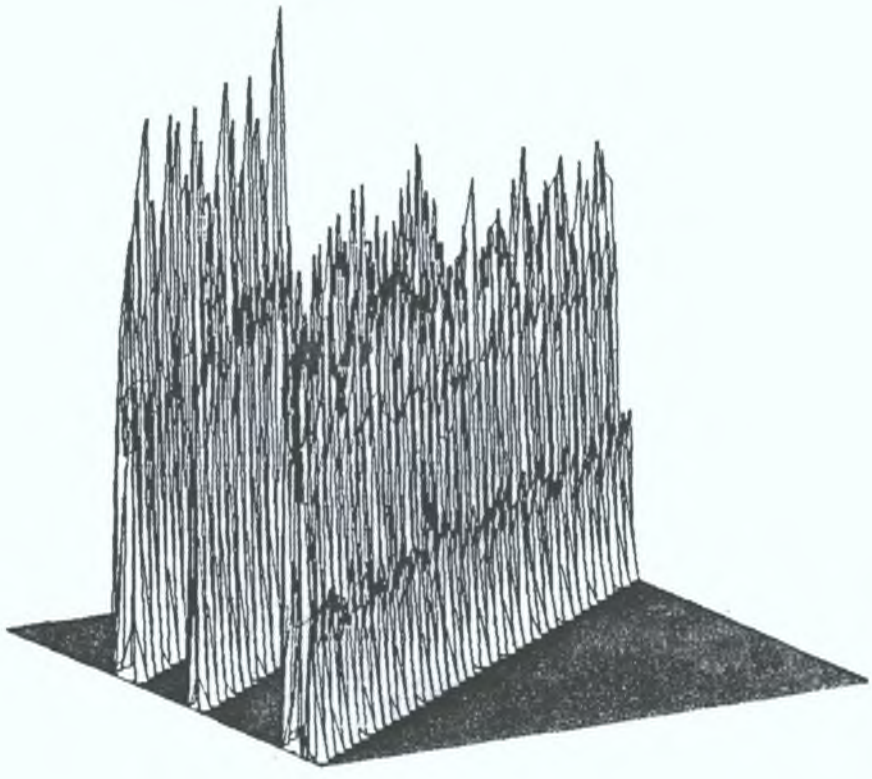

Fig. 4.8. Probability density for C=2/5. Note the non-uniformity of the attractor along the unstable manifold.

$$-\lambda_1^{(n)}\alpha_1 + \lambda_2^{(n)}\alpha_2 = -\lambda_1^{(2n)} \tag{4.30}$$

For the toral map

$$\lambda_1^{(2n)} = 2\lambda_1^{(n)} \tag{4.31}$$

but in general this relationship is not true as is the case for the Henon map. Inserting Eq. (4.31) into Eq. (4.30) we again find that $\alpha_1=1$. Hence this new relationship does not take into account the singularities along the unstable manifold. Eq. (4.29)-(4.31) indicate that the D_q spectrum is constant with a point $f(\alpha)$ spectrum. For the one dimensional version of this toral map (Eq. (3.1)) it has already been shown that non-uniformities along the unstable manifold lead to a nonconstant D_q spectrum.

A computation of the spectrum of dimensions D_q has been undertaken for this map. The results are presented in Fig. 4.9 for the parameter C=2/5. The time series consisted of $N=4*10^5$ data points using an embedding dimension of d=10. The attractor in Fig. 4.7 (b) was rotated through the angle α=-0.33906 rads, so that the

unstable manifold is parallel to the X axis. X′ and Y′ correspond to the rotated time series. The spread in the dimensions for positive q, where q ∈ (0,20), is quite small, i.e. D_q ∈ (1.301–1.325) for X, D_q ∈ (1.318–1.336) for X′ and D_q ∈ (0.375–0.380) for Y′, with errors of ±0.015, 0.015 and 0.008 respectively. These dimensions should be compared to the Lyapunov dimension D_L=1.367. The dimensions calculated form the time series Y′ are reduced by one approximately, which would indicate that the associated Cantor set has been decoupled from the unstable manifold. The rotated X′ time series gives similar dimension results to that of the nonrotated time series X. A surprising result that does not satisfy Eq. (4.14) for the partial dimensions. The expected dimensions form X′ time series is $D_q \approx 1.0$.

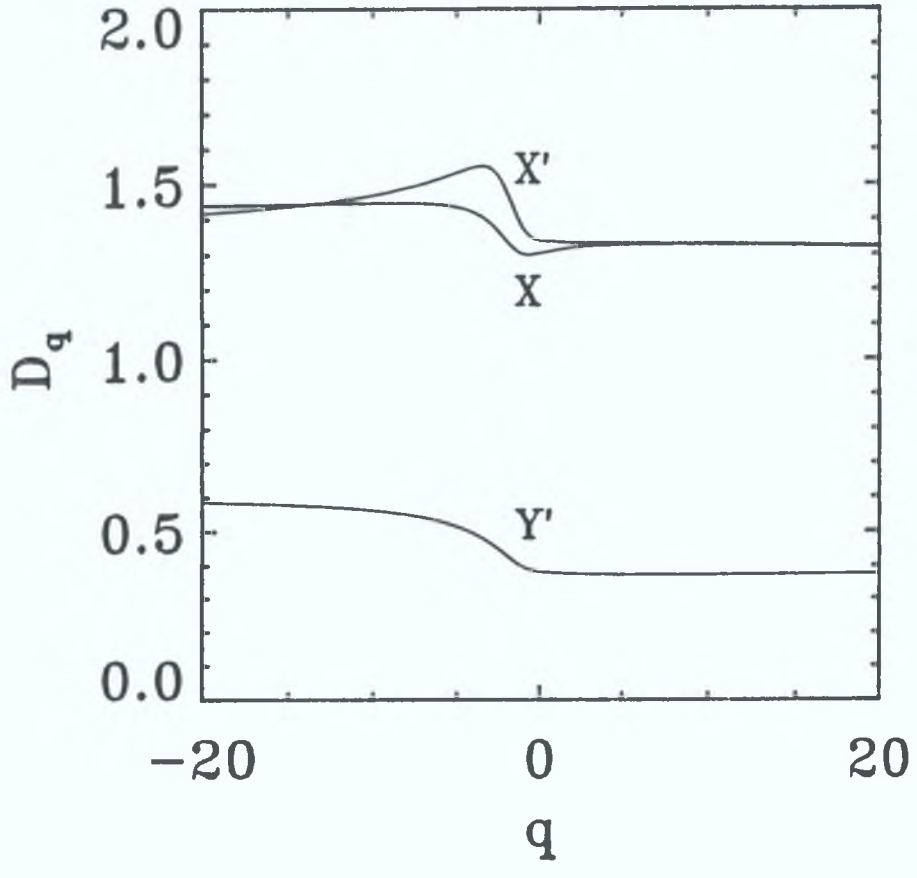

FIG. 4.9. The D_q spectrum for C=2/5 with N=4*10^5 data points. The results for three different time series are shown. X′ and Y′ correspond to rotated time series.

From Eq (2 21) the $f(\alpha)$ spectrum satisfies the conditions $df/d\alpha = q$ and $d^2f/d^2\alpha < 0$. These two conditions make $D_{q'} > D_q$ for $q' < q$, it is obvious from Fig. 4.9 that this is not true for the negative regions of the spectra computed from X' and X time series. Hence the dimensions for negative q are inaccurate, but included for completeness. The essential result is that the fluctuations along the unstable manifold have only a minor effect on the dimensions D_q with D_q approximately constant for positive q indicating a point $f(\alpha)$ spectrum. Similar calculations have been carried out for C=1/5 and 1/2, with D_q in close agreement with D_L.

4.4.3 Structure of Attractor in Three Dimensional Toral Map

The purpose of this section is to examine the possible structures that can exist in $\mathbb{R}^3$ for discrete systems. A new types of structure not previously observed in dynamical systems is analyzed. Consider the hyperbolic toral map. $L_B : T \longrightarrow T$

$$B = \begin{pmatrix} a & b & c \\ d & e & f \\ g & h & i \end{pmatrix} \qquad (4.32)$$

were the parameters of this matrix are $\in \mathbb{R}$. Being able to locate the unstable manifold is an important property that will be made use off in this section. The eigenvalues ε_i of the matrix B will be chosen together with six of the parameters. The other three will be obtained by solving three simultaneous equations The Lyapunov exponents are defined by $\lambda_i = \ln|\varepsilon_i|$ and are ordered as follows $\lambda_1 > 0 > \lambda_2 \geq \lambda_3$. The six parameters pre-selected are b=1 c=1/4, e=0, f=1/5, g=0, h=1 and shown in Table 4.4 are the chosen eigenvalues and the resulting parameters a, d and i obtained from the solution of a set of simultaneous equations.

The eigenvector corresponding to the eigenvalue $\varepsilon_1 = 1.4$ is rotated with the following matrix.

$$\begin{pmatrix} X' \\ Y' \\ Z' \end{pmatrix} = \begin{pmatrix} \mathrm{Cos}(\beta)\mathrm{Cos}(\alpha) & -\mathrm{Cos}(\beta)\mathrm{Sin}(\alpha) & -\mathrm{Sin}(\beta) \\ \mathrm{Sin}(\alpha) & \mathrm{Cos}(\alpha) & 0 \\ \mathrm{Sin}(\beta)\mathrm{Cos}(\alpha) & \mathrm{Sin}(\beta)\mathrm{Sin}(\alpha) & \mathrm{Cos}(\beta) \end{pmatrix} \begin{pmatrix} X \\ Y \\ Z \end{pmatrix} \quad (4.33)$$

This rotation aligns the unstable direction parallel to the X axis. The rotation angles α and β are given in Table 4.4. Coordinates X', Y'and Z' describe the rotated frame.

Table 4.4

The parameter values a, d and 1 for the chosen eigenvalues ε_1, ε_2 and ε_3 obtained from solving a set of simultaneous equations, with ε_1=1 4 When the attractor is rotated α and β are the angles used in Eq. (4.33), they are given in radians.

ε_2	ε_3	a	d	1	α	β
0.5	-0.5	1.51680	-0.12716	-0.11679	0.09993	0.06568
0.7	-0.7	1.82191	-0 47867	-0 42190	0.35526	0.18864
0 8	-0 8	1.95000	-0.63250	-0.55000	0.45360	0.22105
0.5	0.5	0 97185	-0.46205	1 42815	0.05428	-1.09213
0.7	-0.1	0.72471	-0.04578	1.27523	-0.22108	-1.05369
1.2	0.4	1.37155	-0.68650	1 62845	0.39068	-0.72664

The types of structures that will be observed depends on the sign and magnitude of the eigenvalues and hence, the angles between the three eigenvectors. The first case considered is $\varepsilon_2 = -\varepsilon_3$ with Lyapunov dimension $D_L=1-\lambda_1/\lambda_2$ and by varying the magnitude of λ_2 in the range $(-\infty, -\lambda_1/2)$ this dimension changes from 1-3. Figure 4.10 illustrates the type of structure obtained when two contracting directions compete in the formation of a strange attractor. For eigenvalues ε_2=0 5 and ε_3=-0.5, the rotation angles α and β are given in Table 4.4, with the attractor shown in Fig 4 10 (a), for a projection onto the Y'-Z' plane. This attractor has a two dimensional Cantor set structure when viewed in this plane with dimension D_L=1.485. A rotation and a projection onto the X'-Z' plane is shown in Fig. 4.10

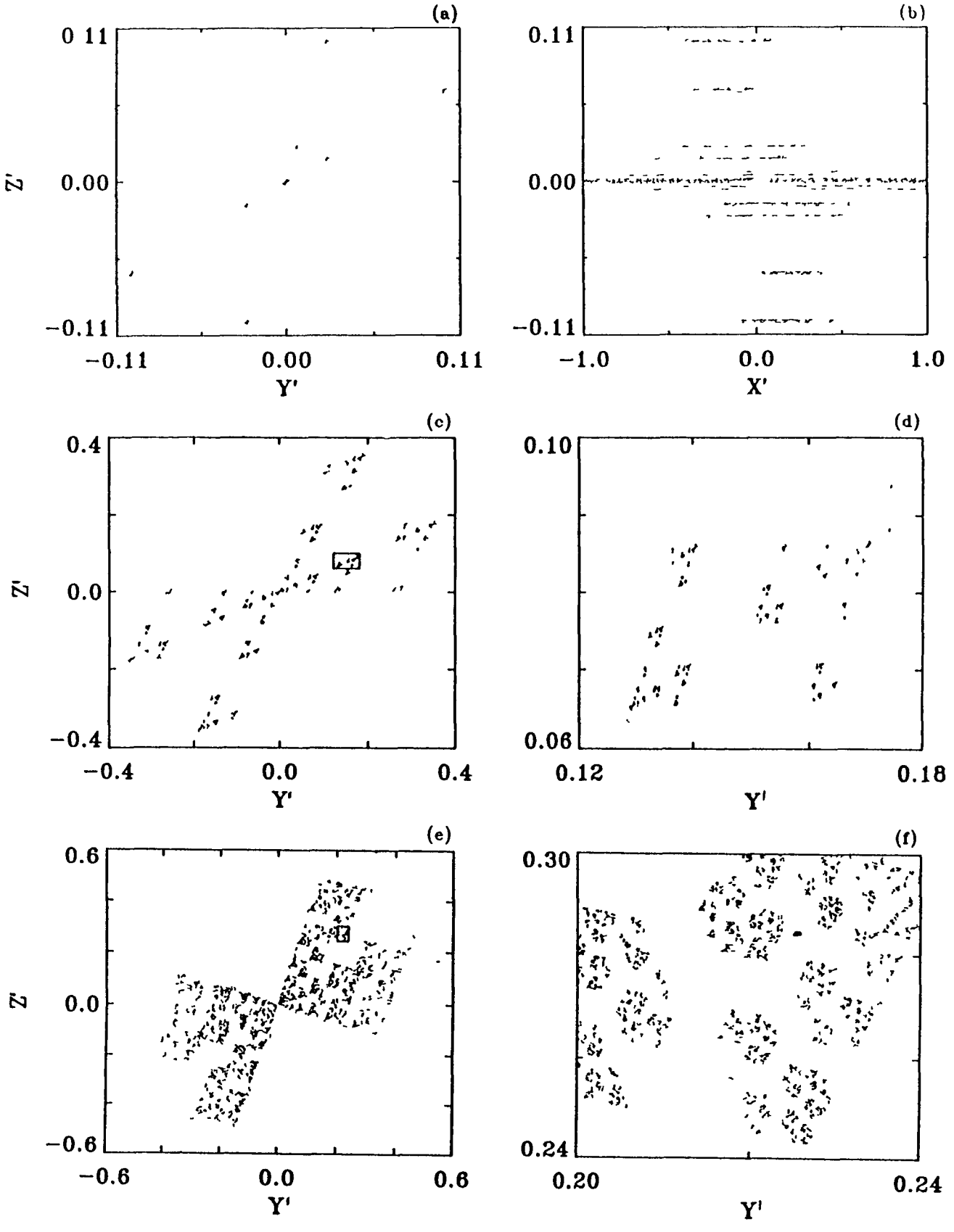

Fig. 4.10. Three attractors for Eq. (4.32). (a) A projection onto the Y′–Z′, with $\varepsilon_2=-\varepsilon_3=0.5$ and (b) a projection onto the X′–Z′ plane. (c) Y′–Z′ plane, with $\varepsilon_2=-\varepsilon_3=0.7$ and (d) a magnification of (c). (e) Y′–Z′ plane, with $\varepsilon =-\varepsilon =-0.8$, and (f) a magnification of (e).

(b), successive magnifications indicate a one dimensional Cantor set. The computation of the correlation dimension from the three rotated time series produced the following results; D_2=1.46±0.03 for the X′ time series and D_2=0.47±0.02 for Y′ and Z′ time series. The same results were obtained for the two dimensional case in the previous section. Shown in Fig. 4.10 (c) is the attractor in the Y′–Z′ plane for ε_2=0.7 and ε_3=–0.7, with a magnification of the indicated region shown in (d). The structure of the attractor is a two dimensional Cantor set when viewed perpendicular to the unstable manifold and a one dimensional Cantor set when viewed parallel to the unstable manifold The dimension of this structure is D_L=1.94. Similar plots are shown in (e) and (f) for ε_2=0.8 and ε_3=–0.8. The dimension is D_L=2.508 and there is a notable filling of phase space.

An optimum separation of eigenvectors is obtained when ε_2=–ε_3. For each of the three figures above the eigenvectors have sign {+,–,–} for ε_1, {+,–,–} for ε_2 and {+,–,+} for ε_3. When the eigenvectors associated with ε_2 and ε_3 are parallel, then the two dimensional structure is not present as is illustrated in Fig. 4.11 (a) for ε_2=0.5 and ε_3=0.5. The projection onto the Y′–Z′ plane has a one

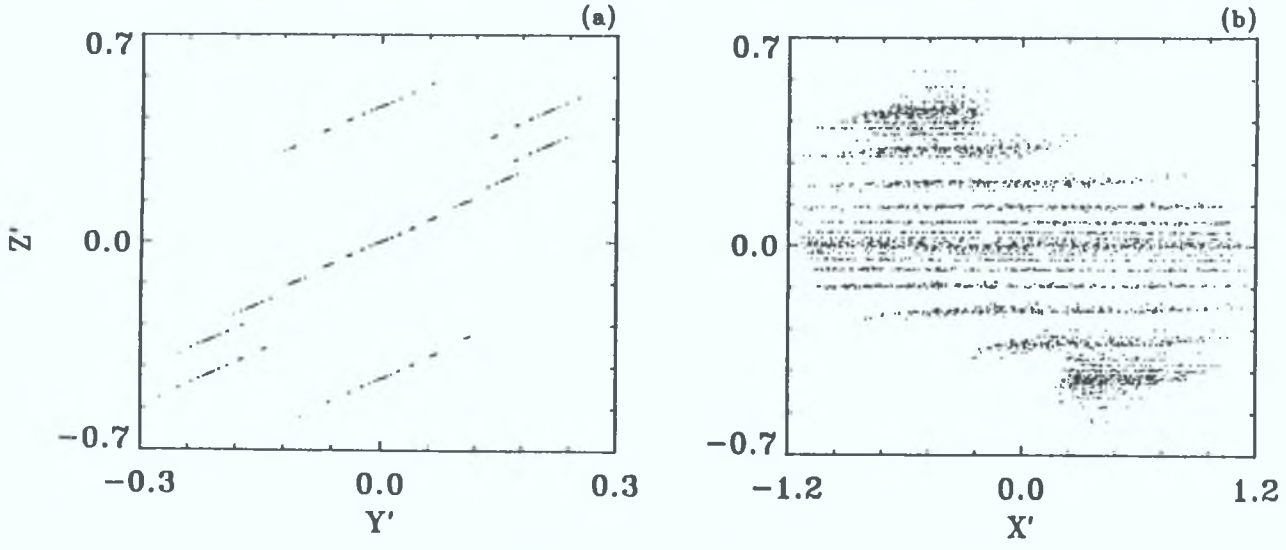

Fig. 4.11. The 3D toral map, with ε_2=0.5 and ε_3=0.5. (a) A projection onto the Y′–Z′ plane, (b) X′–Z′ plane.

dimensional structure, while the projection onto the X'-Z' plane in (b) has properties of a one dimensional Cantor set. For ε_2=0.7 and ε_3=-0.1, the projection of the attractor onto the Y'-Z' plane is shown in Fig. 4 12 (a). This attractor appears to be one dimensional, successive magnifications do not reveal a two dimensional structure. The Lyapunov dimension is D_L=1.94, there is nearly a complete filling of the surface in (b). In both cases the two dimensional Cantor set is not present. These examples illustrate how the magnitude of the eigenvalues and the direction of the eigenvectors can produce dramatic effects on the structure of the attractor.

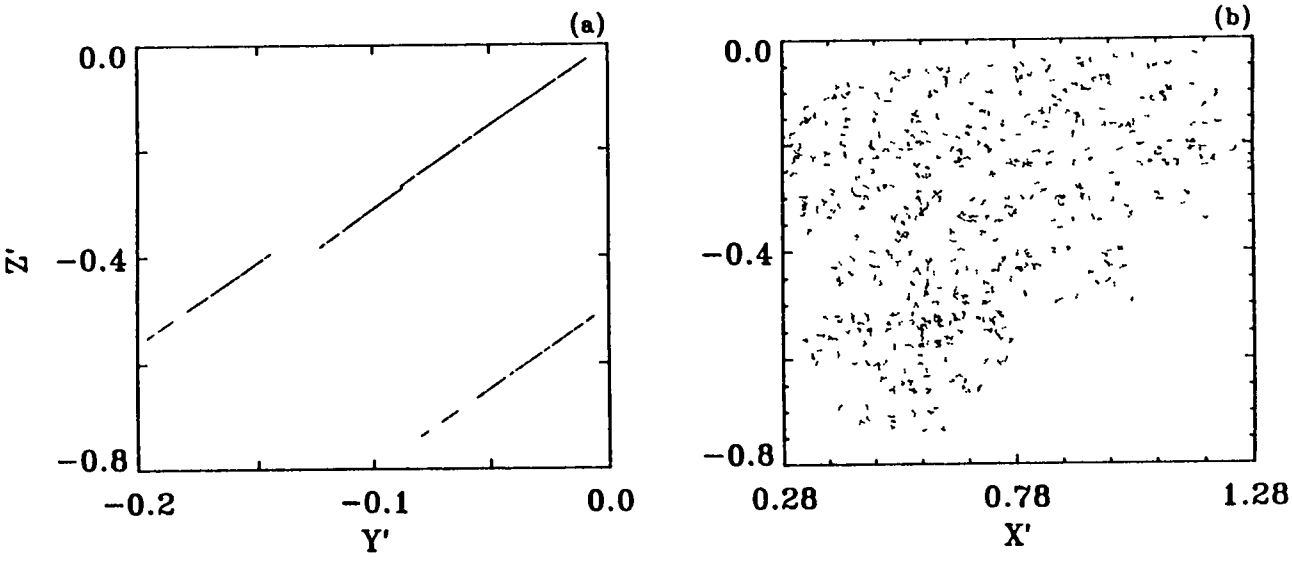

Fig. 4.12. The 3D toral map, with ε_2=0.7 and ε_3=-0.1. (a) A projection onto the Y'-Z' plane, (b) X'-Z' plane.

As a final example an attractor with the following eigenvalues ε_1=1.4, ε_2=1.2 and ε_3=0.4 is considered, with dimension D_L=2.566. At each point in phase space there is expansion in two directions. A visualization of the Cantor set involves taking slices through the attractor. Shown in Fig. 4.13 (a) is the attractor for a rotation by the angles given in Table 4.4, Y'-Z' is plotted when X' is an element of (-0.001,0.001). The Cantor structure can be clearly seen from the magnification shown in (b).

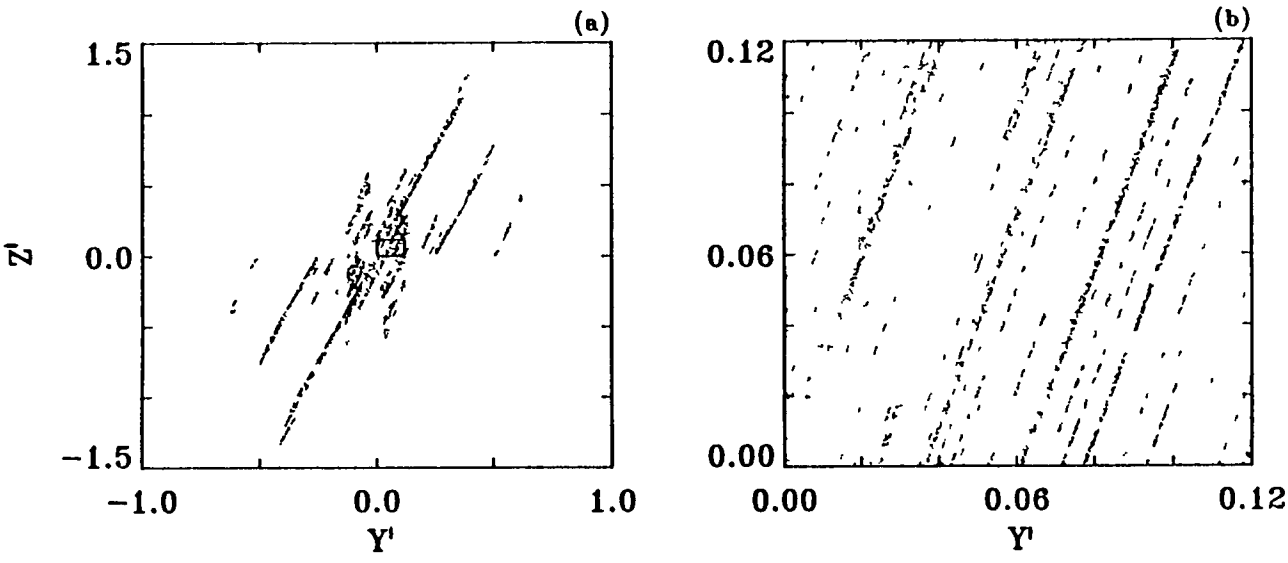

Fig. 4.13. The attractor of Eq. (4.32). (a) Y′-Z′ plane, with ε_2=1.2 and ε_3=0.4, and (b) a magnification of (a).

4.5 CONCLUSION

The local structure of the hyperbolic baker attractor is the product of a line and a Cantor set. The evolution of structure in the baker map is directly related to this Cantor set. It was established that the increase in the Hausdorff dimension D_o is due to changes in the distribution of the unstable periodic orbits. A baker map with an incomplete set of orbits corresponds to a pruned Cantor set. The $f(\alpha)$ spectrum of these pruned Cantor sets have two properties different from normal Cantor sets: one, the maximum of the $f(\alpha)$ spectrum is affected by the degree of pruning and, two, the wings of the spectrum converge not to one but to a set of dimensions greater than one. In the absence of theoretical guidance, the intrinsic properties of the curves would be hardly distinguishable from numerical artifacts. The increase in Hausdorff dimension D_o is due to changes in the structure of the Cantor set, we feel that this is true for typical non-hyperbolic chaotic systems of dimension less than two.

Furthermore, it was shown that the unstable manifold of a hyperbolic toral map does not wind densely around the

torus, but consists of an infinite number of line segments. This leads to the efficient computation of the dimension spectrum D_q through a rotation of this manifold with the result that the spectrum D_q, for $q>0$ is approximately constant. By analyzing a three dimensional toral map it has been shown that whenever two contracting directions compete in the formation of a strange attractor a two dimensional Cantor set structure is to be expected. This structure was obtained from a optimum choice of the eigenvalues.

CHAPTER 5

NON-HYPERBOLIC SYSTEMS AND INTERMITTENCY

5.1 INTRODUCTION

The main theme of this chapter is intermittency in non-hyperbolic systems, also of importance is the study of surface attractors, evolution of structure, dimensions and unstable periodic orbits for this type of system. The term "intermittent crisis" is used primarily to describe sudden changes in a chaotic attractor as a system parameter is varied It has been shown that a good agreement exists between numerical results and a quantitative theory, put forward by Grebogi et al. (1987), for a broad class of low dimensional dissipative systems. The main purpose of this chapter is to investigate the applications of this theory to crises in non-dissipative systems and to investigate the properties of the chaotic attractors for these systems. Statistical behaviour near each crisis is investigated, leading to the analysis of a new type of intermittency that is present in both dissipative and non-dissipative systems.

In Sec. 5.2, the theory of intermittency formulated by Grebogi et al. (1987) is reviewed. The relationship between the critical exponent, γ, and the eigenvalues of an unstable periodic orbit are given for both the heteroclinic and homoclinic tangency. In Sec. 5.3. we discuss the chaotic behaviour of the Henon map. The gradual merging of a two piece attractor into a one piece attractor is explained in terms of the unstable orbits on the attractor. A three dimensional version of the Henon map is given which has a chaotic attractor of dimension greater than two and exhibits an intermittent crisis. In Sections 5.4 - 5.6 an

in depth study is carried out for three different non dissipative mappings. A detailed knowledge of the location of the stable and unstable manifolds of the periodic orbit that collides with the attractor allows both an identification of the type of crisis and a comparison with existing theory. The properties of the chaotic attractors in these systems are examined, together with their evolution. In Sec. 5.7 the symbolic dynamics are examined for a non-dissipative attractor.

5.2 THEORY OF INTERMITTENCY

In dynamical systems, as a system parameter is varied, it is not unusual to encounter sudden changes in a chaotic attractor. The term crisis induced intermittency is used to characterize the temporal behaviour which occurs due to the switching between two (or more) chaotic attractors. This term has also been used to describe the sudden destruction of a chaotic attractor (Grebogi[b] et al., 1986). Crisis can be represented as follows:

$$(\text{chaos}_1) \longrightarrow (\text{chaos}_2) \longrightarrow (\text{chaos}_1) \longrightarrow (\text{chaos}_2) \longrightarrow \text{---------}$$

where chaos_1 and chaos_2 represent chaotic attractors in different regions of phase space and usually of different dimensions. This type of intermittency is to be contrasted with that type of intermittency discussed by Pomeau and Manneville (1980).

$$(\text{chaos}) \longrightarrow (\text{approx. peri.}) \longrightarrow (\text{chaos}) \longrightarrow (\text{approx. peri.}) \longrightarrow \text{---}$$

An example of this latter type will be discussed in Sec. 5.6.1.

Let A denote a relevant system parameter, and let A_c denote the value of A at the crisis, with the intermittency occurring as A increases through A_c. For A less than A_c, there is chaos_1, while for A greater than A_c there is chaos_1 and chaos_2. The temporal dependence of the system can be characterized by a time , τ, which is the average duration spent on the chaos_1 attractor. For a large class

of systems with a crisis the dependence of τ on a system parameter, A, is

$$\tau \approx (A-A_c)^{-\gamma} \tag{5.1}$$

γ is called the critical exponent. For a successful estimate of γ it may be necessary to calculate the critical value A_c to eight decimal places.

A quantitative theory has been developed by Grebogi et al. (1987) for the determination γ for a broad class of low dimensional dissipative systems. In particular, they consider two dimensional maps for which the crisis is due to a tangency of the stable manifold of an unstable periodic orbit with the unstable manifold of another or the same periodic orbit, and are defined as follows

(i) Heteroclinic tangency The stable manifold of an unstable periodic orbit (B) is tangent to the unstable manifold of an unstable periodic orbit (C) on the attractor.

(ii) Homoclinic tangency. The stable and unstable manifolds of an unstable periodic orbit are tangent.

The critical exponent obeys two distinct formulas depending on the type of tangency. The following equations apply to two dimensional discrete systems are three dimensional continuous systems. In the case of a heteroclinic crisis, we have

$$\gamma = \frac{1}{2} - \ln|\alpha_1| \; / \; \ln|\alpha_2| \tag{5.2}$$

where α_1 and α_2 are the expanding ($|\alpha_1| > 1$) and contracting ($|\alpha_2| < 1$) eigenvalues, respectively, of the periodic orbit C. In terms of Lyapunov exponents Eq. (5.2) gives

$$\gamma = \frac{1}{2} - \lambda_1/\lambda_2 \tag{5.3}$$

It is obvious that γ is related to the Lyapunov dimension D_L by

$$\gamma = D_L - \frac{1}{2} \tag{5.4}$$

In the case of a homoclinic crisis

$$\gamma = \ln|\beta_2| \; / \; \ln|\beta_1\beta_2|^2 \tag{5.5}$$

where β_1 and β_2 are the expanding and contracting

eigenvalues of the periodic orbit. In terms of Lyapunov exponents Eq. (5.5) gives

$$\gamma = \lambda_2 / 2 (\lambda_1+\lambda_2) \qquad (5.6)$$

In terms of D_L

$$\gamma = \frac{-1}{2D_L-4} \qquad (5.7)$$

For strictly dissipative maps $|\alpha_1\alpha_2|<1$. For the heteroclinic case γ lies in the range $1/2 \leq\gamma\leq 3/2$, with $\gamma\longrightarrow 3/2$ as $|\alpha_1\alpha_2|\longrightarrow 1$. For the homoclinic case γ lies in the range $1/2 \leq\gamma\leq \infty$, with $\gamma\longrightarrow\infty$ as $|\beta_1\beta_2|\longrightarrow 1$. Larger values of γ correspond to long chaotic transients which tend to persist over larger parameter ranges.

For two dimensional maps that are strictly dissipative these two types of crisis appear to be the only kinds of crisis which can occur. Experimental observations of chaotic bursting in a fluid have been reported by Metcalfe and Behringer (1992). The results of this experiment agree with the scaling given by Eq. (5.1).The existence of a spectrum of critical exponents related to a spectrum of generalized dimensions D_q might be inferred from Eq. (5.4) and Eq. (5.7) In the following parts of this chapter, the application of Eq. (5.3) and Eq. (5.6) to non dissipative systems will be considered.

5.3 HENON MAP

In what follows, a brief account is given of one of the most extensively studied attractors; the Henon attractor. The Henon map (Henon, 1976) still motivates research despite being one of the simplest discrete systems that exhibits chaotic behaviour but the understanding of its dynamics is still incomplete. Previous studies have included: Chaotic transients / intermittency (Grebogi[b] et al., 1986), fractal basin boundaries (Grebogi[a] et al., 1986 and Alligood and Yorke, 1989), coexisting attractors with fractal basins of attraction (Grebogi et al., 1983), period

doubling bifurcations (Derrida et al., 1979), Cantor sets (Henon, 1976), and f(α) spectra (Gunaratne and Procaccia, 1987).

The Henon map $H_{A,B}:\mathbb{R}^2 \longrightarrow \mathbb{R}^2$ is given by

$$\begin{aligned} X_{i+1} &= 1 + Y_i - AX_i^2 \\ Y_{i+1} &= BX_i \end{aligned} \tag{5.8}$$

where A and B are parameters. The Jacobian is defined by

$$DH\begin{pmatrix} X \\ Y \end{pmatrix} = \begin{pmatrix} -2AX & 1 \\ B & 0 \end{pmatrix} \tag{5.9}$$

The symbol DH denotes the matrix of partial derivatives of H. Note that det(DH)=-B, thus the Jacobian determinant is constant and independent of X and Y. The mapping H is a diffeomorphism of $\mathbb{R}^2$ as long as B≠0. A mapping is a diffeomorphism if it is one-one, onto, C^∞, and its inverse is also C^∞. The inverse mapping $H_{a,b}^{-1}$ is given by

$$\begin{aligned} X_{i+1} &= Y_i/a \\ Y_{i+1} &= X_i - 1 + aY_i^2/b^2 \end{aligned} \tag{5.10}$$

For $0 < B \leq 1$ there exist an a & b with $b > 1$ such that $H_{A,B}$ is topologically conjugate to $H_{a,b}^{-1}$ i.e.

$$H_{A,B} \circ R = R \circ H_{a,b}^{-1} \tag{5.11}$$

The linear homeomorphism R is given by

$$\begin{aligned} X &= -Y \\ Y &= -X \end{aligned} \tag{5.12}$$

Mappings which are topologically conjugate are completely equivalent in terms of their dynamics. In fact the mapping $H_{A,B}$ is equivalent to the inverse mapping $H_{a,b}^{-1}$ for

$$B = \frac{1}{b} \quad , \quad A = \frac{a}{b^2} \tag{5.13}$$

One may easily check that orbits of $H_{A,B}$ go over via R to orbits of $H_{a,b}^{-1}$.

The fixed points of the mapping $H_{A,B}$ are given by

$$(X_{1,2}, Y_{1,2}) = \left(\frac{(B-1) \pm \sqrt{((B-1)^2+4A)}}{2A} \, , B\, X_{1,2} \right) \tag{5.14}$$

The eigenvalues of these two fixed points are

$$\varepsilon_{1,2} = -AX \pm \sqrt{(AX^2+B)} \tag{5.15}$$

For B=0 3 the fixed point (X_2,Y_2) is a saddle point for every value of A. The other fixed point is asymptotically stable for A<0.3675 where a flip into a period 2 orbit occurs. A period doubling cascade occurs for increasing A. Derrida et al. (1979) has verified that the cascade converges to the universal Feigenbaum numbers γ and δ. The Henon map which is nonhyperbolic has of yet not being proved to be a strange attractor, but extensive numerical investigation suggests the existence of a strange attractor. In particular Benedicks and Carleson (1991) prove that the attractor is the closure of the unstable manifold. The fact that a trajectory is dense on the unstable manifold excludes the existence of stable periodic orbits. Unfortunately, neither the theorem nor its proof produces any explicit parameter values for which the Henon map is chaotic. A hyperbolic piecewise linear version of the Henon map was proposed by Lozi (1978) and Misiurewicz (1980) was able to demonstrate that the Lozi map has a true chaotic attractor.

The inverse mapping can be used to compute stable manifolds of the unstable periodic orbits. Shown in Fig.

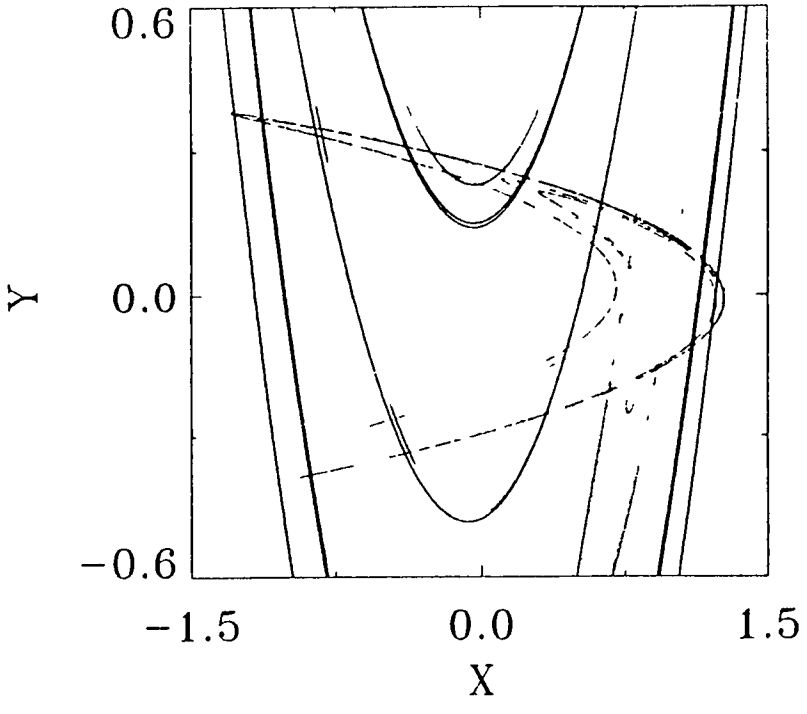

FIG. 5.1. Stable and unstable manifold for the Henon map at A=1.4 and B=0.3.

5.1 is the stable manifold of the period one fixed point. The local stable manifold W^s_{loc} is used to compute the global stable manifold shown in this figure. At a point W^s_{loc} and W^u_{loc} are tangent to the stable and unstable eigenvectors (Eq. (5.15)). While the invariant manifold of flows are composed of the unions of solution curves, those of maps are unions of discrete points. The attractor which is the closure of the unstable manifold is also shown. Figure 5.2 (a) shows the results of a numerical experiment with the classical parameters A=1.4 and B=0.3. A typical strange attractor like that in Fig. 5.2 (a) exhibits a Cantor set structure along directions transversal to the

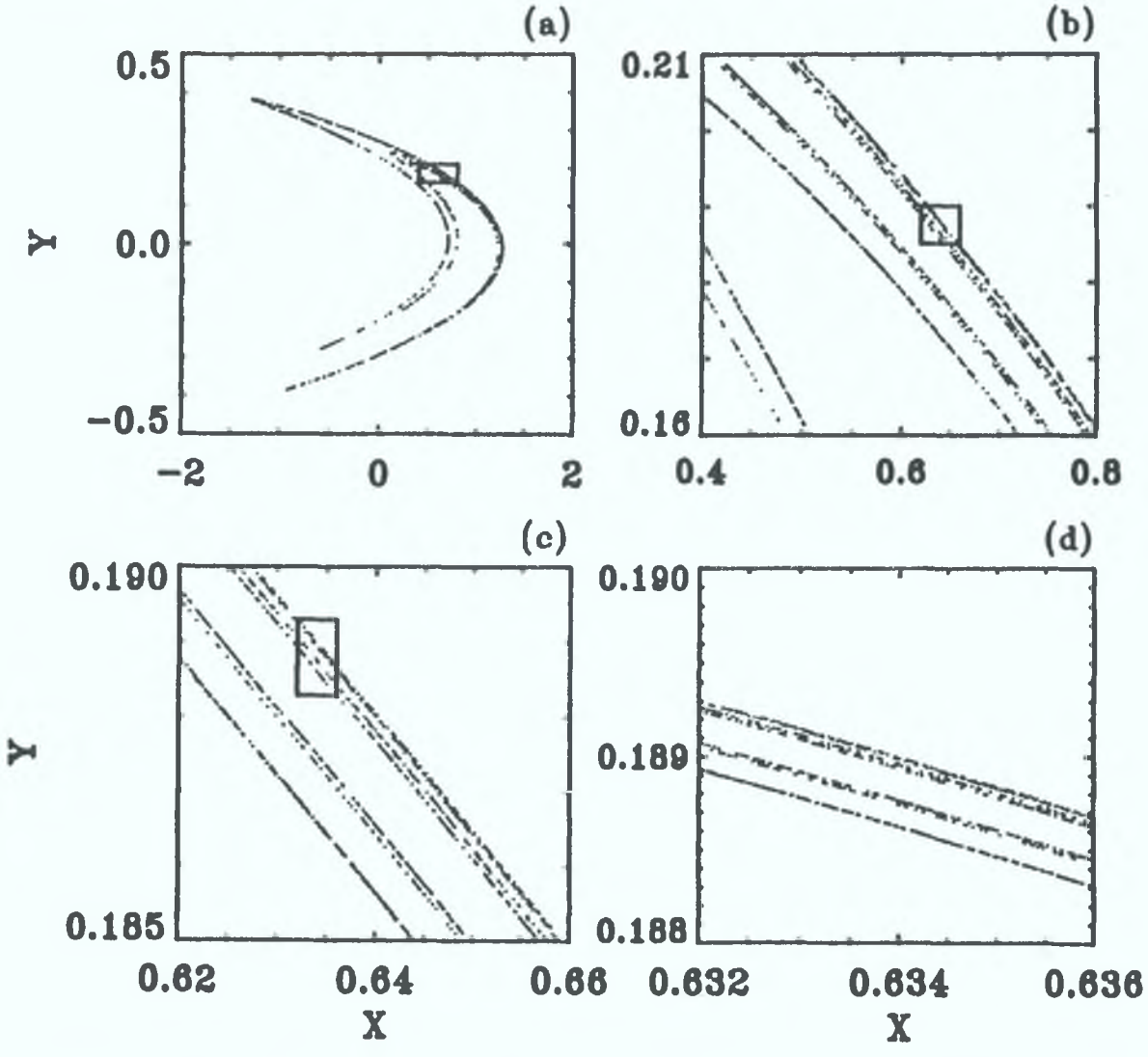

FIG. 5.2. The Henon attractor at A=1.4 and B=0.3. (see text for details). From Henon (1976).

unstable manifolds. Successive points distribute themselves on a complex system of lines. A magnification of the square in Fig. 5.2 (a) yields Fig. 5.2 (b) and this process is repeated to give 5.2 (c) & (d). This system of lines constitute a strange attractor. The self similarity visible in Fig. 5.2, is a typical property of a set which is invariant under time evolution, and makes it a fractal set.

The Lyapunov exponents λ_1 and λ_2 are computed as a function of the parameter A (with B=0.3) and fixed initial conditions. The results are shown in Fig. 5.3 (a). Note there is only one independent exponent since $\lambda_1+\lambda_2=\ln|b|$. $\lambda_1>0$ corresponds to chaotic attractors while $\lambda_1<0$ gives rise to a periodic attractor. With greater resolution many more transitions from chaotic to periodic attractors would be apparent. The Lyapunov dimension for the same range of A is shown in (b). Excluding the periodic windows there is an overall increase in the entropy K_L and the dimension D_L for increasing A. The increasing entropy corresponds to new orbits while the increasing dimension is related to the distribution of these orbits. Three different Cantor sets are shown in Fig. 5.4 for the parameter values A=1.07, 1.21 and 1.40 with dimensions D_L=1.075, 1.209 and 1.260 and entropies K_L= 0.098, 0.318 and 0.422 respectively. As the parameter A is increased more complicated structures with larger dimensions are apparent. Interspersed with these strange attractors, and arbitrarily close to them are stable solutions (Fig. 5.3). The type of structure observed here (although interspersed with stable solutions) should be contrasted with the pruned baker map (Sec. 4.3) where a similar evolution of structure and dimension was observed.

5.3.1 Attractors Merging

Chaotic attractors consisting of many pieces are common to a wide range of dynamical systems. When the orbits on the attractor cycles sequentially through the individual pieces, then they can be mapped onto each other (as in Sec. 5.4.3). The example examined here consists of a

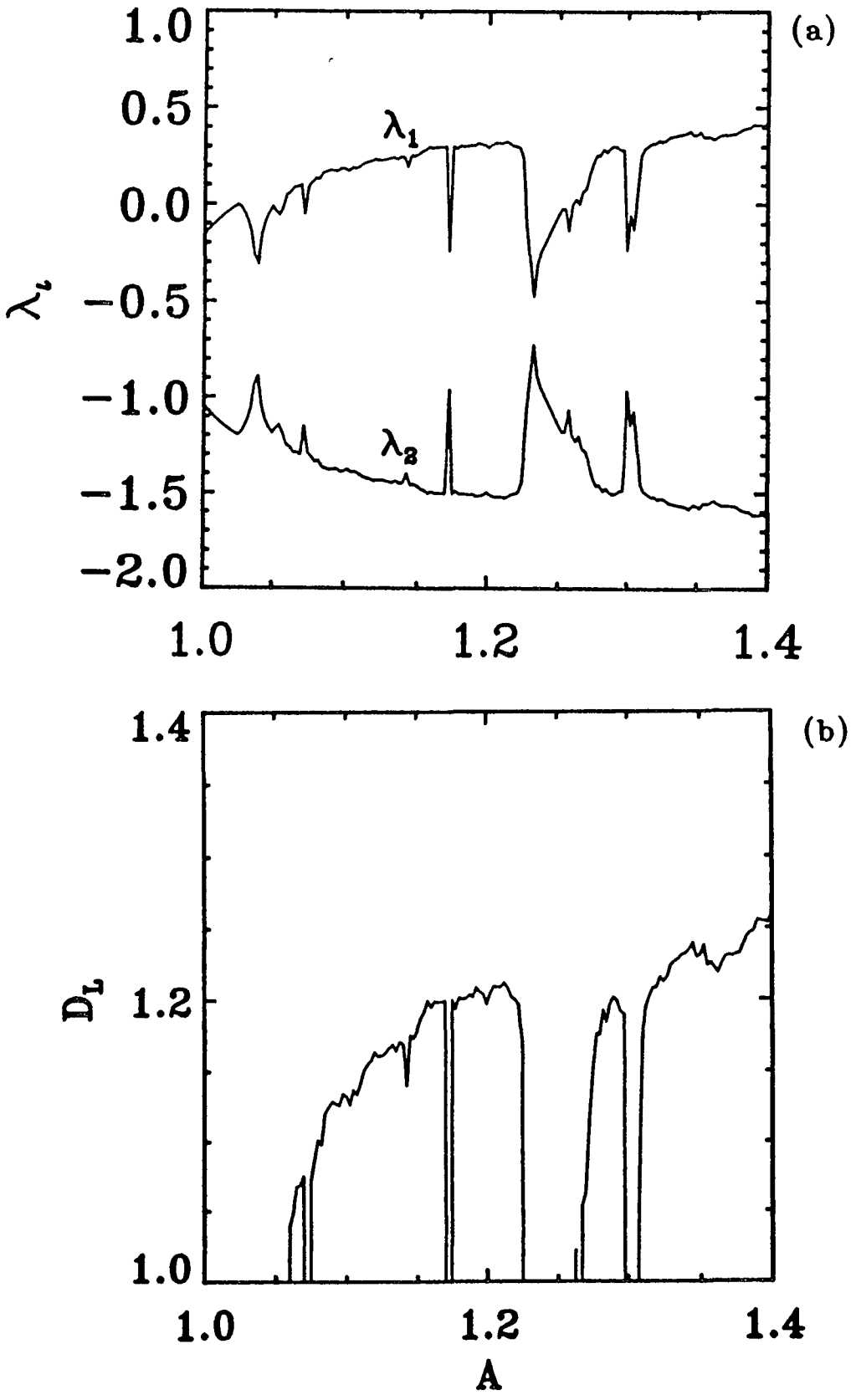

FIG. 5.3. (a) The Lyapunov exponents λ_1 and λ_2 as a function of A, (b) The dimension D_L as a function of A.

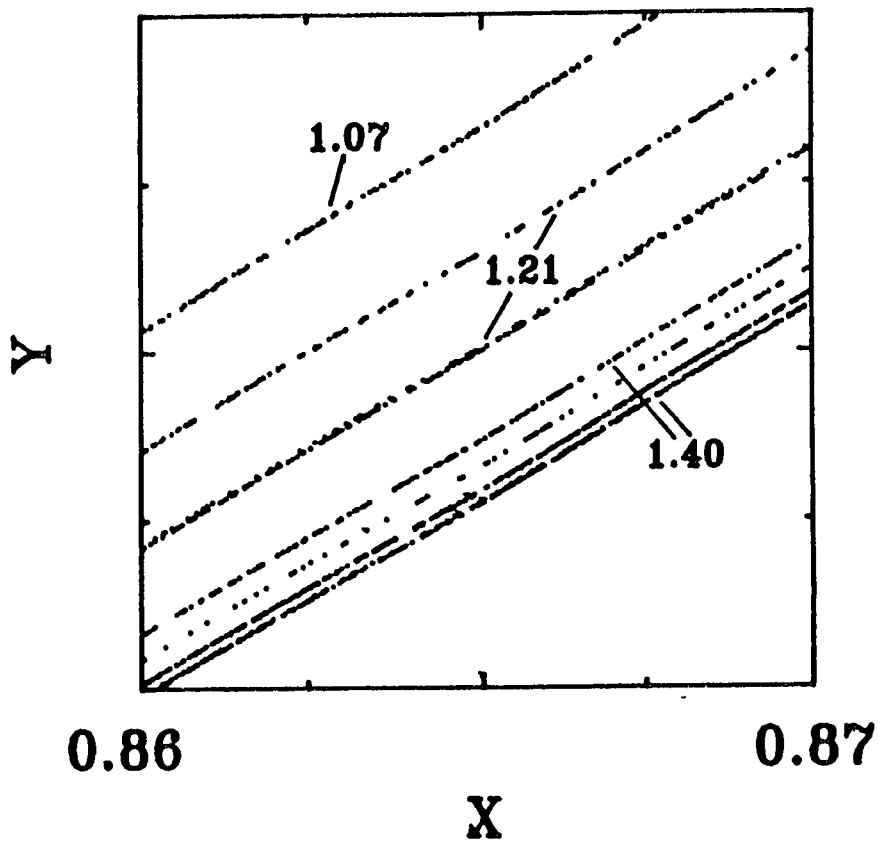

FIG. 5.4. The Cantor set of the Henon map for three values of A namely A=1.07, 1.21 and 1.40.

two piece attractor merging into a one piece attractor where the orbits do not cycle sequentially. The merging process is gradual as opposed to a crisis induced intermittency.

The two piece attractor is shown in Fig. 5.5 (a) for the parameter A=1.12. Sequential iterations of the mapping do not alternate between the two pieces. These two pieces merge to form the attractor in (b) at A=1.2. The unstable period one fixed point is shown in these figures and the unstable directions are indicated. The attractors are located on opposite sides of the stable manifold. It has been seen that orbits of high periodicity provide a dense coverage of the attractor as A is increased and that there is a one to one correspondence between the location of the orbits and the chaotic attractor. A similar expansion of the attractor has been observed for the baker map Eq. (4.17).

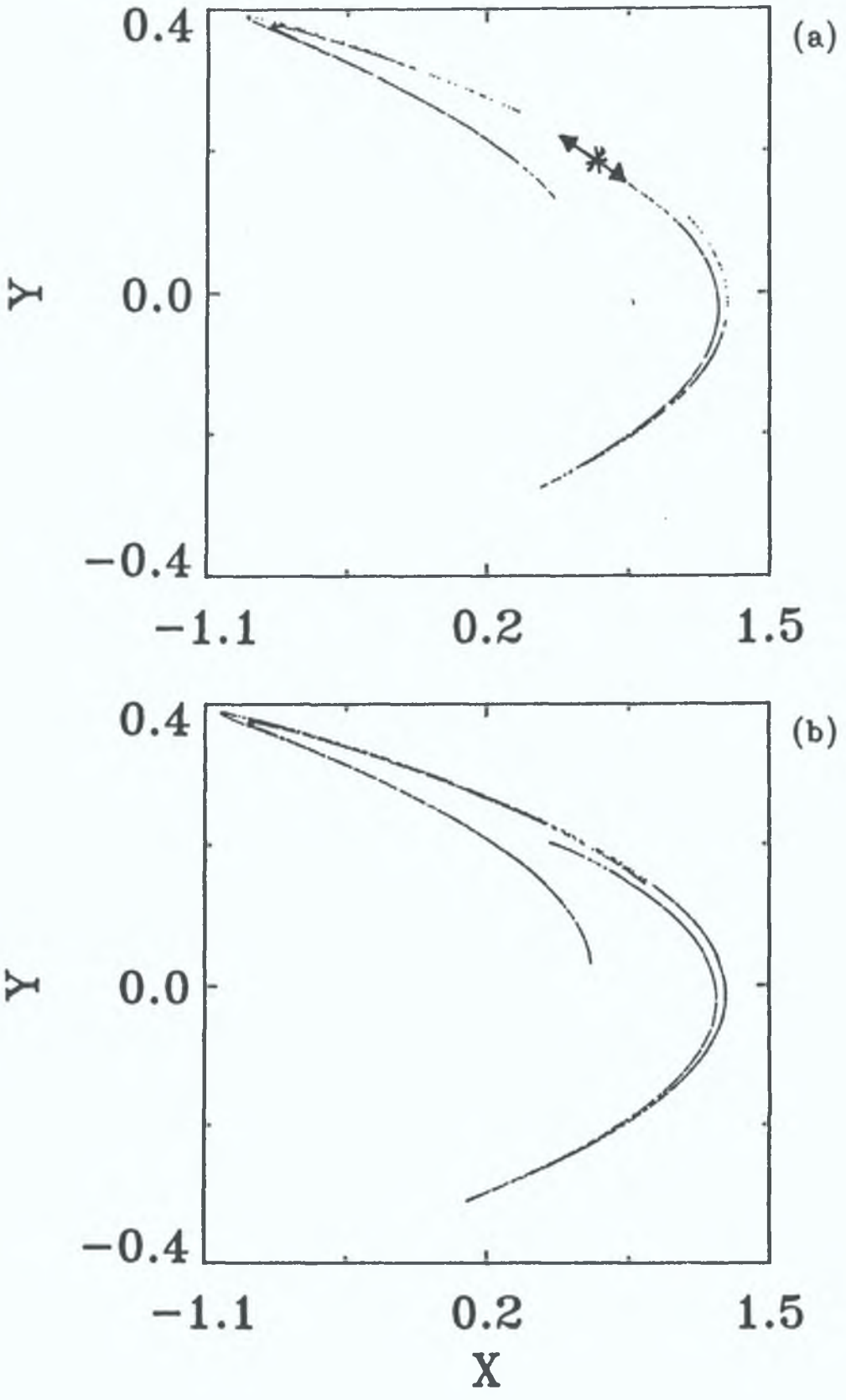

Fig. 5.5. The Henon attractor, at B=0.3. (a) A=1.12, (b) A=1.2

5.3.2 Higher Dimensional Invertible Maps

Consider the map $H_{A,B}\ \mathbb{R}^3 \longrightarrow \mathbb{R}^3$ given by

$$\begin{aligned} X_{i+1} &= 1 - AY_i^2 + Z_i \\ Y_{i+1} &= -X_i \\ Z_{i+1} &= -BY_i \end{aligned} \tag{5.16}$$

where A and B are parameters. The mapping H is a diffeomorphism of $\mathbb{R}^3$ as long as $B \neq 0$. One can compute readily that the determinant Jacobian is B and hence constant and independent of X and Y. An n dimensional discrete map with constant Jacobian has been introduced by Baier and Klein (1990) and a three dimensional map with constant Jacobian which exhibits chaotic behaviour with dimension D_L close to three has been analyzed by Peplowski and Stefanski (1988).

One piece of a four piece attractor is shown in Fig. 5.6 (a) for B=0.17. The dimension D_L=1.55 with Lyapunov exponents λ_1=0 089, λ_2=−0 162 and λ_3=−1.692. For B>0.177 there is an intermittent crisis. Due to the presence of periodic windows and attractors of different structure the critical value B_c can not be determined. Since the intermittency takes place from an attractor of dimension D_L=1.55, Eq (5.3) and Eq. (5.6) may apply. The intermittent transition is to an attractor of dimension D_L>2. Similar types of intermittency will be examined in the following parts of this chapter using two dimensional maps.

The attractor shown in Fig. 5.6 (b) with B=0.3 has dimension D_L=2 15 with Lyapunov exponents λ_1=0.147, λ_2=0.077 and λ_3=−1.43. Since $\lambda_1+\lambda_2>0$ the dynamics take place on a surface. A section through this attractor reveals a Cantor set of low dimension. The dynamics on a surface can be examined using the two dimensional mappings of the following three sections.

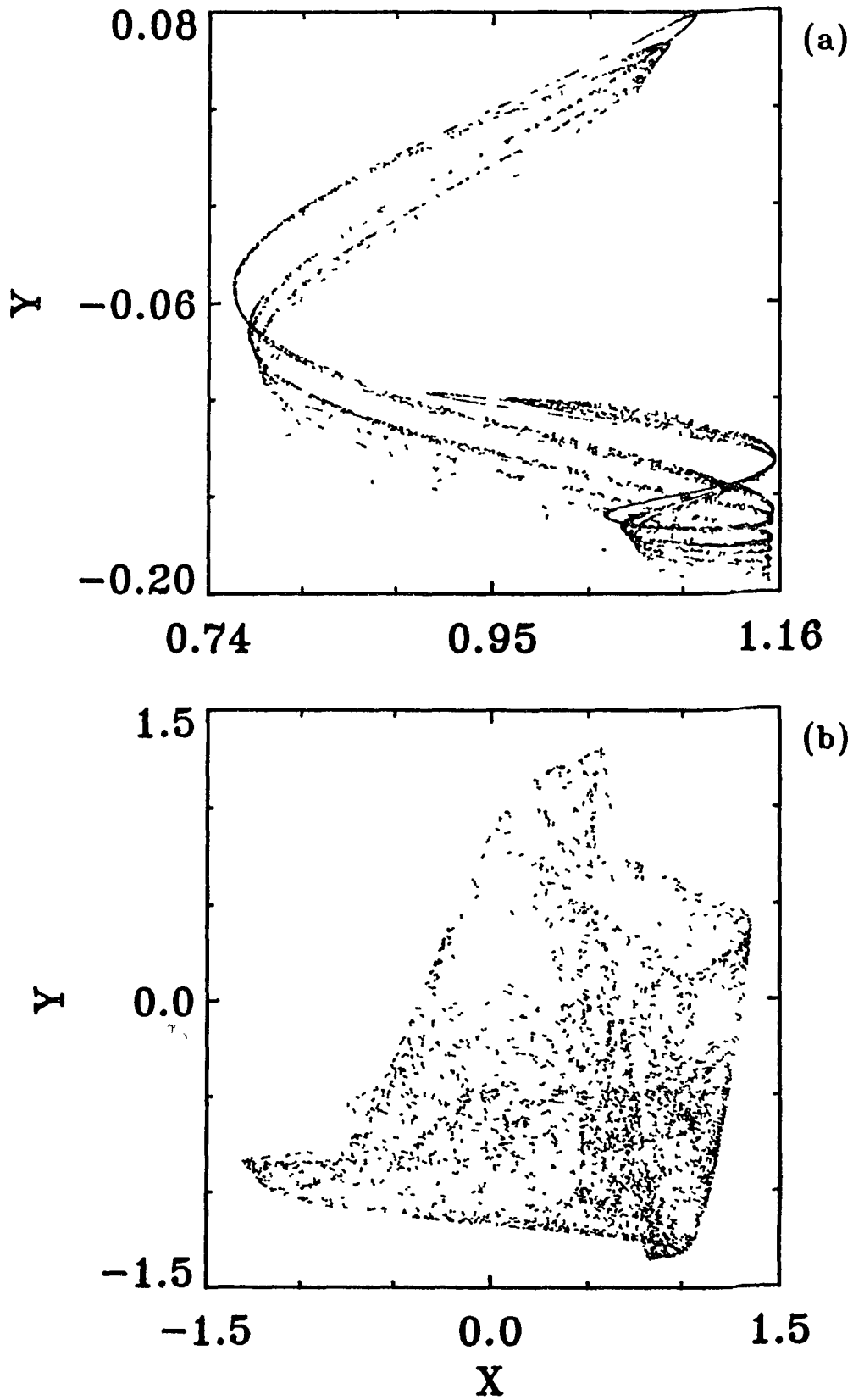

Fig. 5.6. The Henon attractor, at A=1.2. (a) $B=0.17<B_c$, (b) $B=0.3>B_c$

5.4 USHIKI MAP

Consider the two dimensional map $U : \mathbb{R}^2 \longrightarrow \mathbb{R}^2$ given by (Ushiki et al , 1980),

$$\begin{aligned} X_{i+1} &= (A - X_i - B_1 Y_i)X_i \\ Y_{i+1} &= (A - Y_i - B_2 X_i)Y_i \end{aligned} \tag{5.17}$$

with the parameters A, B_1 and B_2, such that

$$A > 1 \ , \quad 1 > B_1, B_2 \geq 0 \tag{5.18}$$

The X axis and the line defined by the equation $A-B_1X-Y = 0$ are mapped onto the X axis. Likewise the Y axis and the line defined by the equation $A-B_2Y-X = 0$ are mapped onto the Y axis. This set is bounded by a quadrangle which is denoted by D, and $U(D) \subset D$. Hence, there is a bounded domain (trapping region) which is a necessary condition for chaos.

There are four fixed points

$$(0,0), \ (A-1,0), \ (0,A-1), \ \left(\frac{(A-1)(1-B_1)}{1-B_1B_2} \ , \frac{(A-1)(1-B_2)}{1-B_1B_2} \right) \tag{5.19}$$

three of which are on the boundary of D and the other is within the interior of D. This chaotic map has been derived from a system of two ordinary differential equations using an Euler's finite difference method. Differential systems with three degrees of freedom are needed for chaotic behaviour which implies that the chaotic mapping above has no direct association with the two differential equations. Three regions of the parameter space A are explored with $B_1=0.1$ and $B_2=0.15$ and the type of behaviour observed is a good representation of the chaotic behaviour of this and the proceeding maps.

5.4.1 Intermittency Between a Dissipative and a Non-Dissipative Attractor.

A dissipative attractor is shown in Fig. 5.7 (a) for A=3.74572. This is a period eight chaotic attractor, of which one piece is shown Apart from a slight distortion the other pieces have identical fractal structure. Fig. 5.7 (b) (for A=3.74571) shows the location of some relevant

periodic orbits, of period 8, 16, 120. Their stability and orbital dimensions are given in Table 5.1. The period 8 is a repelling orbit with two positive Lyapunov exponents. Since this is a period eight chaotic attractor all orbits on the attractor must be some multiple of eight. In fact the orbits of lowest periodicity on the attractor are orbits of period 120, of which there are two. Consecutive orbits are of periods 128, 136, 144,.... Surrounding this attractor are orbits of all periods most of which are repelling The Lyapunov exponents of the attractor are λ_1=0 0191 and λ_2=-0.0582 with Lyapunov dimension D_L=1.33. The correlation dimension is D_2=1.24±0.01, which as expected is a lower bound on D_L. Successive magnifications indicate a structure which is self similar. It should be noted from Table 5 1 that the orbital dimensions of the period 120's is greater than D_L. As the orbital periodicity increases there is convergence towards D_L and for period 400, $D_{orbit}\approx 1.28$.

Table 5.1.

The orbital dimension and Lyapunov exponents of the unstable period orbits in Fig. 5.7 (b) for the parameter A=3.74571

Period	λ_1	λ_2	D_{orbit}
8	0.02129	0.02125	2
16	0.04142	-0.01708	2
120	0 01976	-0.04068	1.486
120	0.01912	-0.03618	1.528

The unstable and stable manifolds of the period 16 orbit is shown in Fig. 5.7 (a). The stable manifold consists of 11 disconnected pieces which bound the attractor. All iterations inside this stable manifold terminate on the attractor. The attractor appears to be the closure of that part of the unstable manifold which is

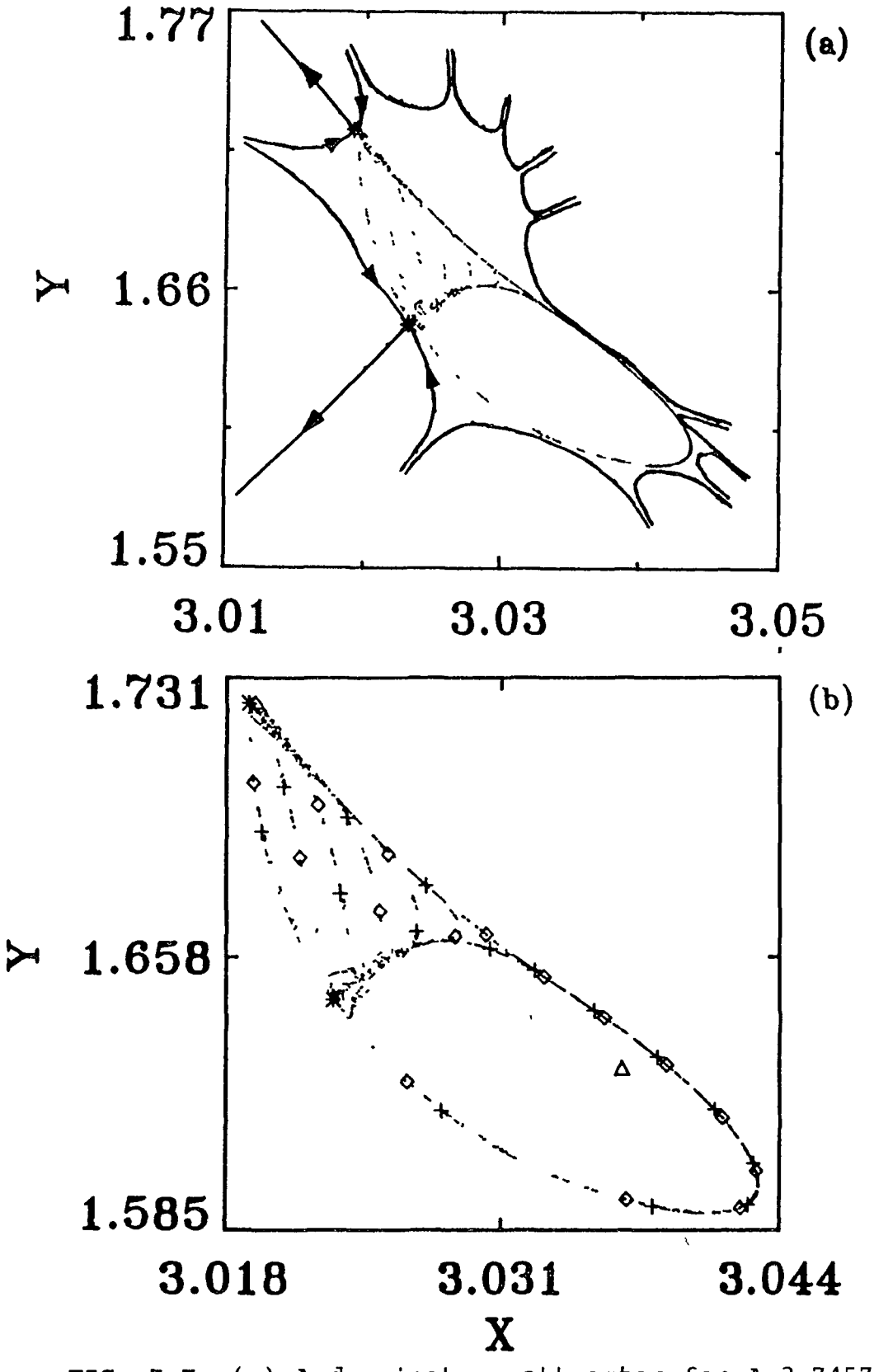

FIG. 5.7. (a) A dissipative attractor for A=3.74572. The manifolds of the period 16 orbit are also shown. (b) The attractor for A=3.74571. The symbols identify the following orbits, triangle period 8, asterisks period 16, pluses period 120 and diamonds period 120.

bounded by the stable manifold segments as illustrated. This manifold was obtained by plotting a set of initial points that pass through the period 16 orbit, exiting via the unstable manifold At the resolution used the stable manifold consists of 11 pieces; higher resolution could result in more than 11 pieces.

The period 16 orbit collides with the attractor as A is reduced below a critical value A_c= 3.7457099470.... Figure 5.8 shows Y_i versus i for three different values of A. In Fig. 5.8 (a) A is greater than A_c, while Figs 5.8 (b) and (c) show results for successively smaller A values below A_c. It is evident from this diagram that the time between bursts is seen to decrease with increasing A_c-A.

Figure 5 9 (a) shows the non-dissipative chaotic attractor after the intermittency for $A=3.745<A_C$. The diamonds shown in this figure indicate the position of the dissipative attractor at A=3.74571. The area occupied by the dissipative attractor is less than 0.3% of that occupied by the non-dissipative attractor. This attractor at A=3.745 has mainly repelling periodic orbits and the associated Lyapunov exponents are λ_1=0.26 and λ_2=0.06. Because $\lambda_1+\lambda_2>0$ the Lyapunov dimension D_L=2 from Eq. (2.8) while the correlation dimension computed from 40000 points is D_2=1.55±0 05. This type of chaotic behaviour with two positive Lyapunov exponents has also been observed in coupled logistic maps (Hogg and Huberman, 1984) and in a two dimensional discrete map (Kitano et al., 1984).

The result of an experiment to determine the critical exponent, γ, is shown in Fig. 5.9 (b). The calculation of the average lifetime, τ, from the data of the numerical experiment was done as follows. The initiation of a burst is via the unstable manifold of the period 16 orbit and by choosing a suitable region on the unstable manifold of the period 16 orbit, it is possible to detect such an burst. By placing a box around one of the period eight chaotic attractors it is possible to detect the termination of a burst. Hence, the accurate computer determination of τ for

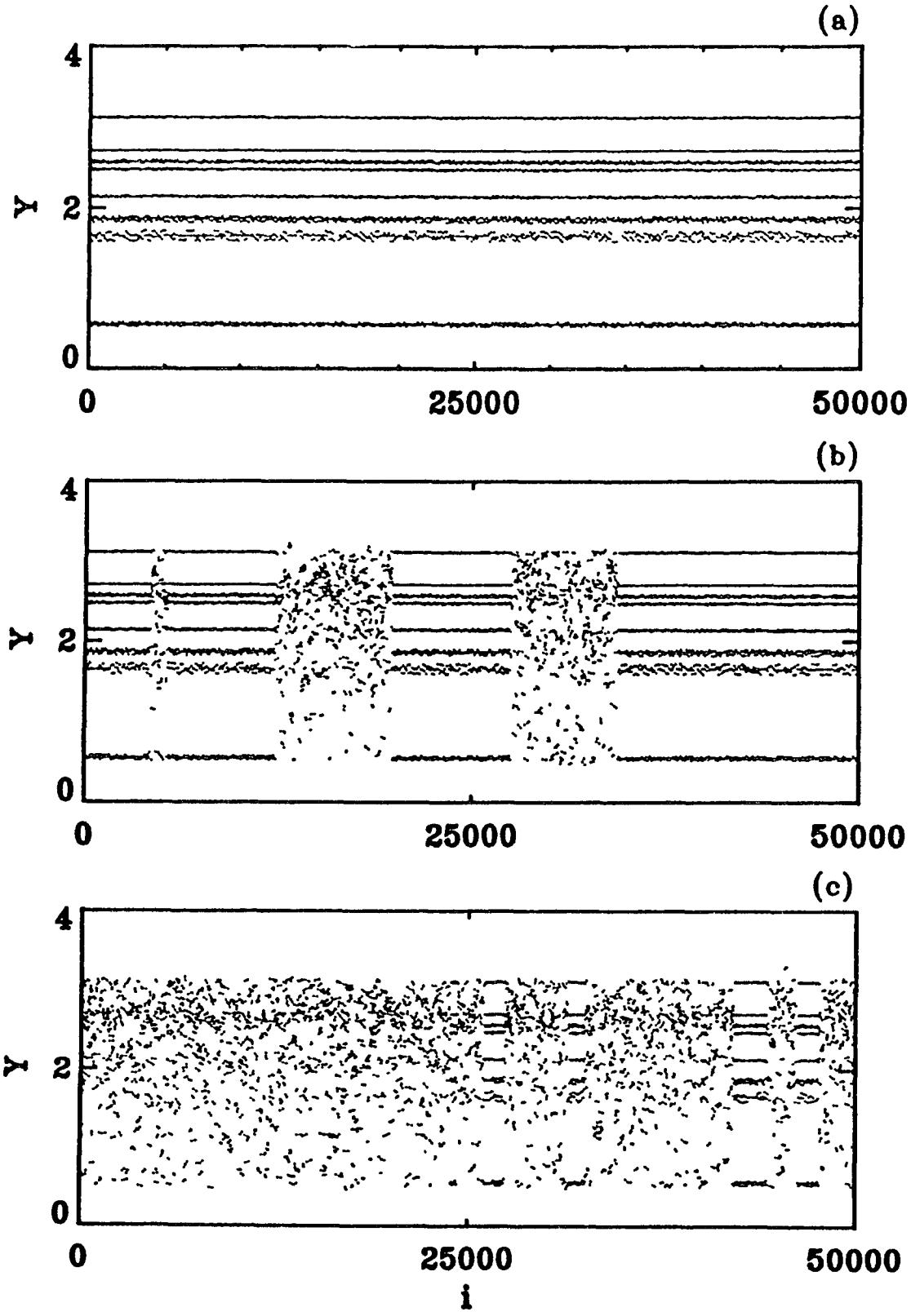

Fig. 5.8. Time series Y_i versus i for (a) A=3.74571 $>$ A_c (b) A=3.7457109 $<$ A_c (c) A=3.7457105 $<$ A_c.

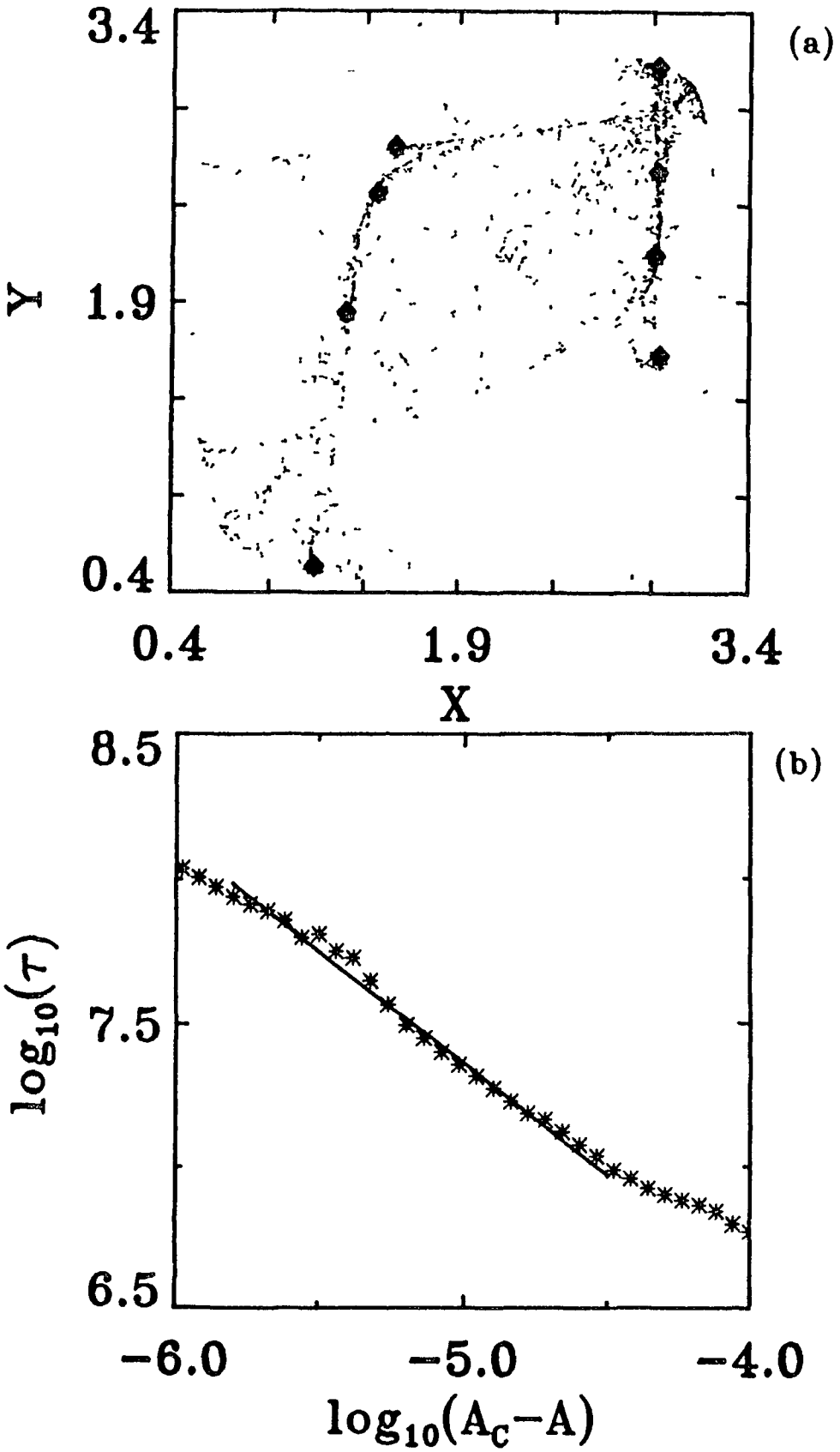

Fig. 5.9. (a) The non-dissipative attractor at A=3.745 $<A_c$. The diamonds locate the position of the dissipative attractor similar to the one at A=3.74571. (b) $Log_{10}\tau$ vs $Log_{10}(A_c-A)$. The computed value is $\gamma=0.78\pm.02$.

an arbitrarily long orbit is facilitated. The result, from Fig. 5.9 (b), for the critical exponent is $\gamma=0.78\pm0.02$.

The attractor before the crisis is the closure of the unstable manifold of the unstable periodic orbits on the attractor. Details of the possible collisions are, a homoclinic tangency (involving the stable and unstable manifold of the period 16 orbit) or a heteroclinic tangency (involving the stable manifold of the period 16 orbit with an unstable manifold of an orbit on the attractor). The unstable manifolds on the attractor have orbits of period 16, 120, 128 etc.. A homoclinic tangency is ruled out because the period 16 orbit has positive divergence. According to Grebogi et al. (1987) for a heteroclinic tangency, where the orbit that collides with the attractor also bounds the attractor, the second orbit involved must be of the same period. Clearly the theory does not cover this case, since there is only one period 16 orbit. It is not possible to isolate the contribution of each orbits unstable manifold from the attractor. Hence, the global eigenvalues are used in Eq. (5.3) for a heteroclinic tangency, the exponent is $\gamma=0.82$ which is in close agreement to the computed value. Therefore a heteroclinic type tangency is concluded to be responsible for the crisis.

5.4.2 Intermittency Between a Line Attractor and a Non-Dissipative Attractor.

In this section, intermittency between a line attractor and a surface attractor is analyzed. At A=3.572 in Eq. (5.17) there is a line attractor (at $\approx 44^{\circ}$ in the X-Y plane) with Lyapunov exponents $\lambda_1=0.0499$ and $\lambda_2=-0.2027$ and dimension $D_L=1.246$. There is a steady increase in this dimension as A increases. At A=3.581 the Lyapunov exponents are $\lambda_1=0.101$ and $\lambda_2=-0.055$ with dimension $D_L=2$. Correlation dimension studies give $D_2=0.91\pm0.01$ for all line attractors for $A \in (3.572, 3.581)$, see Table 5.2. This dimension is consistent with what is expected for a one dimensional

chaotic attractor. When the geometrical properties of the attractor are taken into account $D_L=1$. This example illustrates the caution which is needed when using the Kaplan Yorke conjecture

Three time series are shown in Fig. 5.10 for three values of the parameter A (successive Y_1 are joined by straight lines), after a rotation through $\approx -44^\circ$ so that the line attractor is parallel to the X axis. Note the change in scale between Fig. 5.10 (b) and (c). The critical value for the intermittency was $A_c=3.581833641.....$ and numerical calculation of the critical exponent γ, for $10^{-8} < (A-A_c) < 10^{-2.5}$ gives a γ that is zero to four decimal places. This value of γ indicates that the durations of the bursts are extremely short. Shown in Fig. 5.11 (a), for $A=3\ 582 > A_c$, is one piece of a chaotic period four line attractor. Orbits of period 4, 8, and 16 are located on this line and all have one positive and one negative Lyapunov exponent For the range A=3.572 to A_c the negative Lyapunov exponent decreases in value from -0.2027 to -0.055, making the line attractor less attracting. The band of period 12 and 24 orbits, with two positive Lyapunov exponents, shown in this plot, block a trajectory from visiting the complete attractor shown in Fig. 5.11 (b) resulting in the γ being approximately zero as stated earlier. For this particular case the orbit that causes the intermittency has not been identified.

For A=3 6 there is a surface attractor with two positive exponents (similar to Fig. 5.11 (b) at A=3.583). According to the Kaplan Yorke conjecture D_L is undefined (Eq. (2.7)) while Eq. (2.8) gives the maximum value of $D_L=2$. As given in Table 5.2, the correlation dimension is $D_2=1.55$. To validate that $D_L=2$ it would be necessary to show that the following inequality is true $D_0 \geq D_L$. The results for a of calculation of D_0 will be given in the next section

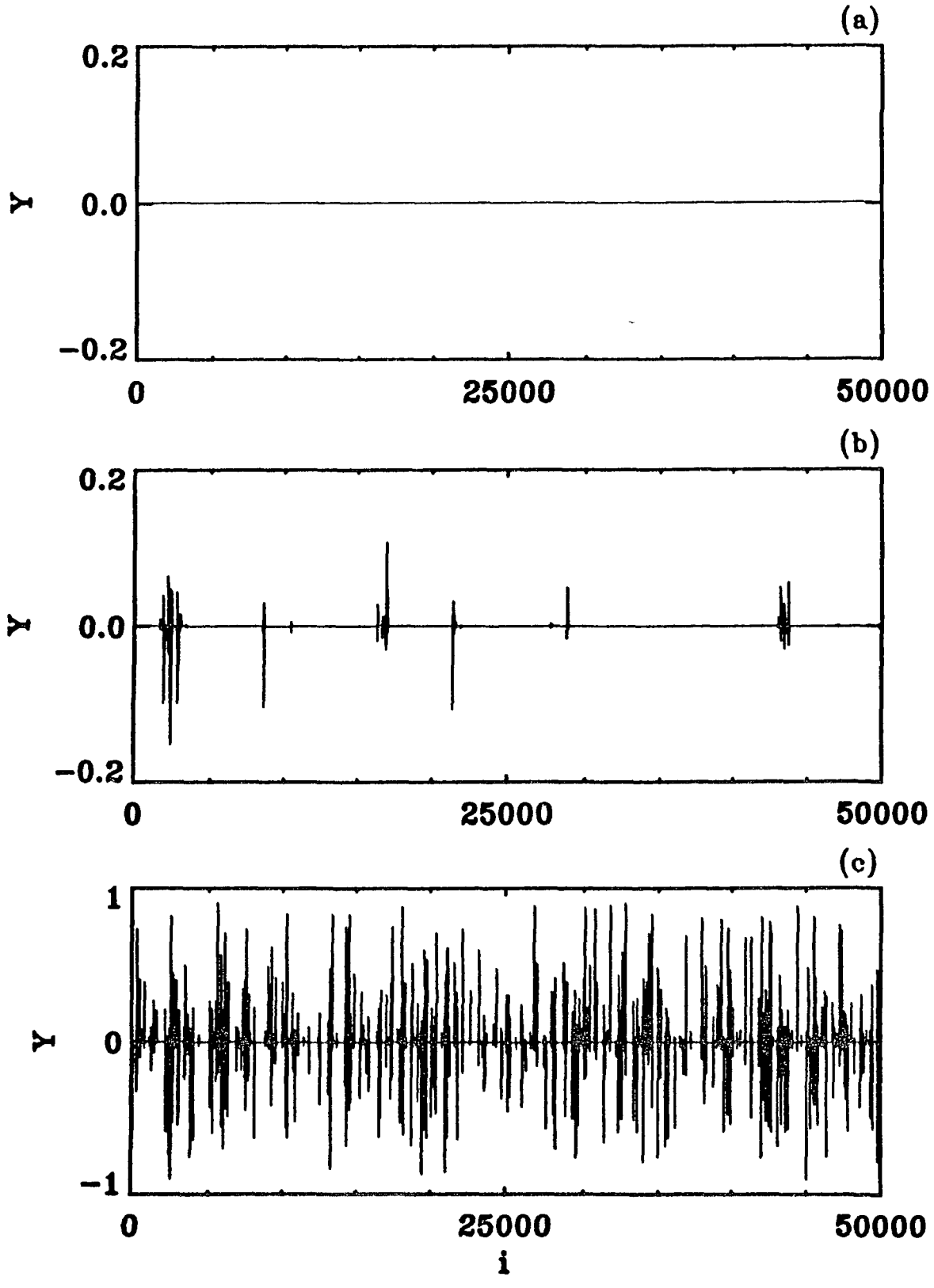

Fig. 5.10. Time series Y_i versus i for Ushiki map near the intermittency, (a) A=3.581 $<A_c$, (b) A=3.582 $>A_c$, (c) A=3.583 $>A_c$

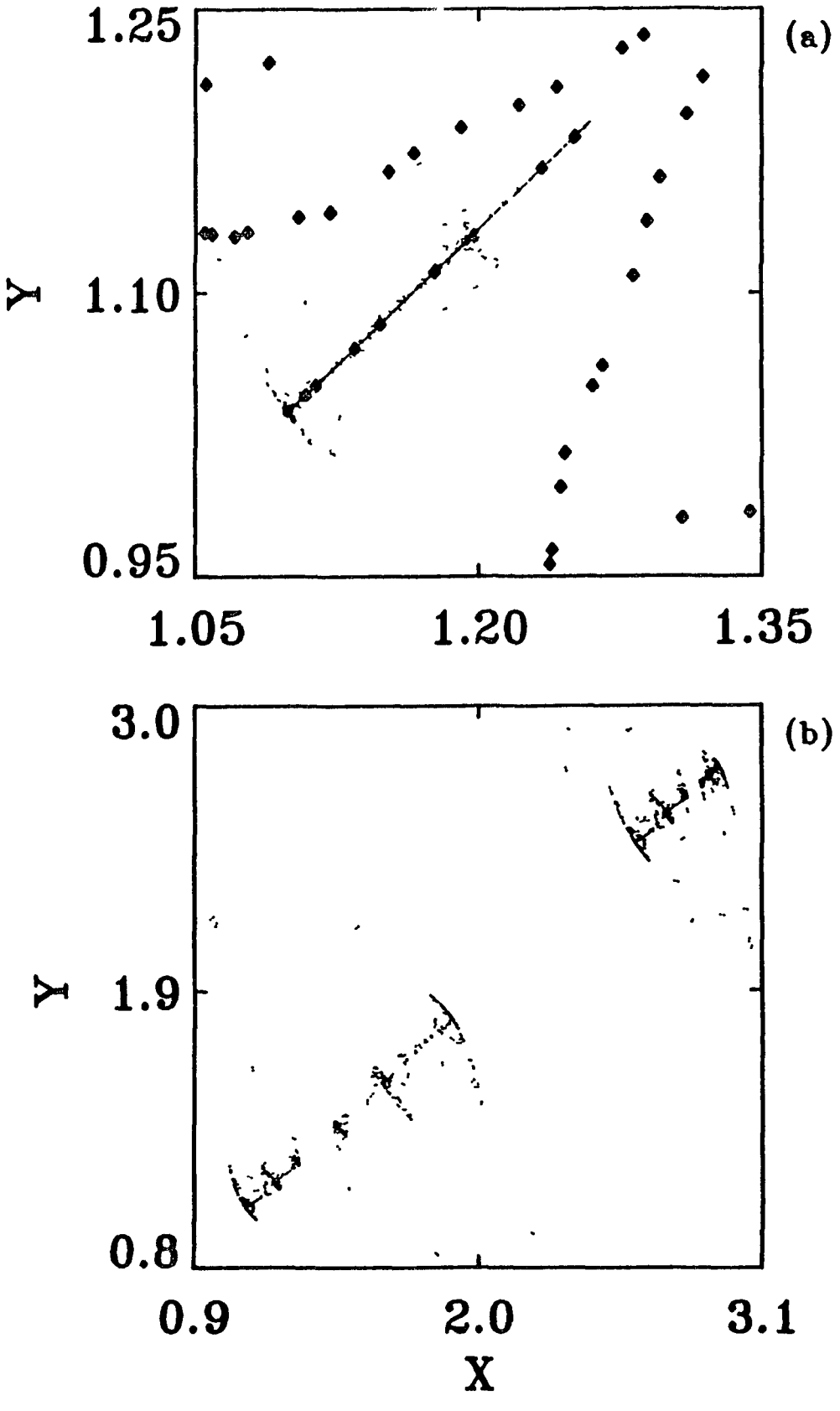

Fig. 5.11. Phases space plots for (a) A=3.582 $>A_c$, Orbits of period 4, 8, and 16 are located on the line, other orbits are of period 12 and 24, (b) A=3.583 $>A_c$.

Table 5.2

Comparison of the correlation dimension, D_2, and the Lyapunov dimensions, D_L, for line and surface attractors. D_2 was computed using 40000 points, the statistical variation in the slope is ± 0.01.

A	D_2	D_L	Type of Chaos
3.572	0.91	1.246	line
3.575	0.91	2	line
3.581	0.91	2	line
3.600	1.55	2	surface

5.4.3 Attractor Merging, Intermittency and Evolution

Initially at A=3.635311 in Eq. (5.17) there is a 72 piece chaotic attractor. Two of these 72 pieces are shown in Fig. 5.12 (a) with the dimension D_L=1.21. It is apparent that the pieces are related geometrically. Also located on this figure is the fundamental orbit of period 72, with orbital dimension D_{orbit}=1.347. The other orbit shown is of period 36, with D_{orbit}=1.45. As A is increased the two pieces of the attractor shown converge towards the period 36 orbit and for A >3.63531143... the 72 piece attractor has been reduced to a 36 piece attractor. This should be compared with the Henon map, where a two piece attractor merges to form a one piece attractor (Sec. 5.3.1). At the critical value A_c=3.635318594.. each of 36 attractors simultaneously experience a collision with the stable manifold of a period 36 orbit. This orbit has Lyapunov exponents λ_1=0.0371 and λ_2=-0.0308. The manifold of the orbit that collides with the attractor is shown in Fig. 5.12 (b) and in this case the stable manifold does not bound the attractor. At the intermittent crisis a trajectory crosses over from one side of the stable manifold before shooting out along the unstable manifold.

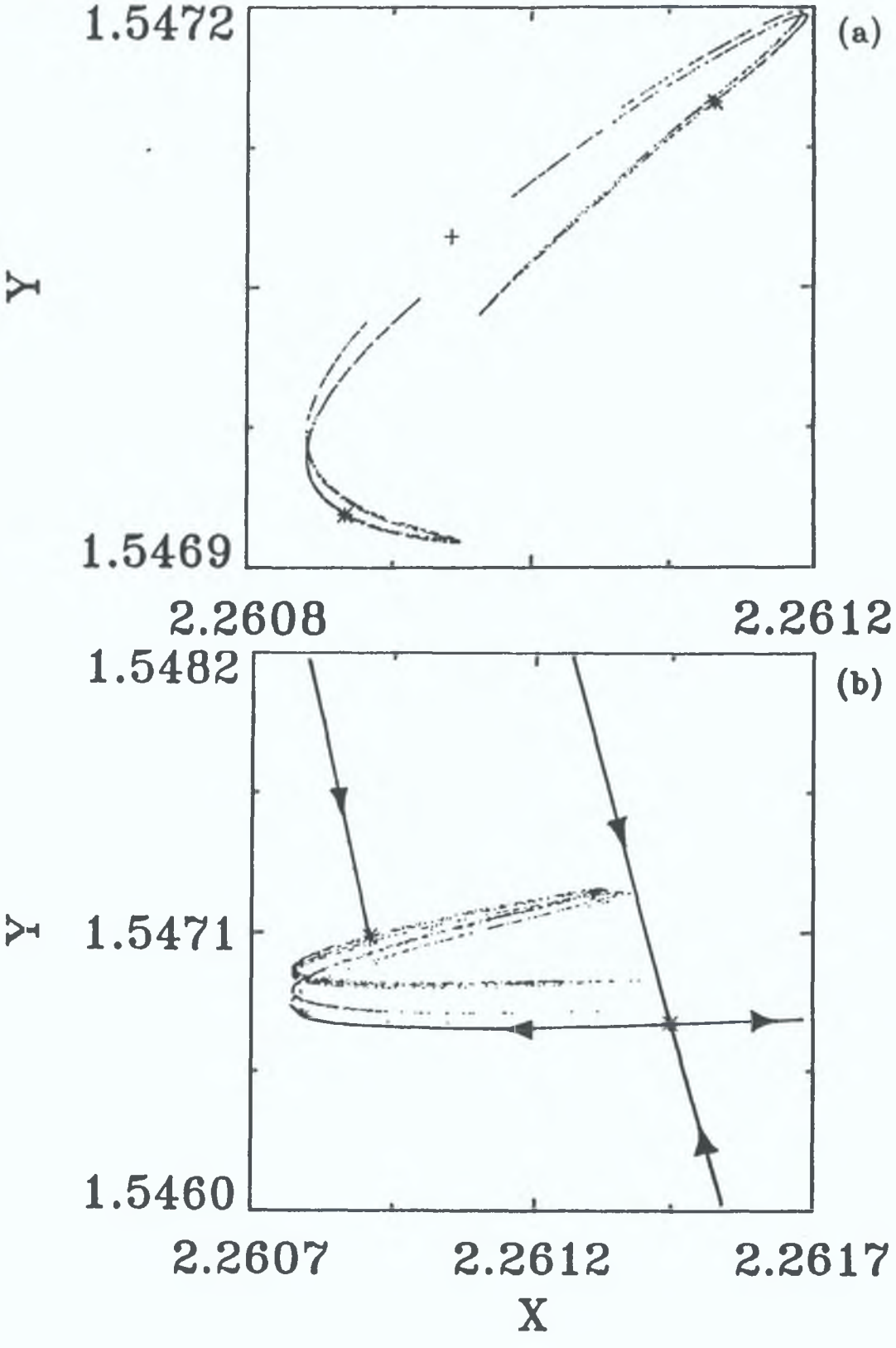

FIG. 5.12. (a) The attractor for A=3.635311 $<A_c$. The symbols identify the following orbits, asterisk period 72, crosses period 36. (b) The attractor for $A=A_c$. The directions of the unstable and stable manifolds of the period 36 orbits are indicated.

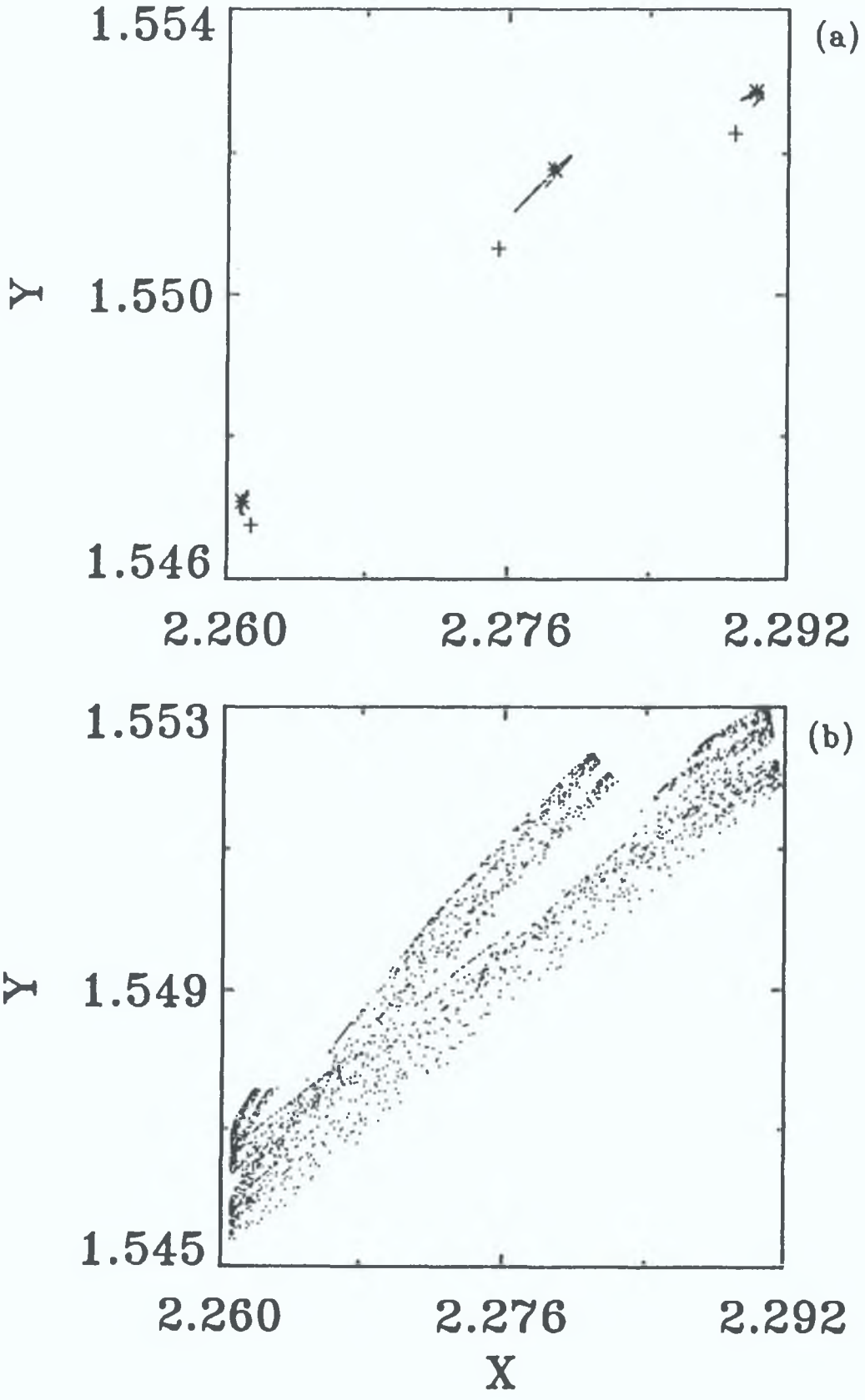

FIG. 5.13. (a) The attractor for A=3.635314 $<A_c$. Asterisks period 36 and crosses period 36. (b) The 12 piece attractor for A=3.63534 $>A_c$, one piece shown.

Shown in Fig. 5.13 (a) is three of these pieces for $A<A_c$. A period 36 orbit that collides with the attractor is also shown with an orbit of the same period on the attractor. This dissipative attractor has Lyapunov exponents $\lambda_1=0.0151$ and $\lambda_2=-0.0302$ and dimension $D_L=1.50$. Following the crisis there is a 12 piece attractor, as illustrated in Fig. 5.13 (b) where one of the 12 pieces is shown. Orbital dimensions give $D_L=2$ for this attractor. This is substantiated by the absence of structure. The dimension D_L is plotted against the parameter A in Fig. 5.14 (a) for the region of interest. As indicated in this diagram there is a sharp increase in dimension for $A>A_c$. For comparison purposes D_2 and D_L are given in Table 5.3 for four values of A.

The calculation of the average lifetime τ from a numerical experiment is shown in Fig. 5.14 (b). The computed critical exponent is $\gamma=0.78\pm.01$. For each value of A, τ was computed using the technique described in Sec. 5.4.1. The orbit that collides with the attractor produces a result in clear disagreement with the above γ when its eigenvalues are inserted in Eq. (5.6) for a homoclinic tangency. Hence this leads to the possibility of a heteroclinic tangency with the period 36 orbit on the attractor with Lyapunov exponents $\lambda_1=0.0159$ and $\lambda_2=-0.0307$ and dimension $D_L=1.52$. Inserting these exponents into Eq. (5.3) gives $\gamma=1.02$, significantly greater than the numerical value. This theoretical value assumes that the bursts are of a longer duration than those measured numerically. This orbit's unstable manifold has not been identified to be involved in the crisis. It is interesting to note that the global eigenvalues give $\gamma=1.00$.

A calculation of D_2, D_L and D_0 is given in Table 5.3 for four values of A. Attempts were made to calculate D_0 from the generalized correlation integral Eq. (2.42). For the first two values of A in Table 5.3 it has been verified that $D_2< D_L< D_0$. Despite using extremely long time series ($4*10^5$ data points), conclusive results were not obtained

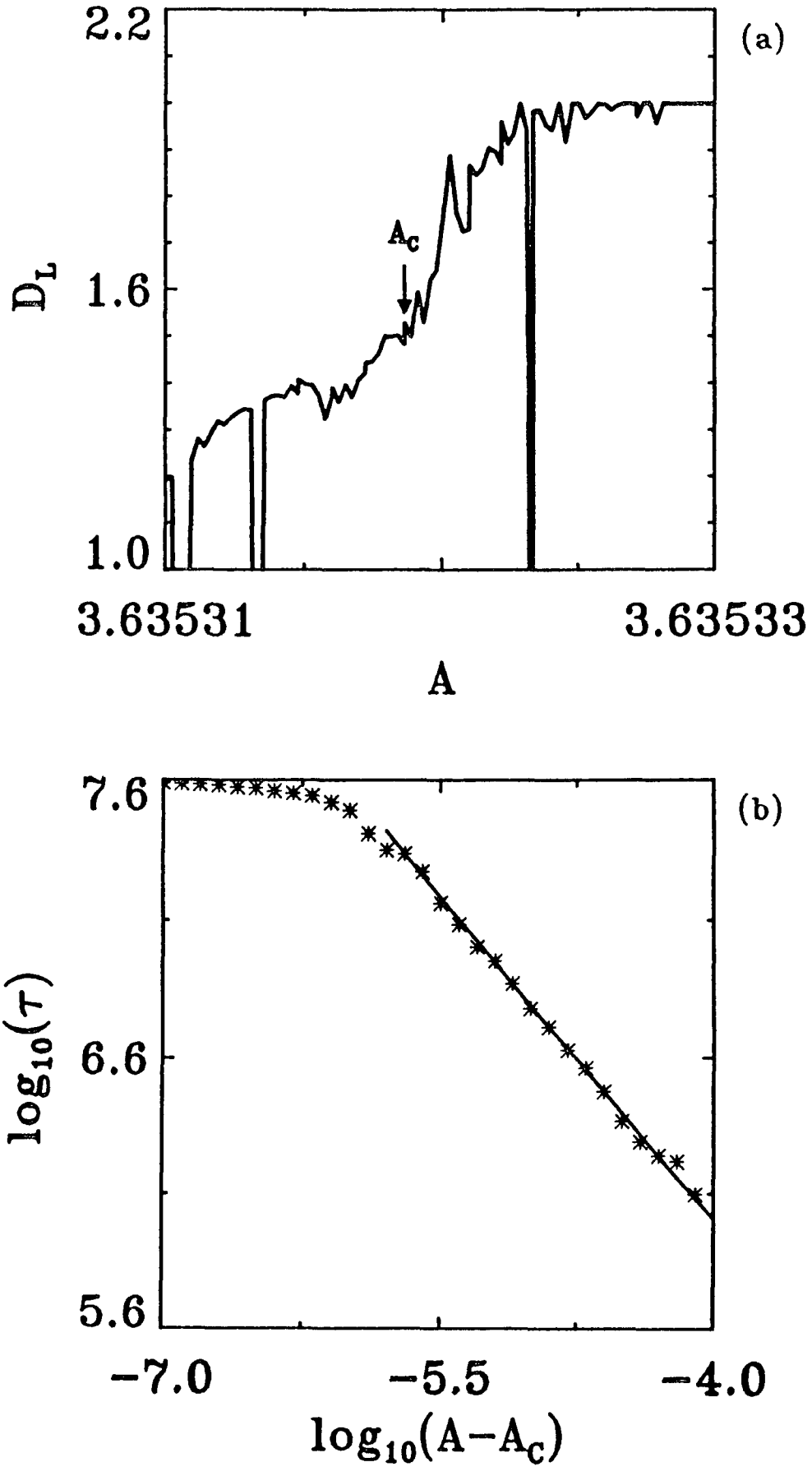

FIG. 5.14. (a) Lyapunov dimension D_L versus A. (b) $\text{Log}_{10}\tau$ vs $\text{Log}_{10}(A-A_c)$. The computed value is $\gamma=0.78\pm.01$.

to prove that $D_o \geq D_L$, when $D_L \approx 2$ due to the large error in D_0. This is one of the difficulties encountered when trying to determine the D_q spectrum.

Table 5.3

Comparison of correlation dimension D_2, Lyapunov dimension D_L and Hausdorff dimension D_0 for different types of chaotic attractors. D_2 was computed from 15000 data points, sampling at the period of the attractor.

A	D_2	D_L	D_0	Type of Chaos
3.635311	1.115±0 003	1.24	1.28±0.03	72 piece
3.635315	1.35±0.02	1.40	1.43±0.03	36 piece
3.635330	1.41±0 02	1.96	———	12 piece
3.635340	1.55+0 05	2	———	12 piece

5.5 WARWICK MAP

Chaos in the two dimensional mapping $W : \mathbb{R}^2 \longrightarrow \mathbb{R}^2$ given by

$$\begin{aligned} X_{i+1} &= (2X_i^2 + 2Y_i^2 - A)X_i - 0.5(X_i^2 - Y_i^2) \\ Y_{i+1} &= (2X_i^2 + 2Y_i^2 - A)Y_i + X_i Y_i \end{aligned} \qquad (5.20)$$

which involves the adjustable parameter A, is considered (Stewart, 1989). The evolution of chaotic behaviour and intermittency are examined as the parameter A is increased. Table 5.4 summarized the behaviour of the unstable periodic orbits as the parameter A is increased and the global Lyapunov exponents, together with D_L and D_2.

5.5.1 Intermittency Between Two Dissipative Attractors

Initially there is a 90 piece chaotic attractor at A=1 8932 with a Lyapunov dimension D_L =1.1. The fundamental orbit on this attractor is of period 90 and all successive orbits are a multiple of this. Each of these 90 pieces is visited periodically and they have the same symmetry. It is a fractal attractor with an unstable and a stable manifold

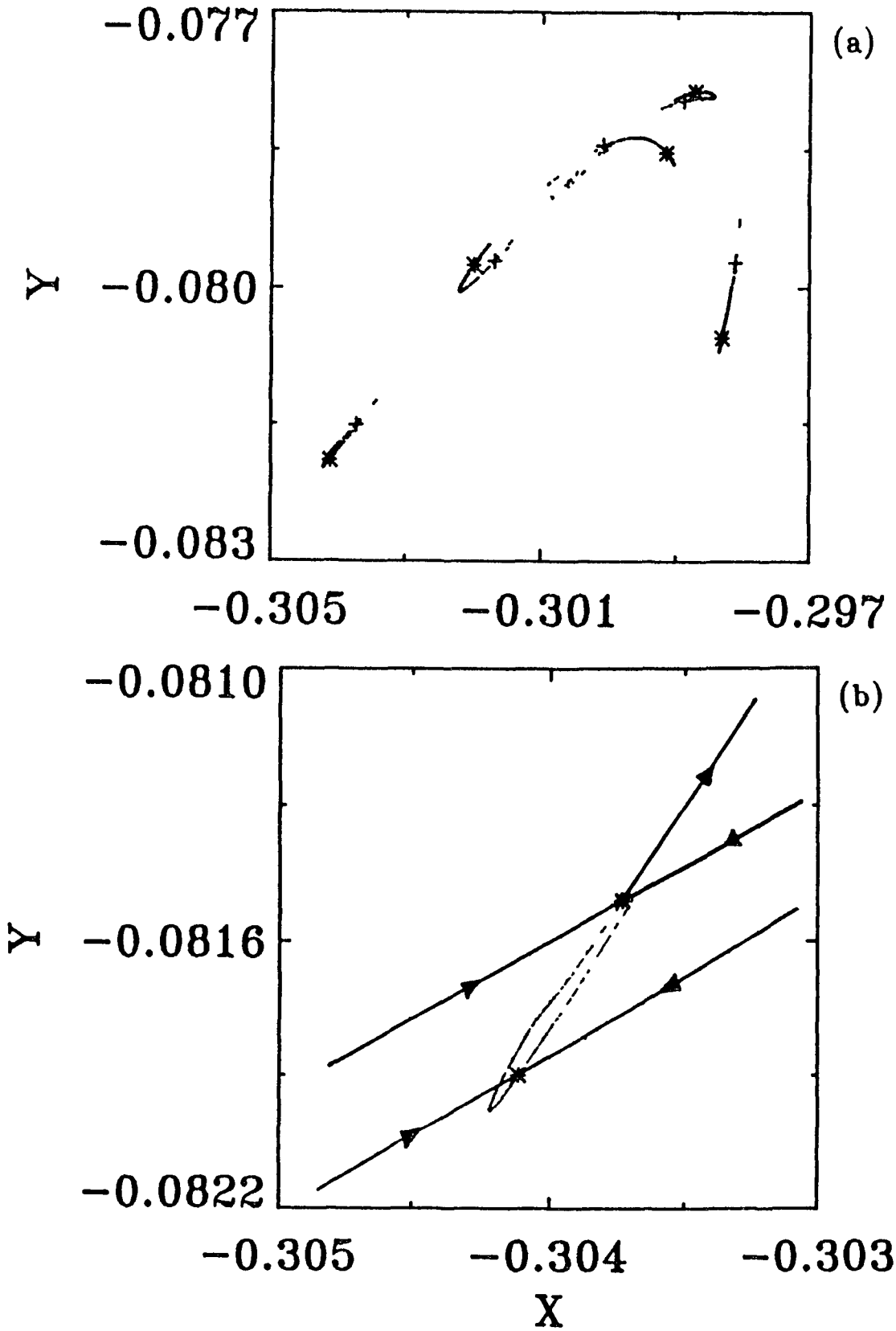

FIG. 5.15. The attractors for $A=A_c$. (a) Five of the ninety pieces. Asterisks and crosses are of period 90. (b) The manifolds of the period 90 orbits.

with one positive and one negative Lyapunov exponent

Through an intermittent crisis for $A > A_c = 1.893205605...$ the number of pieces are reduced from 90 to 18 as illustrated in Fig. 5.15 (a) for $A=A_c$. The intermittency has resulted from the collision of a period 90 unstable periodic orbit with the 90 piece chaotic attractor. Also located on this plot are two orbits of period 90, asterisks denoting the orbit on the attractor, crosses denoting the orbit that collides with the attractor. One of the 90 pieces is shown in Fig. 5.15 (b) together with the positions of the manifolds of both period 90 orbits. The intermittent crisis occurs when a trajectory crosses the stable manifold of the period 90 orbit shooting out along the unstable manifold. This is defined as a heteroclinic tangency. The Lyapunov exponents of the period 90 orbits on the attractor are $\lambda_1=0.0119$ and $\lambda_2=-0.0655$, (Table 5.4) which when substituted into Eq. (5.3) gives a value of $\gamma=0.682$.

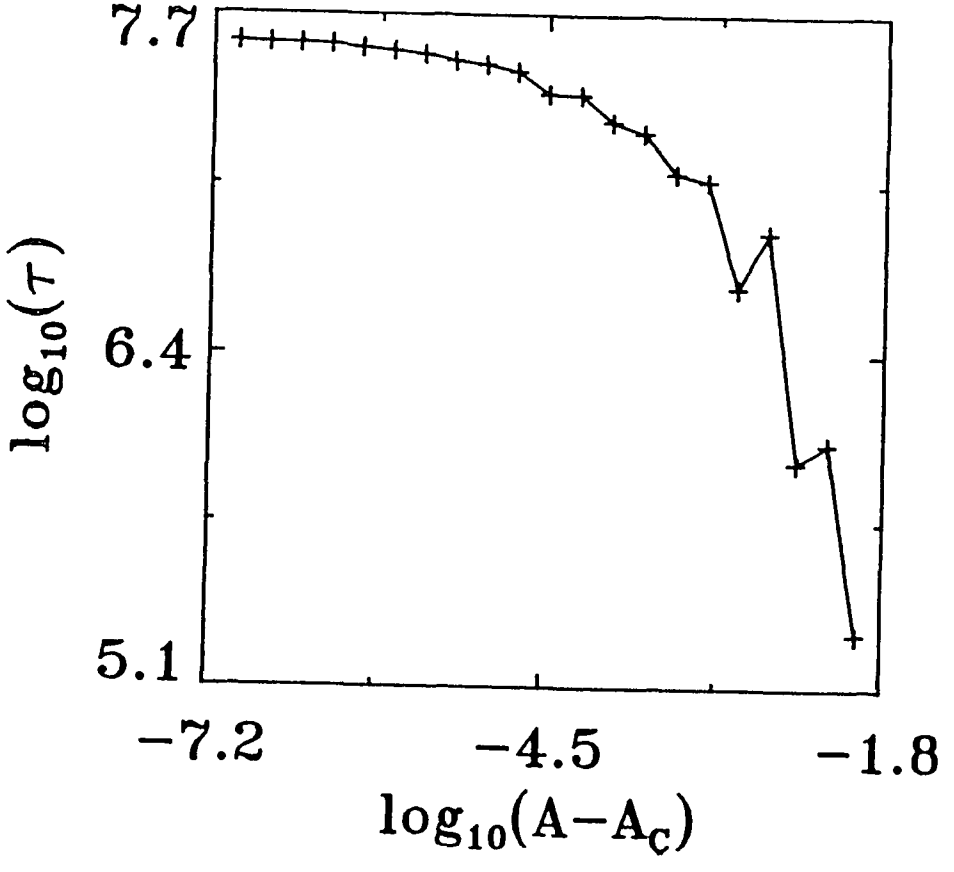

FIG. 5.16. $\mathrm{Log}_{10}\tau$ vs $\mathrm{Log}_{10}(A-A_c)$. The slope is $\gamma=0.049\pm0.005$.

The result of a numerical experiment to determine γ is shown in Fig 5.16. For $10^{-8} < (A-A_c) < 10^{-4.5}$ the computed critical exponent is $\gamma=0.049\pm0.005$. Significantly less then the minimum of 1/2 for both types of crisis. In this cases the attractor before and after the intermittency is dissipative The reason for the small values of γ is apparent from Fig. 5.16, once an intermittent burst has started it is quickly terminated by colliding with another piece of the attractor. This new type of intermittency only takes place for an attractor with more than one piece and is due to the direction of the unstable manifolds. A second example of this type of intermittency will be illustrated in Sec. 5.6.2 between a dissipative and a non-dissipative attractor.

5.5.2 Evolution

Of specific interest here is the evolution of the chaotic attractors of Eq. (5.20) for the parameter value A in the range A=1.8932-1.8965 The chaotic development we shall consider here involves the transition from a strange attractor, with a one dimensional unstable and stable manifold, to an attractor with a two dimensional unstable manifold We first examine the Lyapunov exponents, the corresponding Lyapunov dimension and the correlation dimension for different values of the parameter A. More specific information about the chaotic attractor can be obtained by examining the unstable periodic orbits (see Table 5.4)

Five pieces of a period 90 chaotic attractor are shown in Fig. 5.17 (a). A Period 90 orbit is located on the attractor. Other orbits shown are of period 18 and 36. For A greater than A_c there is another coexisting attractor with its own basin of attraction. These two coexisting attractors merge together to form the attractor in Fig. 5.17 (b) at A=1.8938. Orbits of period 18 and 36 are located on this attractor which has a dimension D_L=1.36. It should be noted from Table 5.4 that one of the period 18 orbits has the maximum D_L=2.0.

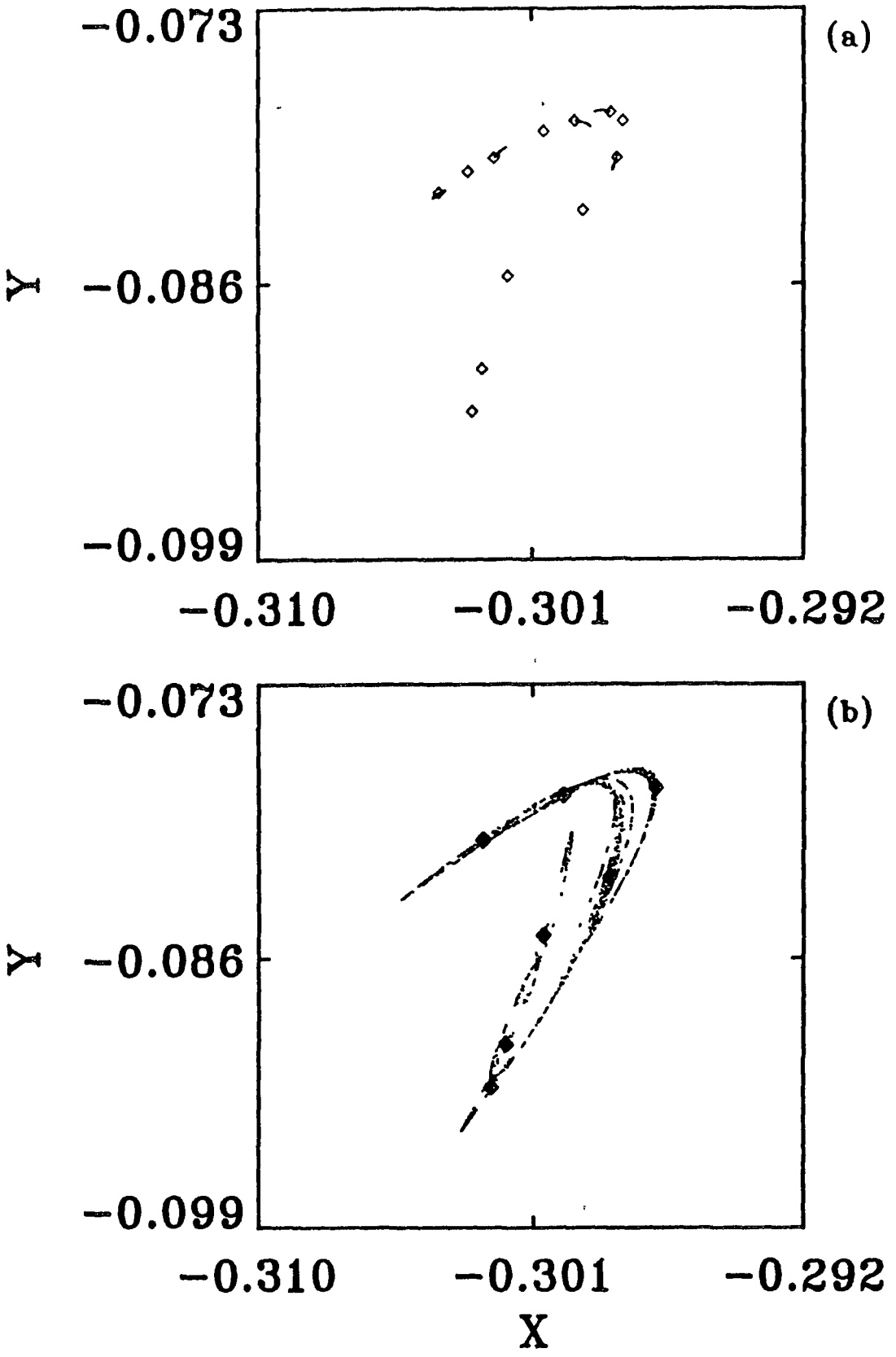

FIG. 5.17. The attractors for (a) A=1.8932, (b) A=1.8938.

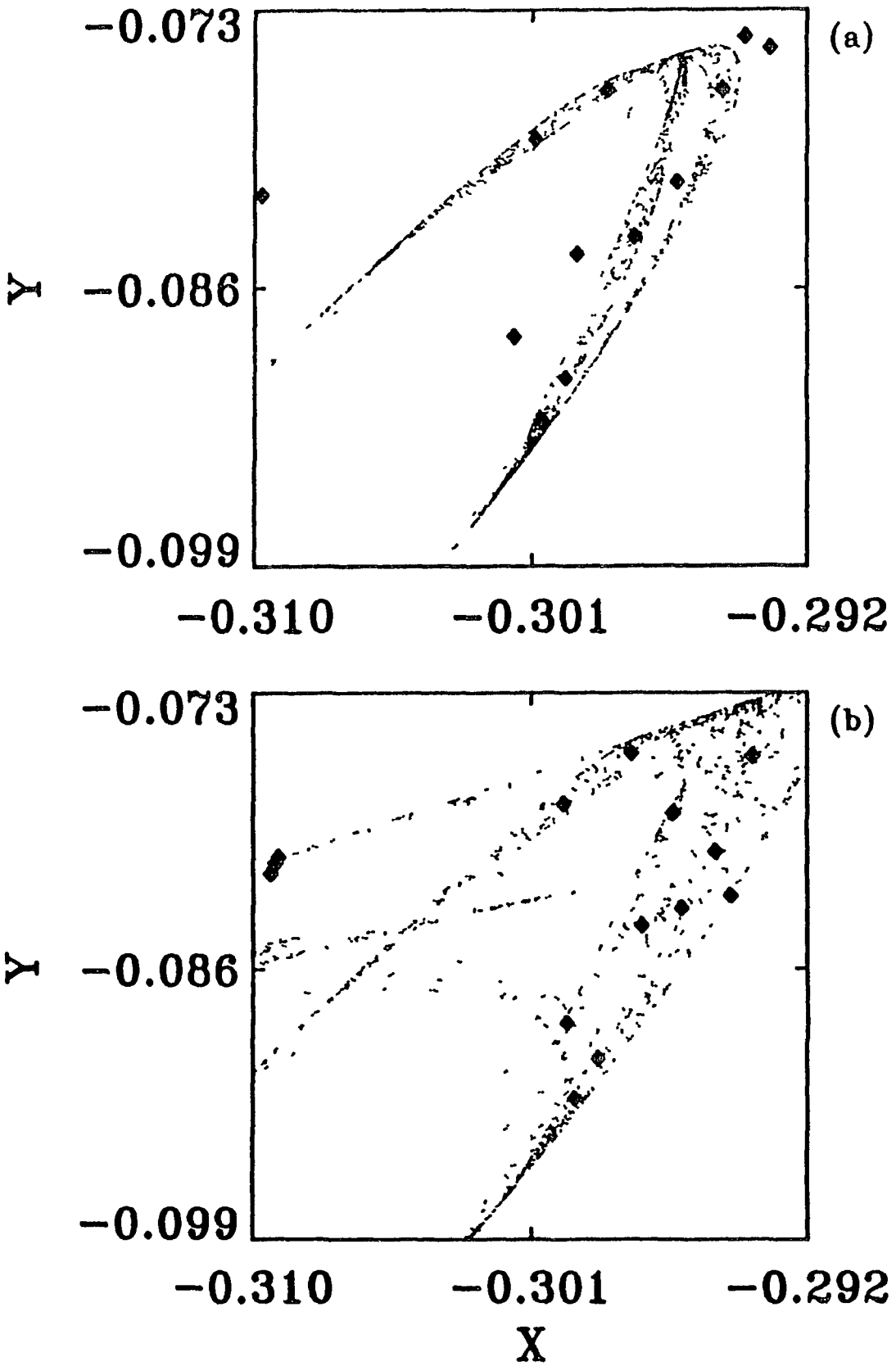

FIG. 5.18. The attractors for (a) A=1.8955, (b) A=1.8965.

Table 5.4

Summary of periodic orbits stability for a range of values of A

A	Period	λ_1	λ_2	D_{orbit}	D_2
1.8932	90	0.0119	−0.0655	1.182	
	90	0.0158	−0.0689	1.229	
	⋮	⋮	⋮	⋮	
	∞	0.0065	−0.0596	1.109	1.06
1.8938	18	0 0434	−0 0587	1.739	
	18	0.0435	−0.0591	1.735	
	18	0.0527	−0.0476	2	
	36	0 0433	−0.0498	1.868	
	36	0 0434	−0 0501	1.867	
		·	⋮	⋮	
	∞	0 0286	−0 0732	1.391	1.36
1.8955	18	0.0613	−0.0334	2	
	18	0.0613	−0.0336	2	
	18*	0.0654	−0.0017	2	
	36	0 0630	−0.0071	2	
	36	0 0629	−0.0071	2	
	⋮	·	⋮	⋮	
	∞	0 0446	−0.0375	2	1.55
1.8965	18	0 0695	−0.0213	2	
	18	0 0694	−0.0207	2	
	18	0 0750	−0 0437	2	
	18	0 0736	0.0152	2	
	18	0 1077	0.0172	2	
	36	0 1076	−0.0180	2	
	36	0 0719	0.0047	2	
	36	0 0775	0.0004	2	
	36	0 0718	0.0041	2	
	36	0.0864	−0.0471	2	
	36	0 0863	−0.0471	2	
	36	0.0778	0.0003	2	
	⋮	⋮	⋮	⋮	
	∞	0.0608	−0.0331	2	≈2
1.9500	∞	0.2746	0.0933	2	≈2

In Fig. 5 18 (a) the attractor is shown for the parameter value A=1.8955. Orbits of period 36 not previously present exist outside the attractor. The period 18 orbit ceases to be on the attractor in Fig. 18 (a) due to the decrease in the magnitude of the Lyapunov exponent λ_2 (denoted by a * in Table 5.4). The global structure of the attractor has increased in complexity. The Lyapunov dimension of this attractor is D_L=2 while the correlation dimension is D_2 = 1.55.

At A=1 8965 in (b) the attractor has expanded to include those orbits on the fringes. A gradual merging of the 18 pieces into 6 pieces has taken place and there is no structure in this attractor due to the fact that $\lambda_1+\lambda_2>0$ with the dynamics taking place on a surface. Figures 5.17 to 5.18 have shown the gradual evolution of structure for the parameter range A=1.8933 to 18965. The dimensions D_L and D_2 have both increased from 1 to the maximum value 2. At A=1.95 there is an one piece attractor which occurs through a process of merging.

5.6 DISPPREY MAP

Two more intermittent examples will be presented. The first is an example of a transition from a stable periodic attractor to a chaotic one. This is the type of intermittency considered by Pomeau and Manneville (1980). The second example substantiates the result obtained in Sec. 5.5.1 for the value of the critical exponent $\gamma \ll 1/2$, with γ=1/2 being the minimum for both the homoclinic and heteroclinic tangency discussed in Sec. 5.2. The following map is chosen (Maynard Smith 1986), and is referred to as the dispprey map

$$\begin{aligned} X_{i+1} &= A\,X_i(1-X_i) - X_iY_i \\ Y_{i+1} &= X_iY_i/B \end{aligned} \qquad (5.21)$$

As the parameters are varied in Eq. (5.21) the solutions undergo a remarkable sequence of bifurcations, ranging from

simple to highly complex chaotic attractors. B is fixed at 0.31.

5.6.1 Type 2 Intermittency

The intermittent transition from a periodic to a chaotic attractor is classified into three types. Type 1 occurs when a eigenvalue crosses a unit circle at (+1); type 2: complex crossing, and type 3; crossing at (-1). Type 1 is a saddle node bifurcation, type 2 a Hopf bifurcation and type 3 an inverted period-doubling bifurcation. At A=3.57 there is a stable periodic attractor of period 62 with two negative Lyapunov exponents. Intermittent bursting consisting of laminar and chaotic regions occurs as A is increased through the critical value A_c= 3.5701978616... The chaotic attractor and the periodic attractor are shown in Fig. 5.19 (a) for A > A_c. A numerical calculation of the critical exponent, γ, is shown in (b). The estimated γ = 0 206±0.003. An examination of the Lyapunov exponents of the period 62 orbit at A_c indicates that the exponents are complex conjugates. Although this intermittency has been classified as type 2, this is the first observation of intermittency between a periodic and a non dissipative surface attractor. A theoretical verification of the numerical exponent, γ, is required.

5.6 2 Intermittency Between a Dissipative and a Non-Dissipative Attractor.

Shown in Fig. 5 20 (a) is one piece of a 15 piece chaotic attractor for A=3.740921008... Each piece is visited sequentially. As A is reduced the critical value for intermittency is A_c=3.740921006... Figure 5.20 (b) shows the chaotic attractor after crisis for A=3.74 <A_c. This is a non dissipative attractor with dimension D_L=2. Before the crisis the Lyapunov exponents are λ_1=0.032 and λ_2=-0.064, with dimension D_L=1.5. It is interesting to note that the period 15 orbit located on the attractor is non

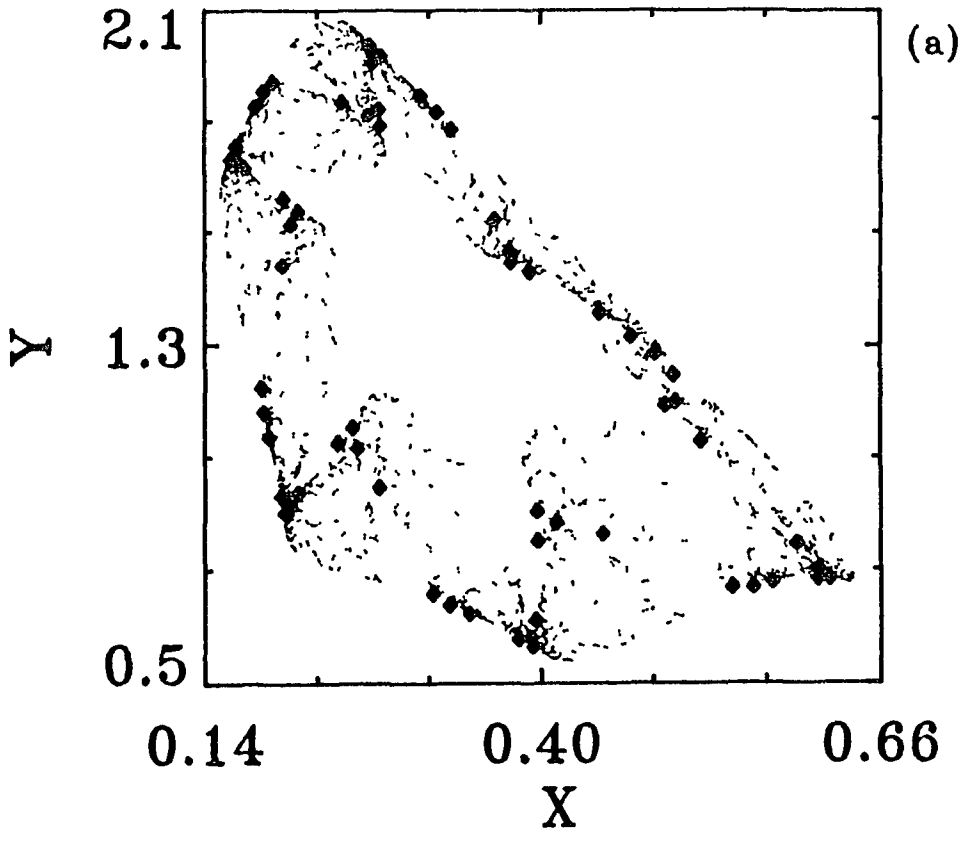

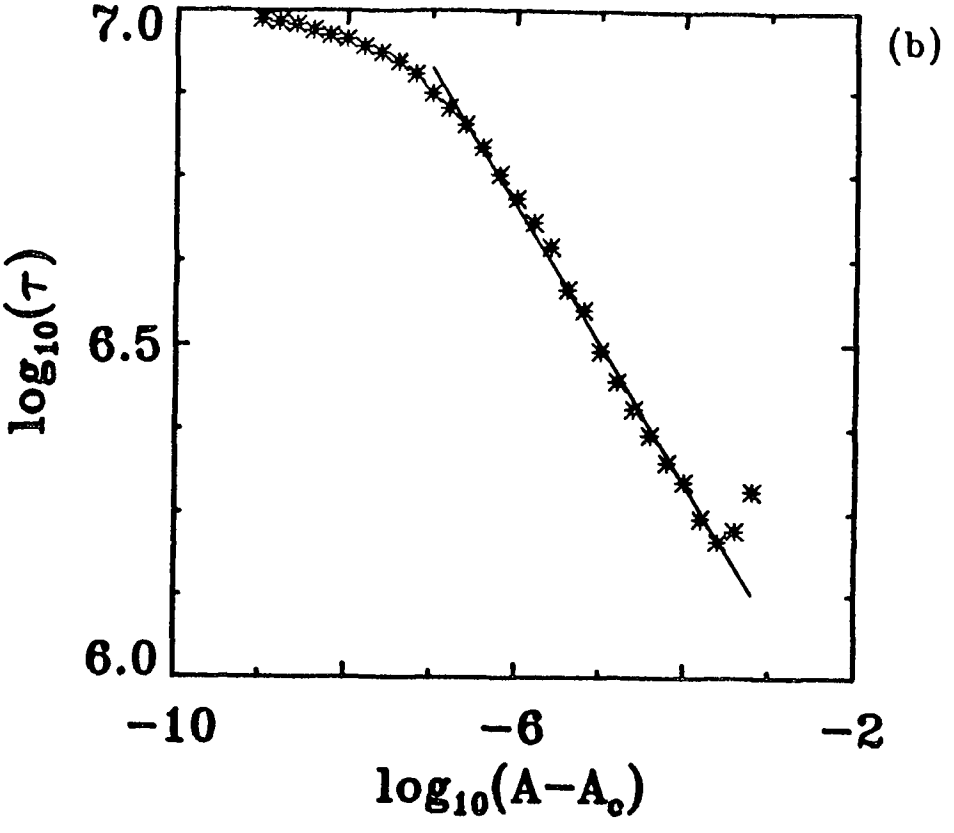

Fig. 5.19. (a) Attractor for the Dispprey map at A=3.575 >A_c. Also located on this plot is a period 62 orbit. (b) $Log_{10}\tau$ vs $Log_{10}(A-A_c)$. The computed value is γ=0.206±0.003.

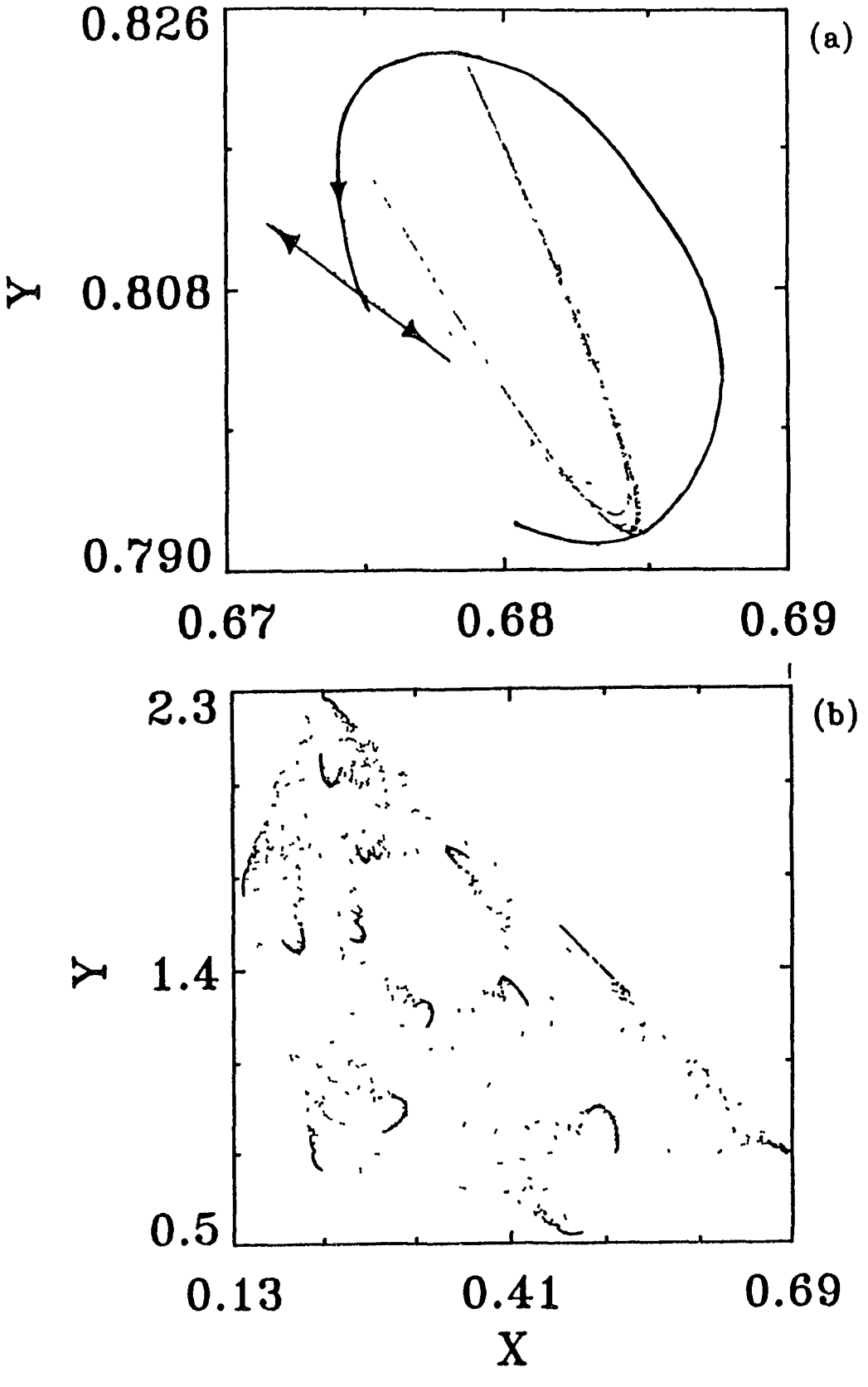

Fig. 5.20. (a) Piece of period 15 attractor for the Dispprey map at A=3.740921008 $>A_c$. (b) Attractor after crisis, A=3.74 $<A_c$

dissipative with exponents λ_1=0.045 and λ_2=−0.037 (compare with Warwick map, table 5.4 at A=1.8955). Consecutive orbits on the attractor have periods that are multiples of 15, with D_L<2. The period 15 orbit that collides with the attractor is also shown in (a), with its stable and unstable manifolds. This orbit has Lyapunov exponents λ_1=0.073 and λ_2=−0.163 with D_L=1.45. The stable manifold of this orbit bound the attractor. Intermittent bursting occurs when an trajectory crosses the stable manifold shooting out along the unstable manifold. This is described as a heteroclinic tangency. A numerical calculation of the critical exponent gives γ=0.0007±0.0002 for 10^{-8}< $\log_{10}(A_c-A)$ <$10^{-3.5}$. This magnitude of γ indicates short transitions to the non dissipative attractor. Upon shooting out along the unstable manifold the trajectory quickly collides with another piece of the period 15 chaotic attractor. In this example a heteroclinic tangency has been identified, a period 15 orbit's stable manifold bounds the attractor and another orbits of period 15 on the attractor is non-dissipative. The eigenvalues of the attractor give γ=1.0, for a heteroclinic tangency (Eq. (5.3)), in total disagreement with the numerical γ. As A is increased past 3.741 intermittent bursting also occurs. Small parameter windows exist, consisting of periodic and chaotic attractors of different structure. This has prevented the calculation of the critical value A_c and hence, a comparison of the numerical exponent γ with the theoretical γ.

5.7 UNSTABLE PERIODIC ORBITS AND THE SYMBOLIC DYNAMICS

In the case of the baker map the extraction of the periodic orbits and the identification of each orbit by a unique symbolic name was a useful method for the characterization of the topology of the attractor. In this framework each periodic orbit X_p, p=1,...,n of period n is identified by a symbol name S_p, p=1,...,n, where for the

baker map S_p can take on two symbolic values such as 0 and 1. This is usually done by dividing the phase space into two or more regions and giving each one of them a symbolic name

Two methods have been proposed for partitioning the attractor. Grassberger and Kantz (1985) studied the Henon map and constructed the partition by first calculating a set of points of homoclinic tangencies (between stable and unstable manifolds), then choosing a subset of them as primary tangencies and connecting them with a line. For the parameter values they studied, this line provides a good partition in the sense that, each periodic orbit has a unique symbolic sequence.

In the method of Biham and Wenzel (1989) the symbolic sequence is chosen and the associated periodic orbit is then calculated. Thus, the construction of the partition is an integral part of the process. They proceed as follows. For the Henon map Eq (5.8)

$$F_i(\mathbf{X}) = -X_{i+1}+1 -aX_i^2 +bX_{i-1} \qquad (5.22)$$

A system of coupled differential equations is assumed

$$\frac{dX_i}{dt} = S_i F_i(\mathbf{X}) \qquad i=1,...n , \qquad (5.23)$$

with periodic boundary conditions $X_{n+1}(t)=X_1(t)$ For the Henon map $S_i=\pm 1$. If $F_i=0$ then X_i is an orbit of the Henon map. Thus, periodic orbits of the Henon map correspond to stationary solutions of (5 23) Grassberger and Kantz (1989) discuss some of the limitations of the above technique.

When this technique is applied to the three dimensional Henon map Eq. (5 16), the partition is a two dimensional manifold in a three dimensional phase space and thus hard to construct and visualize. Primary tangencies could not be used to construct a partition for the four piece chaotic attractor shown in Fig. 5.6 (a) with A=1.2 and B=0.17

In the Henon map the number of periodic orbits of period n is less than 2^n. The above technique can be

modified to calculate orbits in a system where the total number is $\leq 4^n$. Consider the Ushiki map Eq. (5.19) four symbols are required to represent the dynamics say 0,1,2,3. Each of the four fixed points are represented by one of these symbols. The coupled differential equations are given as follows;

$$\begin{aligned} \frac{dX_i}{dt} &= S_i[-X_{i+1} + (A - X_i - B_1 Y_i)X_i] \\ \frac{dY_i}{dt} &= T_i[-Y_{i+1} + (A - Y_i - B_2 X_i)Y_i] \end{aligned} \tag{5.24}$$

for $i=1,\ldots,n$ with boundary conditions $X_{n+1}(t)=X_1(t)$ and $Y_{n+1}(t)=Y_1(t)$ Two differential equations have to be used. The coefficients S_i and T_i are both ± 1. For example to calculate S_i and T_i for a particular orbits of period 4, of which there is a possible 256, a symbolic sequence is chosen say 3231 in binary form this is 11101101. Converting the 0's to -1's the S_i's and T_i's are given by $(S_1,T_1,S_2,T_2,S_3,T_3,S_4,T_4) = (1,1,1,-1,1,1,-1,1)$. The above calculations were implemented for the attractor at A=3.6 (similar to Fig. 5 11 (b)) The attractor is partitioned into four regions The partition is unique in the sense that each orbit has a unique symbolic sequence. It should be noted that for this particular attractor homoclinic tangencies can not be calculated.

5 8 CONCLUSION

In summary intermittent crisis, due to a heteroclinic tangency has been investigated. This type of crisis occurs when the stable manifold of an unstable periodic orbit collides with the chaotic attractor. Two types of heteroclinic crises have been observed by examining the statistical behaviour near each crisis point. For the first type the observed behaviour agrees with a theoretical model based on the stability of an unstable periodic orbit, despite the fact that one of the attractors is a non-dissipative surface attractor. The second type of crisis produces a numerical γ less than the theoretical γ.

Crises have been analyzed where the numerical γ is significantly less than the minimum theoretical value of $\gamma=1/2$ for both a homoclinic and heteroclinic tangency. This type of crisis only occurs for multiple piece attractors regardless of whether the attractor is dissipative or non-dissipative The placing of the colliding orbit's unstable manifold in relation to the pieces of the attractor has a profound effect on the critical exponent γ. Further study is needed in order to obtain a theoretical understanding of this particular crisis. This type of crisis is likely to be encountered in experimental simulations similar to the coupled nonlinear oscillators of Buskirk and Jeffries (1985)

Although the theory of Grebogi et al. (1987) has been confirmed to apply for some crises in non-dissipative systems the following inconsistencies have been found

(i) clear evidence has been obtained to show that for a heteroclinic tangency periodic orbit's (B) and (C) need not be of equal period, even when the stable manifold of periodic orbit (B) bounds the attractor (Sec 5.4.1).

(ii) the distinction between a heteroclinic and homoclinic tangency is not obvious particularly in light of the example in Sec.'s 5.4.1, 5.4.3 and 5.5.1.

(iii) although an attractor may be dissipative the individual orbits on the attractor need not be dissipative as in the examples of Sec.'s 5.5.2 and 5.6 2, this has obvious limitation for a heteroclinic tangency.

(iv) the unstable manifolds of the individual orbits on the attractor can not be isolated from the attractor.

The non-dissipative surface attractors with two positive Lyapunov exponents, encountered in these two dimensional maps can be thought of as arising from three dimensional dissipative maps. Dimension calculations for these surface attractor are consistent with the following inequality $D_2 \leq D_L \leq D_0$ and attractors have been found where

$D_2=D_L=2$ with 2 been the maximum dimension of a surface. This is substantiated by the absence of structure in the attractor. The evolution of chaos in these maps is consistent with the analytic results for the baker map of Sec. 4.2

A numerical technique has been extended to calculate unstable periodic orbits for a system requiring four symbols This technique has been applied to the Ushiki map, a good partition is obtained in the sense that each orbit has a unique symbolic label

CHAPTER 6

POINCARE MAPPINGS OF DIFFERENTIAL EQUATIONS

6.1 INTRODUCTION

The idea of reducing the study of a continuous time system (flows) to the study of an associated discrete time system (maps) is due to Poincaré (1899) who first utilized it in his studies of the three body problem in celestial mechanics The problem is defined as: given a three dimensional chaotic differential system, find a two dimensional map from which it originates. The objective of this chapter is to examine the circumstances under which it is possible to construct a global map. The Wiggins (1991) approach is the construction of a local map about some fixed point. Bernussou (1977) constructs approximate maps for nonlinear differential systems with periodic coefficients These maps are used to examine local properties One area not considered is Hamiltonian systems where the forcing is through Dirac impulses. For this type of system, maps are routinely constructed (Lowenstein (1991) and Normura et al. (1992)). The chapter is organized as follows; In section 6.2 three dimensional differential systems are introduced together with their Poincaré return maps which are obtained numerically. Section 6.3 considers the possibility of constructing a Poincaré map from a numerical and analytic standpoint.

6 2 DIFFERENTIAL SYSTEMS

The following set of coupled differential equations have been used by Rabinovich and Fabrikant (1979) to model a plasma.

$$dX/dt = Y(Z - 1 + X^2) + \gamma X$$
$$dY/dt = X(3Z + 1 - X^2) + \gamma Y \qquad (6.1)$$
$$dZ/dt = -2Z(\alpha + XY)$$

The Jacobian determined is given as $2(\gamma-\alpha)$. With the parameters chosen to be γ=0.87 and α=0.11. The phase space solution obtained numerically is shown in Fig. 6.1 (a) with the corresponding Poincaré section in (b). The Poincaré section is constructed from the set of points that intersect the surface Y=−1 with dY/dt>0. The correlation dimensions are D_2=2.19 for (a) and D_2=1.19 for (b).

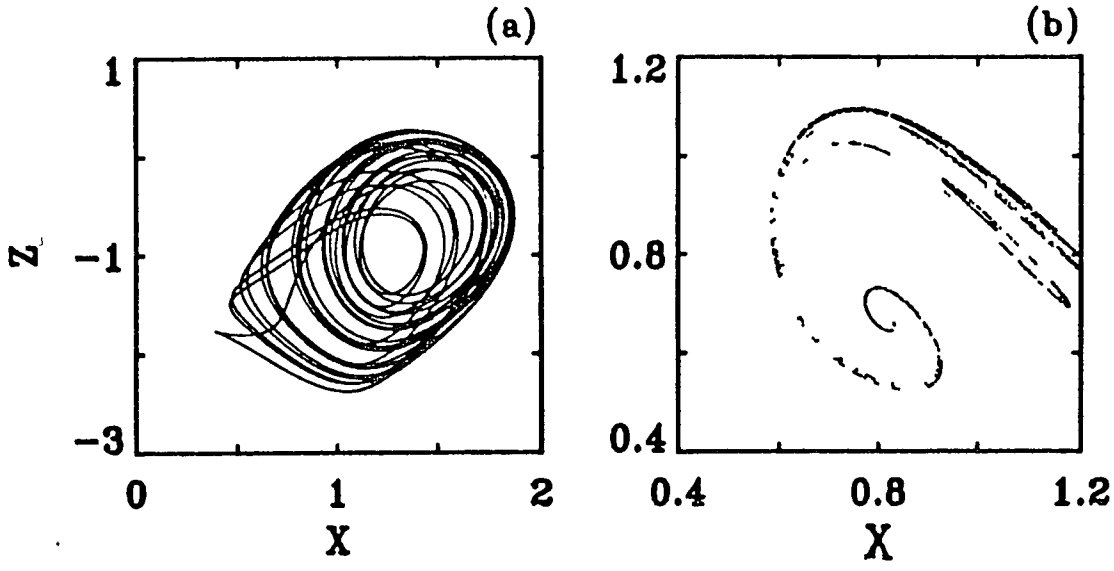

FIG. 6.1. (a) The phase space attractor for Eq. (6.1) plotted in the X–Z plane. (b) The Poincaré section.

The Japanese oscillator equations are defined as

$$dX/dt = Y$$
$$dY/dt = X - X^3 - AY + BCos(t) \qquad (6.2)$$

with A=0.1 and B=10. This is a periodically forced oscillator with a cubic stiffness term. It is an nonautonomous system in $\mathbb{R}^2$. However, the appropriate phase space to use is $\mathbb{R}^2 * S$ since the third variable, time figures into the system as the argument of the periodic function. Its phase space and Poincaré section are shown in Fig. 6.2 (a) and (b) respectively. The Poincaré section is constructed from the set of points $X(2n\pi)$, $dX(2n\pi)/dt$. In

the next section the possibility of obtaining a functional set of discrete equations for these numerical Poincaré maps is examined.

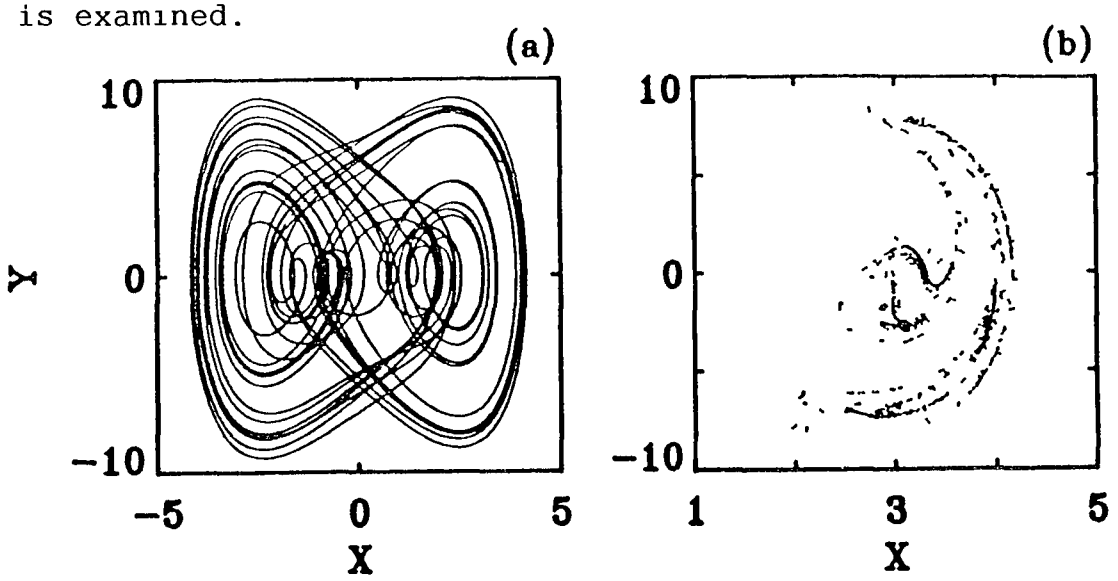

FIG. 6.2. (a) The phase space attractor for Eq. (6.2) plotted in the X–dX/dt plane. (b) The Poincaré section.

6.3 POINCARÉ MAPS

The construction of a Poincaré section reduces the dimension of the system by one. The goal is to produce a map that corresponds to the differential system as the control parameter is varied. The behaviour of the solution of maps presents more variety than those of differential equations of the same order. For instance in maps there is the case of an eigenvalue equal to -1, whereas there is no analog of this in differential systems. Due to sensitive dependence on initial conditions the chaotic solutions of the discrete and continuous systems would diverge. How rapidly the two solutions would diverge would depend on the magnitude of the positive Lyapunov exponents. Two approaches will be adopted: (a) construct the Poincaré section from the differential system numerically and use a curve fitting routine to obtain the equations for the map and (b) use analytic methods to construct equations from the differential system. The former method is equivalent to

forecasting the future of a continuous system using a discrete system, Farmer and Sidorowich (1987).

6.3.1 Construction of a Poincare Map

Given a time series (X_i, Y_i) i=1,N the equations are constructed as follows. Assume knowledge of the general form of the equations. For a second order polynomial would have the form

$$\begin{aligned} X_{i+1} &= \alpha_1 X_i^2 + \alpha_2 Y_i^2 + \alpha_3 X_i Y_i + \alpha_4 X_i + \alpha_5 Y_i + \alpha_6 \\ Y_{i+1} &= \beta_1 X_i^2 + \beta_2 Y_i^2 + \beta_3 X_i Y_i + \beta_4 X_i + \beta_5 Y_i + \beta_6 \end{aligned} \tag{6.3}$$

By randomly selecting six points from the attractor together with their consecutive points the above 12 equations can be solved for the unknown coefficients α_i and β_i, using a standard mathematical routine. The validity of this construction has been tested by applying it to some well-known dynamical systems; The Henon Map Eq. (5.8) and the Ushiki Map Eq. (5.17) which are second order polynomials and the Warwick Map Eq. (5.20) a third order polynomial. In each case all coefficients have been obtained to a specified accuracy. The construction is independent of the data points used and the order of the polynomial above a critical value, periodic or chaotic data sets may be used The main limitation of this method is that the form of the equations are required for the construction. Giona et al (1991) uses a construction method that does not need any kind of parameter fitting, and is used to examine local prediction of chaotic times series. Baake et al. (1992) use a boundary-value-problem approach for fitting ordinary differential equations to chaotic data. Although twelve data points are sufficient for a second order polynomial construction, a least square fitting routine can be implemented which uses a predetermined number of data points, the results are not improved for the above three test sets.

When these methods are applied to Poincaré sections obtained from Eq. (6 1) and (6.2) no functional map is

obtained. To rule out the possibility that the map can not be constructed due to sensitive dependence on initial conditions the construction was implemented for periodic orbits. Due to the difficultly in obtaining periodic orbits of large period only second and third order polynomials were used. Again no map was obtained. To examine the reasons for this failure, analytic methods will now be considered

6.3.2 Poincare Map of Quasiperiodic Orbits

Consider the second order linear differential equation

$$\frac{d^2X}{d^2t} + A\frac{dX}{dt} = B\sum_{i=1}^{N} Cos\ (\sqrt{i}t) \qquad (6.4)$$

with periodic forcing. A=0.2 and B=0.3. For N=3 we have three incommensurable frequencies ($\sqrt{1}/2\pi, \sqrt{2}/2\pi$ and $\sqrt{3}/2\pi$) and the motion is on a 3-torus while, for N=2 the motion is on a 2-torus Our goal here is to study the nature of the solutions of Eq. (6.4) in the context of Poincaré maps. Recall (see Wylie and Barrett (1982)) that the general solution of Eq (6.4) is the sum of the solution of the homogeneous equation B=0 and a particular solution B≠0.

The homogeneous solution is $X_h(t)$ with characteristic equation

$$m^2 + A\ m = 0 \qquad (6.5)$$

and since the roots are $m_1=0$ and $m_2=A$, the solution is

$$X_h(t) = C_1 + C_2e^{-At} \qquad (6.6)$$

The particular solution $X_p(t)$ is of the form

$$X_p(t) = \sum_{i=1}^{N} \alpha_i Cos\ (\sqrt{i}t) + \beta_i Sin\ (\sqrt{i}t) \qquad (6.7)$$

The constants α_i and β_i are determined by substitution and are given by

$$\alpha_i = \frac{-B}{(i+A^2)}\ ,\quad \beta_i = \frac{AB}{\sqrt{i}(i+A^2)} \qquad (6.8)$$

As $t\longrightarrow \infty$, $X_h(t) = C_1+C_2$. We will set C_1 and C_2 to zero. Therefore the phase space solution is

$$X(t) = \sum_{i=1}^{N} \alpha_i \text{Cos}\ (\sqrt{i}t) + \beta_i \text{Sin}\ (\sqrt{i}t)$$
$$Y(t) = \sum_{i=1}^{N} -\alpha_i \sqrt{i}\ \text{Sin}\ (\sqrt{i}t) + \beta_i \sqrt{i}\ \text{Cos}\ (\sqrt{i}t) \qquad (6.9)$$

where $Y(t) = dX(t)/dt$. The Poincaré map is constructed from the set of points $(X(t),Y(t))$ for $t=2\pi n+\phi$ where n is an integer, and $\phi \in (0,2\pi)$. By varying ϕ we can select different Poincaré maps. For $\phi=0$ the co-ordinates of the points on the Poincaré map are given by

$$X_n = \sum_{i=1}^{N} \alpha_i \text{Cos}\ (\sqrt{i}2\pi n) + \beta_i \text{Sin}\ (\sqrt{i}2\pi n)$$
$$Y_n = \sum_{i=1}^{N} -\alpha_i \sqrt{i}\ \text{Sin}\ (\sqrt{i}2\pi n) + \beta_i \sqrt{i}\ \text{Cos}\ (\sqrt{i}2\pi n) \qquad (6.10)$$

where $X_n = X(2\pi n)$ and $Y_n = Y(2\pi n)$. The Poincaré map is defined as

$$X_{n+1} = F(X_n, Y_n) \text{ and } Y_{n+1} = G(X_n, Y_n) \qquad (6.11)$$

What remains is to determine the functions F and G. The phase space solutions for N=2 is shown in Fig. 6.3 (a) with the corresponding Poincaré map in (b).

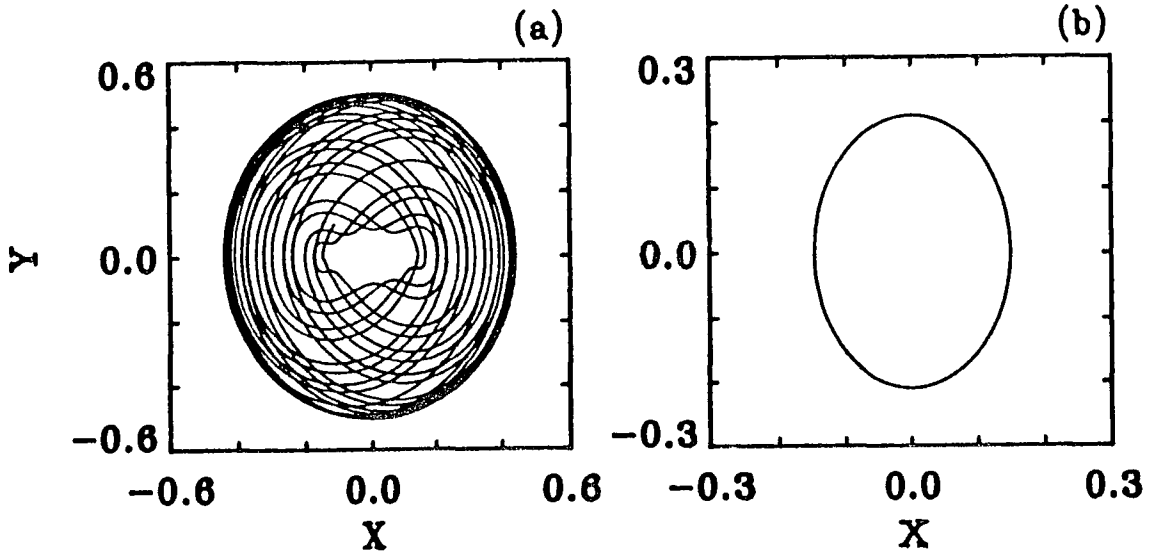

Fig. 6.3. (a) Phase space solution for a 2 torus and (b) the Poincaré section

For N=2 the Poincaré map of the quasiperiodic orbit is an invariant ellipse defined by the following map

$$X_{n+1} = X_n \cos(\sqrt{8}\pi) + Y_n \sin(\sqrt{8}\pi)/\sqrt{2}$$
$$Y_{n+1} = -\sqrt{2}\, X_n \sin(\sqrt{8}\pi) + Y_n \cos(\sqrt{8}\pi) \qquad (6.12)$$

This map was obtained by substituting Eq. (6.10) into Eq. (6.11). The constants α_1 and β_1 have been neglected since they only off set the ellipse and do not effect the dynamics. The initial conditions for this map (X_0, Y_0) are related to the parameter ϕ. Different initial conditions correspond to different invariant ellipses. The fixed point is at the origin with complex eigenvalues given by $\cos(\sqrt{8}\pi) \pm j\sin(\sqrt{8}\pi)$. As expected the modulus of the eigenvalues are one.

The phase space solutions for N=3 is shown in Fig. 6.4 (a) with the corresponding Poincaré map in (b). For N=3 no Poincaré map can be formulated from Eq. (6.11).

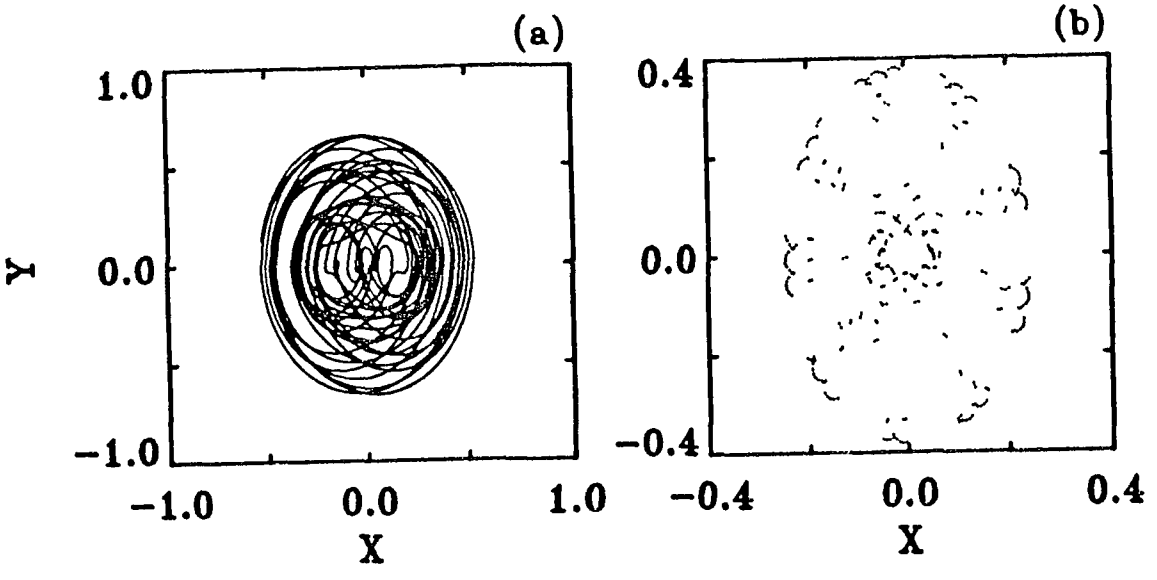

Fig. 6.4. (a) Phase space solution for a 3 torus and (b) the Poincaré section.

The reason for this can be explained with the following example. Consider the Legendre's differential equation

$$tX'' + (1-t)X' + nX = 0 \qquad (6.13)$$

where n is a positive integer. It is a second order autonomous system in $\mathbb{R}^3$. For n=3 the polynomial solution is given by

$$X(t) = 6-18t+9t^2-t^3$$
$$Y(t) = -18+18t-3t^2 \qquad (6.14)$$

where $Y(t)=dX/dt$ Although all solutions of Eq. (6.13) are infinite for large t, is there a map which describes this approach to infinity. The Poincaré map consists of those points for which t is an integer. Is there function F and G such that

$$(-4-3t+6t^2-t^3) = F\{(6-18t+9t^2-t^3),(-18+18t-3t^2)\}$$
$$(-3+12t-3t^2) = G\{(6-18t+9t^2-t^3),(-18+18t-3t^2)\} \qquad (6.15)$$

It is obvious from Eq (6 15) that the forward evolution of the variable X can not be determined from previous discrete values of X.

6.4 CONCLUSION

In this chapter the connection between differential and discrete systems has been examined. It has been shown by means of analytic and numerical considerations that only in a limited number of cases is there a one to one correspondence. These include some linear systems and the well known chaotic differential systems with delta functions.

CHAPTER 7

DELAYED DIFFERENTIAL EQUATIONS

7.1 INTRODUCTION

An first order ordinary differential equation can be written in the form

$$\frac{dX(t)}{dt} = f(X(t)) \tag{7.1}$$

In this equation the function f(X(t)) and its derivatives are all evaluated at the same instance in time t. A more general type of differential equation can be written in the form

$$\frac{dX(t)}{dt} = f(X(t),X(t-\tau)) \tag{7.2}$$

In this case the present rate of change of X(t) depends upon the value at the times t and $t-\tau$ where τ is the delay time. An introduction to linear delayed differential equations (DDE's) can be found in Driver (1977) and references cited within In this book references can be found for DDE's applied to the following problems: control systems, nuclear reactors, neutron shielding, transistor circuits, transmission lines and the production of red blood cells. Delayed differential equations are infinite dimensional, because it is necessary to specify a infinite number of initial conditions to calculate the function X(t) for a time greater than t.

Typical nonlinear differential equations of interest are

$$\frac{dX(t)}{dt} = \frac{aX(t-\tau)}{1+X(t-\tau)^{10}} - bX(t) \tag{7.3}$$

a, b and τ are constants Farmer (1982). This equation was proposed by Mackey and Glass (1977) to model blood production in leukemia patients.

$$\frac{dX(t)}{dt} = \frac{u\pi}{T}\left[1-\varepsilon COS\ [\ X(t-\tau)+X_B\ ] - X(t)\right] \qquad (7.4)$$

u,π,T,X_B,τ, and ε are constants. This equation models a hybrid optical device, Derstine et al (1983).

$$\frac{dX(t)}{dt} = \frac{\pi}{T}\left[A-uSIN^2[\ X(t-\tau)+X_B\ ] - X(t)\right] \qquad (7.5)$$

A,π,T,X_B,τ, and u are constants. This equation models a acoustic optical device, Vallee and Delisle (1985).

$$\frac{dX(t)}{dt} = X(t-\tau)\{A-0.01X(t-\tau)\} - X(t) \qquad (7.6)$$

$$\frac{dX(t)}{dt} = A\ SIN\{X(t-\tau)\} - X(t) \qquad (7.7)$$

A and τ are constants, Olivera and Malta (1987), which arise in biology to describe the isolated population of Drosophila Stervants flies.

The following DDE

$$\frac{dX(t)}{dt} = A\ X(t-\tau)^2\ ^4exp(\ X(t-\tau)^2) - B\ X(t) \qquad (7.8)$$

and Eq. (7.3) and Eq (7 7) are examined in detail in this chapter. The properties of the solution of the nonlinear time-delayed differential equations are investigated as a function of two parameters: the delay τ and the nonlinearity A The structure and evolution of the attractors will be examined while emphasizing the connections with the previous chapters. To date the most extensive numerical study of chaos in a delayed differential equation has been done on the Mackey Glass DDE (cf. Eq. (7.3)) by Farmer (1982).

Numerical integration was carried out with a fourth order Runge-Kutta method The integration step is a function of A and τ. The accuracy of the integration, for some trial cases, was tested by using smaller integration steps and examining the effects on the Lyapunov dimension. A random initial function provides rapid convergence onto the attractor, the results are consistent with a constant initial function.

7.2 EXPERIMENTAL DDE'S

In this section we review experimental results whose time evolution is described by delayed differential equations. In Fig. 7.1 an acoustic optical bistable device is shown The acousto-optic device has delayed feedback and the system is modelled by Eq. (7.5). Experimental details can be found in Chrostowski et al. (1983). The sine squared term in this equation is due to the modulation effect of the acoustic optic crystal.

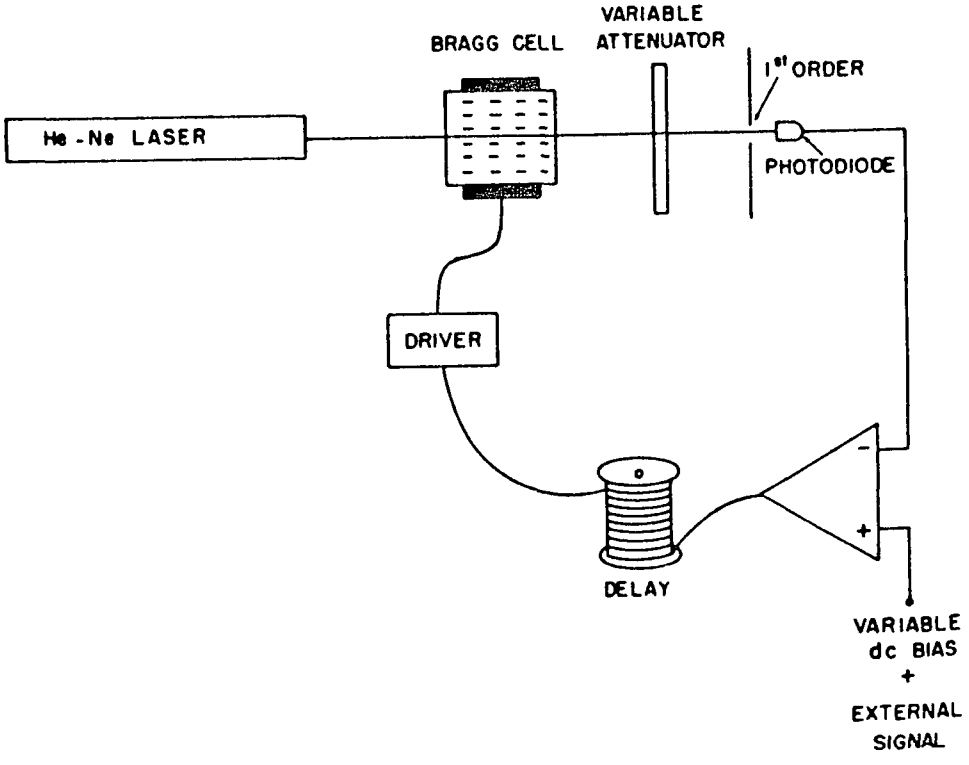

Fig. 7.1. Experimental layout of a delayed acoustic-optic system, (From Vallee and Delisle (1985)).

The universal Feigenbaum constant δ which describes the rate of period doubling has been measured experimentally, Vallee et al. (1985), and found to agree with theory. The bifurcation sequence, in the presence of addictive and multiplicative noise, shows excellent agreement between theory and experiment, Vallee et al. (1984). Periodic windows within the chaotic domain have also shown excellent agreement between experiment and numerical simulations, Vallee and Delisle (1986). An

alternative experiment based on a potassium dihydrogen phosphate (KDP) crystal has been studied by Derstine et al. (1983).

The following result pertains to the chaotic behaviour in the hybrid optical device. Dimension and correlation entropy measurements have been made by Hopf et al. (1986). Measured dimensions were found to be significantly less than dimensions consistent with the Kaplan-Yorke conjecture. When the correlation dimension of a continuous system is plotted as function of the sampling time, there are two plateaus corresponding to the dimension of the Poincare section and the dimension of the complete system. It is possible that inconsistencies in this experimental result could be explained in terms of these plateaus.

7.3 HOPF BIFURCATION

The fact that a DDE in one variable actually describes a time evolution in an infinite dimensional functional space enables it to undergo a Hopf bifurcation, a property that requires at least two degrees of freedom in an autonomous system of ordinary differential equations. A Hopf bifurcation occurs when a parameter in the system is changed resulting in a bifurcation from a fixed point to a limit cycle By examining the stability of this fixed point it is possible to determine the parameter value for this bifurcation. Assume the following general form

$$\frac{dX(t)}{dt} = g(X(t-\tau))-bX(t) \qquad (7.9)$$

The fixed points of this equation are obtained by setting $dX/dt = 0$, and $X(t)=X(t-\tau)=X_p$. A linear stability analysis involves examining the stability about the fixed point X_p:

$$\frac{d\delta X(t)}{dt} = \frac{\delta F}{\delta X(t)}\,\delta X(t) + \frac{\delta F}{\delta X(t-\tau)}\,\delta X(t-\tau) \qquad (7.10)$$

where $F(X(t),X(t-\tau))= g(X(t-\tau))-bX(t)$. The partial derivatives are evaluated at the fixed point X_p.

$$\frac{d\delta X(t)}{dt} = -b\delta X(t) + g'(X_p)\delta X(t-\tau) \qquad (7.11)$$

assume solution of the form $\delta X(t)=X^{*}\exp(\lambda t)$ and $\delta X(t-\tau)=X^{*}\exp(\lambda(t-\tau))$. Substituting into Eq. (7.11)

$$\lambda = g'(X_p)\exp(-\lambda\tau) - b \qquad (7.12)$$

If Eq. (7.12) is separated into its real and imaginary parts, $\lambda=r+iw$, with a little rearrangement it becomes

$$\begin{aligned} r(w) &= - b - w/\tan(w\tau) \\ w(r) &= [\, g'(X_p)^2 \exp(-2r\tau) - (r+b)^2 \,]^{1/2} \end{aligned} \qquad (7.13)$$

Marginal stability occurs when the largest solution is r=0, i.e.

$$\tau = \frac{\tan^{-1}(w(0)/b)}{w(0)} \qquad (7.14)$$

For Eq. (7.3) (with a=0.2, b=0.1 and c=10) a Hopf bifurcation occurs for $\tau>4.53$. Numerically we have found the existence of a Hopf bifurcation for Eq. (7.8) (with A=1.6 and B=0.3) at τ =3.52. Longtin (1991) examines the postponement of the Hopf bifurcation in Eq. (7.3) with the inclusion of additive and multiplicative noise.

7.4 FOURIER ANALYSIS AND PHASE PORTRAITS

The first DDE investigated is

$$\frac{dX(t)}{dt} = A\, X(t-\tau)^{2.4}\exp(\, X(t-\tau)^2) - B\, X(t) \qquad (7.15)$$

Parameter values are A=1.6 and B=0.3. The qualitative changes in the nature of the attractor will be described as the parameter τ is varied. A linear stability analysis shows that, with A given as above, there is a stable fixed point attractor for $\tau<3.52$. For $3.52<\tau<8.75$ there is a stable limit cycle. At τ=8.75, the period of the limit cycle doubles, initiating a period doubling sequence which accumulates at τ=11.65. Olivera and Malta (1987), has verified that the period doubling sequence is characterized by the two universal constants α=2.502907.... and δ=4.66920.... For $\tau>11.65$ numerical simulations show chaotic attractors at most parameter values, with limit cycles interspersed in between. The period doubling route

is the only route observed in the differential equations considered here. Boe and Chang (1991) examine coupled DDE's and observe the quasiperiodic route to chaos both experimentally and numerically. The nature of the periodic solution of DDE's have been extensively studied (Mallet-Paret et al. (1989)). Each of the functions considered here have a negative Schwarzian derivative (Eq. (3.7)) for some of the parameter space τ and A. Using this derivative it is possible to examine the existence and uniqueness of the periodic solutions. Type 3 intermittency has also been observed in a DDE with Gaussian nonlinearity,

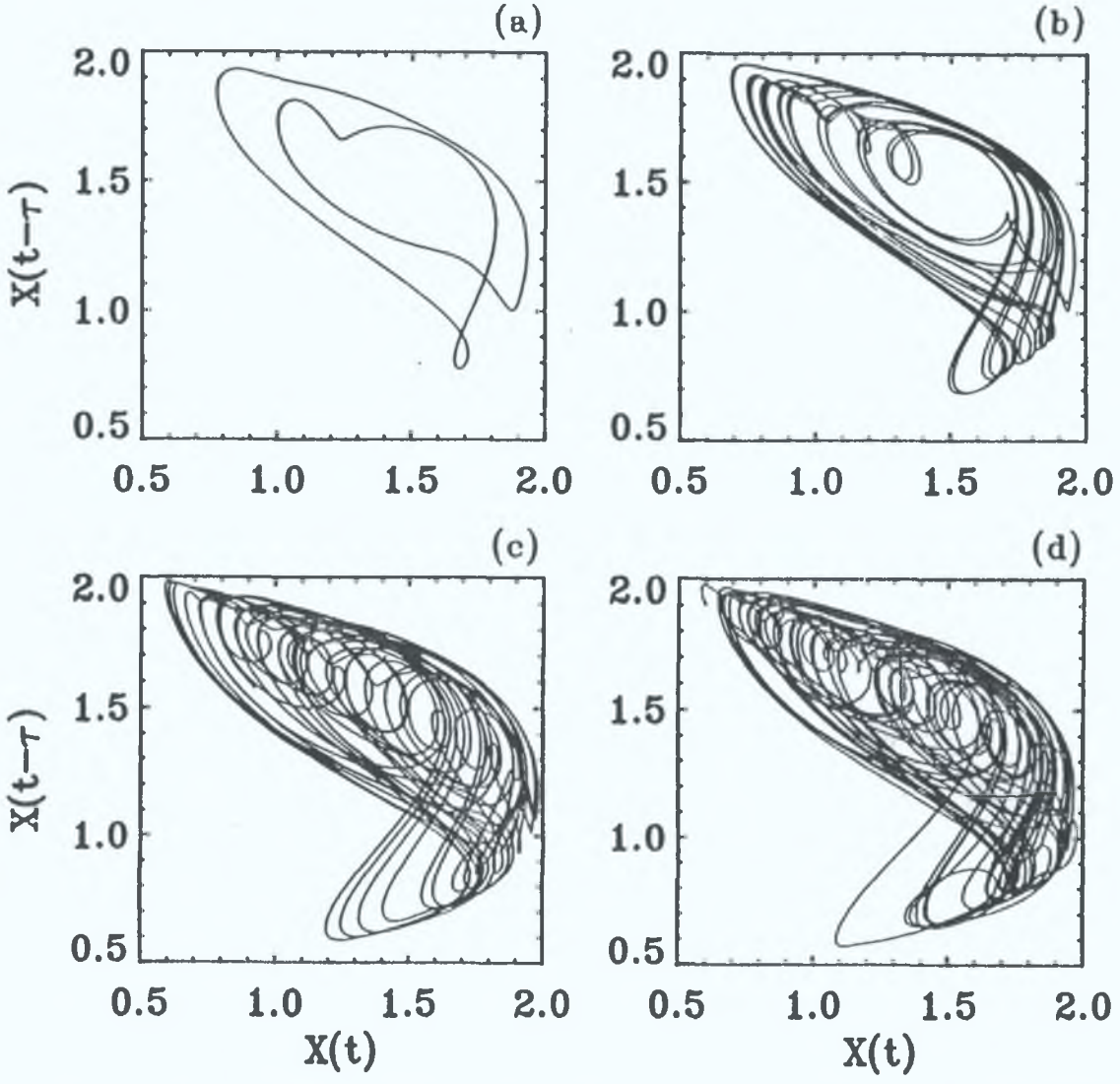

FIG. 7.2. Phase plots obtained by plotting X(t) against X(t−τ) for Eq. (7.8), with A=1.6 and B=0.3. (a) τ=10, (b) τ=12, (c) τ=18 and (d) τ=200, where τ is the delay parameter.

Hamilton (1992).

Phase plots (Fig. 7.2) and power spectra (Fig. 7.3) are employed to study the qualitative nature of the attractor. These are sufficient to distinguish periodic behaviour from chaotic behaviour but provide little information to distinguish between different types of chaotic behaviour. The phase plots are obtained by plotting $x(t)$ against $x(t-\tau)$. Each power spectrum consists of 100 averages of 4096 samples at intervals $\Delta t=5$ time units. The integration step was $\Delta h=0.025$. All power spectra are on a semi-log scale.

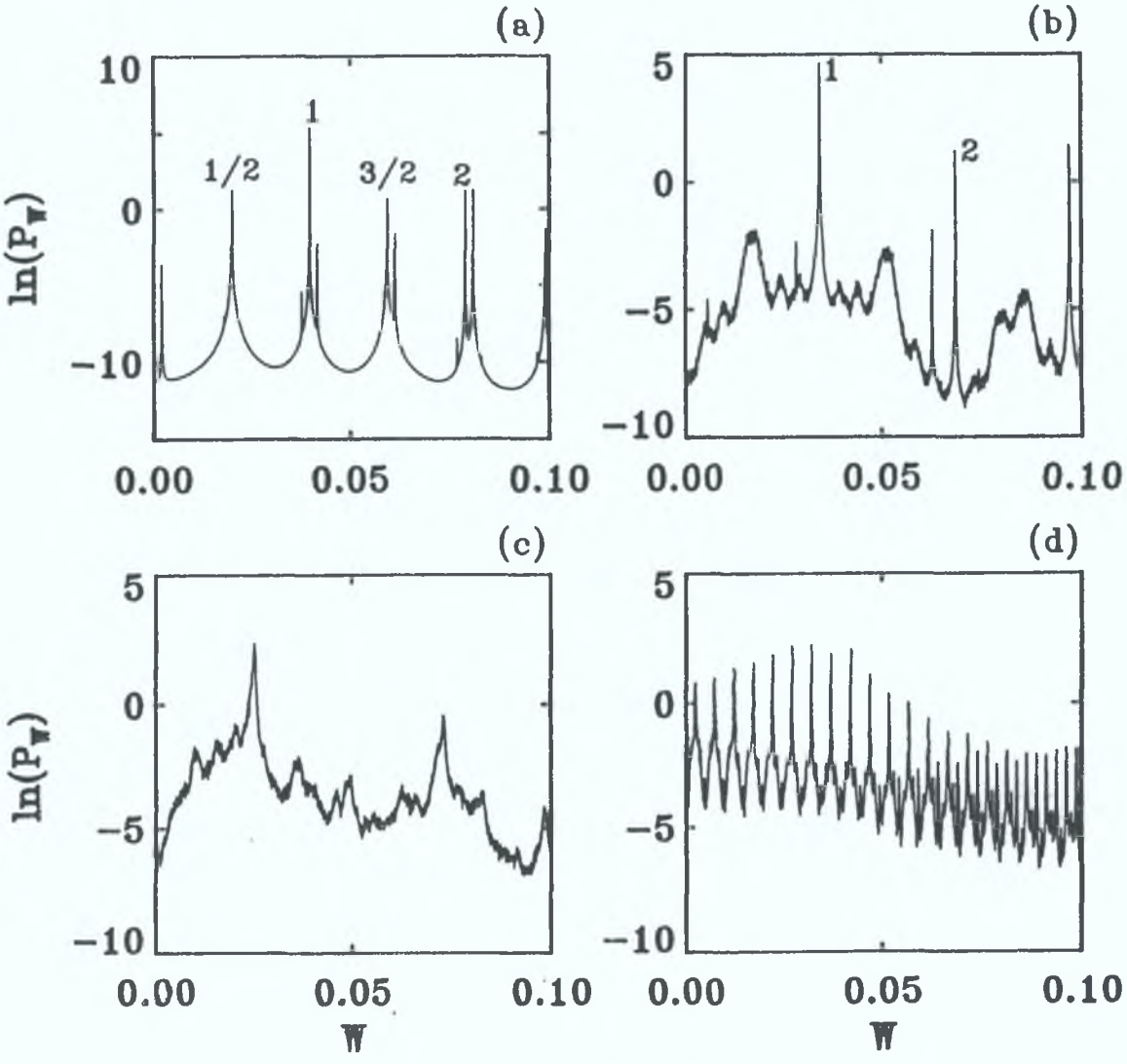

FIG. 7.3. Power spectra of the phase plots shown in Fig. 7.2. Each spectrum consists of 100 averages of 4096 samples taken at intervals $\Delta t=5$.

The power spectrum of the limit cycle in Fig. 7.2 (a), for τ=10, is shown in Fig. 7.3 (a) and consists of delta functions. The broadening of these delta functions is due to the finite length of the time record. The fundamental frequency is labeled with a 1 and the harmonics are labeled with n/m where, n and m are integers. The frequency of this fundamental is f=0.0396, therefore the period is T=25.245. The actual period of this period two orbit is T_2=50.49 which is equivalent to the sum of the two secondary peaks close to the fundamental. In summary the power spectrum does not have a fundamental at the period of the orbit but at T_n/n where n is period of the orbit.

A chaotic attractor for τ=12 is shown in Fig. 7.2 (b) with its corresponding power spectrum in Fig. 7.3 (b). For this chaotic attractor the spectrum contains sharp peaks with a broadband component. The sharp peaks have altogether disappeared for τ=18 in Fig. 7.3 (c). At τ=200 the spectrum is shown in Fig. 7.3 (d). The broadband component has many harmonics separated by a $\Delta f=4.9*10^{-3}$. This spectrum would indicate that the individual orbits which constitute the attractor have frequency components that are rationally related. It appears from Fig 7.2 that as τ is increased the phase space plots increase in complexity, specifically the difference between (b) and (c). This point will be investigated further in the next section where dimension and structure is examined.

7.5 STRUCTURE OF ATTRACTOR AS A FUNCTION OF DELAY PARAMETER τ AND GAIN PARAMETER A.

From the analysis so far a number of important questions remain unanswered. What is the reason for the increased complexity of the phase space? Is there an Cantor set associated with the attractor? How does the dimension and entropy change with the parameters A and τ? What is the maximum dimension of an infinite dimensional system? Up to what dimension is the concept of a strange attractor useful? A more detailed understanding requires an

examination of the Poincaré section and a computation of the Lyapunov spectrum

Shown in Fig. 7.4 is the Lyapunov dimension plotted as a function of the delay parameter τ, in the range 11.0 to 20 0 with increments 0.2. From the onset of chaos at τ=11.8 there is a steady increase in dimension from D_L=2.0 to 4.0. The four largest Lyapunov exponents are plotted in Fig. 7 5. There are two positive Lyapunov exponents in this region, one is zero, indicating that along the flow there

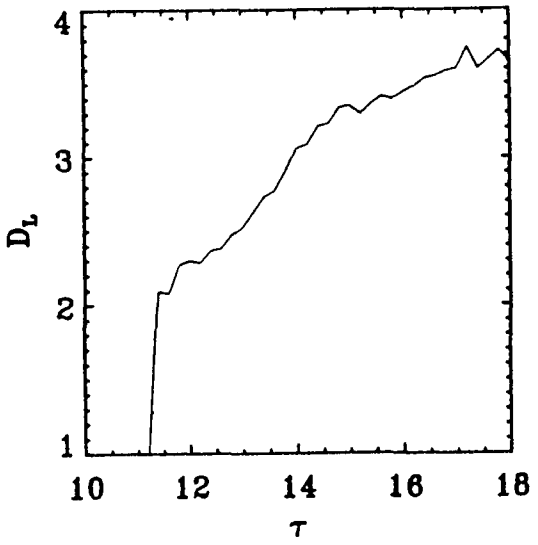

FIG. 7.4. The Lyapunov dimension D_L as a function of τ for τ in the range 11.0 to 18.0 with increments of 0.2.

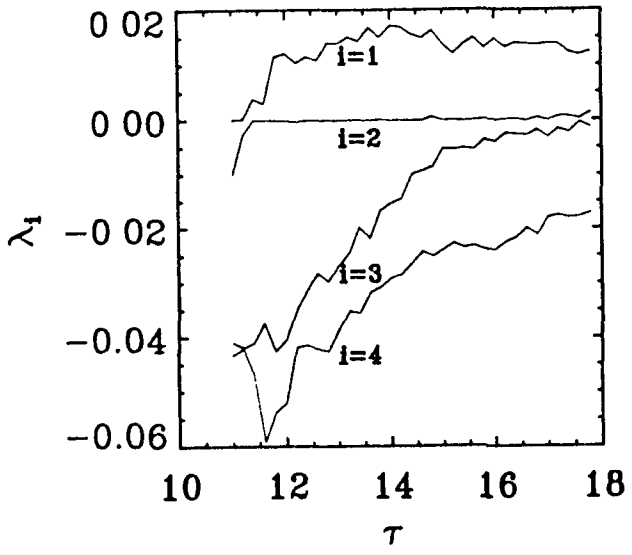

FIG. 7.5. The four largest Lyapunov exponents as a function of τ for τ in the range 11.0 to 18.0 with increments of 0.2.

is neither contraction or expansion, while the other exponent is equivalent to the Lyapunov entropy K_L. The Lyapunov exponents calculated represent the global stability of the system and it is possible that individual orbits have stability such that there are more than two positive Lyapunov exponents for the parameter range of interest. After an initial increase in K_L, there are only small fluctuations about the average value $\overline{K}_L=0.014$. The constant value of K_L indicates that the number of orbits in the system is constant

The causes for the increase in dimension (Fig. 7.4) can be found by examining the geometrical structure of an attractor. To observe the structure we will examine the Poincaré section of the attractors shown in Fig. 7.2. By plotting $X(t-\tau)$ against $X(t-2\tau)$ when $dX(t)/dt>0$ and $X(t)$ is constant we obtain an adequate representation of the Poincaré section. The plane of intersection is chosen to be $X(t)=1.5$ For the limit cycle shown in Fig. 7.2 (a) the Poincaré section would consist of two dots.

Shown in Fig 7.6 (a) is a cross section of the attractor for $\tau=12.0$, with magnifications shown in (b) and (c). The structure is reminiscence to that observed for the discrete systems in Chapters 4 and 5. Repeated magnifications show that there is a nested set of attracting curves, up to a maximum possible magnification which is dependent on the numerical integration step. These figures strongly suggest that the cross section might indeed be a Cantor set. The dimension is $D_L=2.28$. A probability distribution of the cross section in Fig. 7.6 (a) shows complicated singularities along the unstable manifold Dorizzi et al. (1987) concluded that the chaotic solution of DDE's behaves as a Gaussian-Markovian process for an one dimensional probability distributions. This is clearly not the case when the probability distribution is examined in a dimension space of two or greater. It is interesting to note that the first three negative Lyapunov exponents have similar magnitude. The two dimensional Cantor set structures observed in Sec. 4.4 are not present

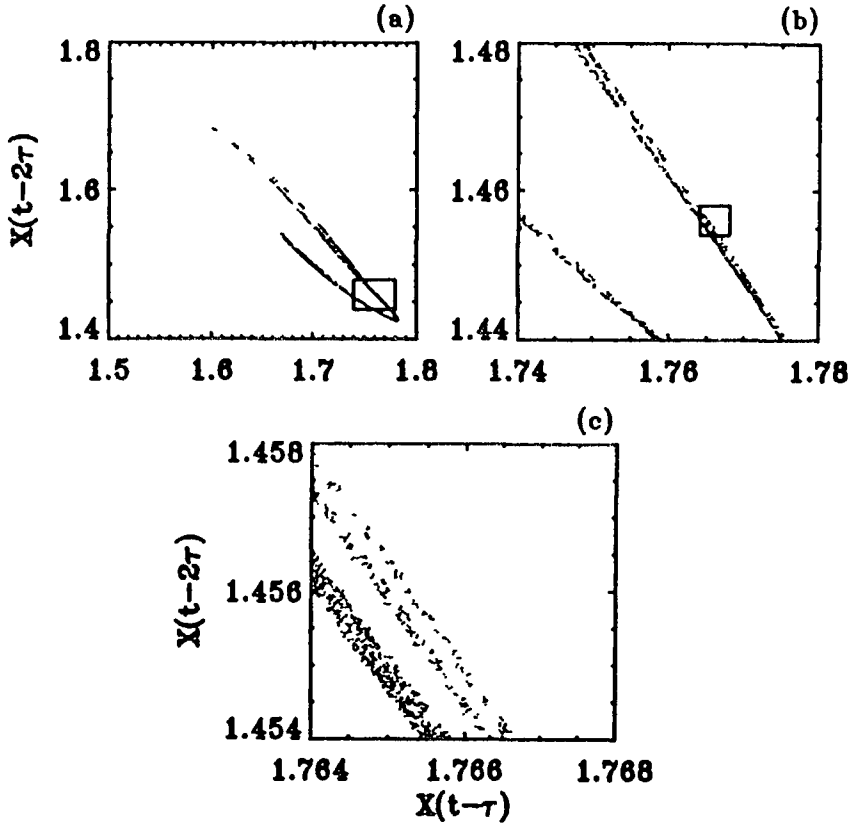

FIG. 7.6. A cross section of the attractor for τ=12.0. The sections are constructed by plotting $X(t-\tau)$ against $X(t-2\tau)$ when $X(t)$=2.0 and $X(t+\Delta t)>2.0$. In this figure as well as Fig.'s 7.7-7.9, the magnifications shown in (b) nd (c) are constructed by plotting only those points that lie within the box indicated. The dimension is D_L=2.28.

which would indicate that the eigenvectors of the Lyapunov exponents have common directions. At τ=13.0 the dimension has increased to D_L=2.51, which is reflected in a more complex structure as shown in Fig. 7.7. For τ=14, the dimension is greater than three (D_L=3.05) despite the fact that there are only two positive Lyapunov exponents. An analogous situation for discrete systems is when the dimension is greater than two despite the existence of only one positive Lyapunov exponent (Sec. 4.4.3). The structure of the attractor is shown in Fig. 7.8, again an increase in complexity is evident. At τ=18 there are still only two positive Lyapunov exponents, with expansion along one manifold As is shown in Fig. 7.9 the structure is reminiscent of a scatter plot. The associated dimension for

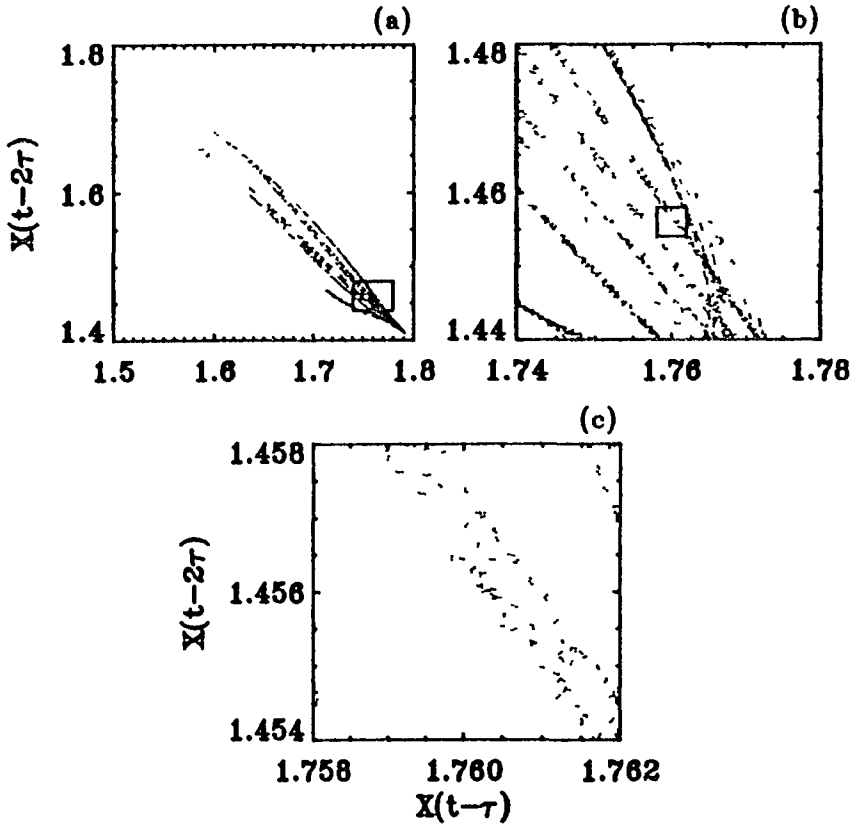

FIG. 7.7. See caption of Fig. 7.6. The delay parameter is τ=13.0 with dimension D_L=2.51.

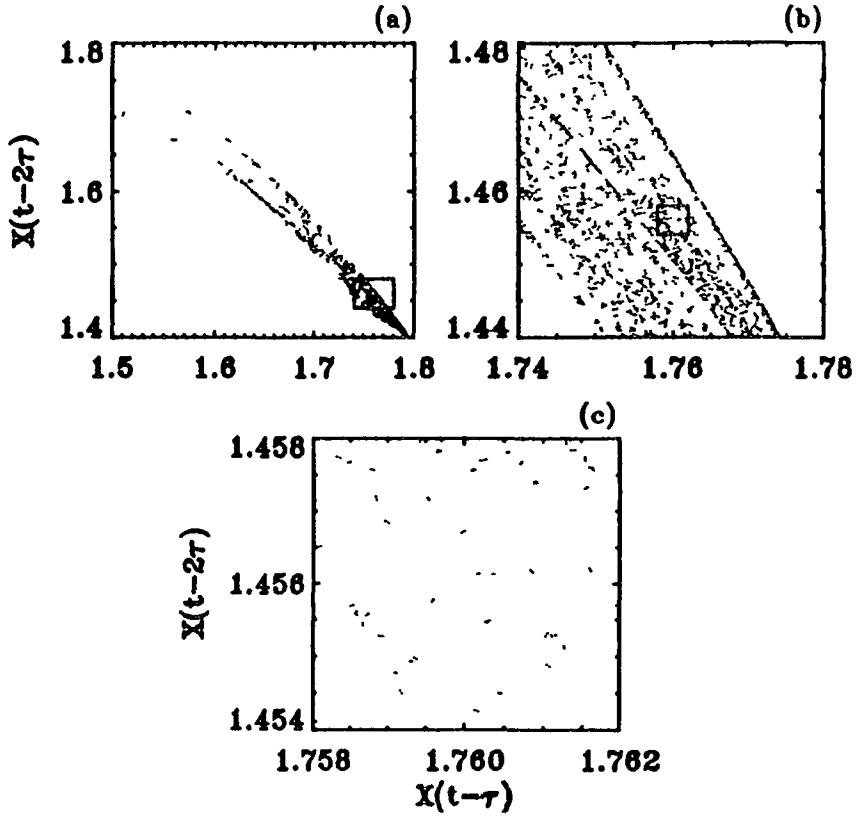

FIG. 7.8. See caption of Fig. 7.6. The delay parameter is τ=14.0 with dimension D_L=3.05.

this value of τ is D_L=3.74.

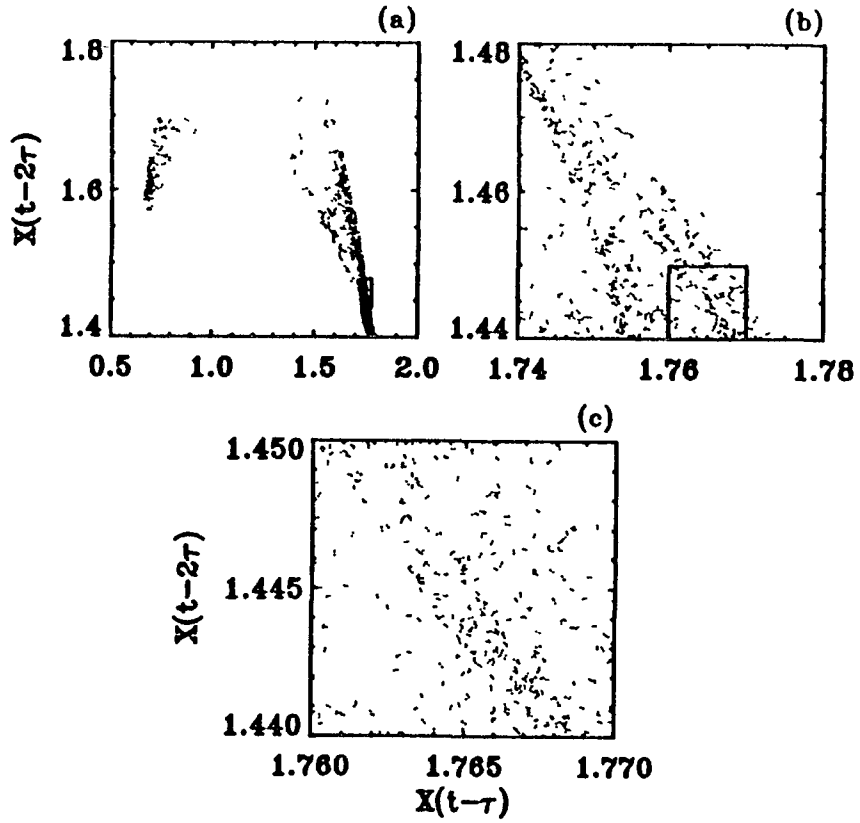

FIG. 7.9. See caption of Fig. 7.6. The delay parameter is τ=18.0 with dimension D_L=3.74.

Are chaotic attractors with periodic components in their power spectra of low dimension and simple structure? This was the case for τ=12. It was observed that these periodic components disappeared as τ increased. This type of attractor occurs after the onset of chaos. There is a periodic window between τ=34 and 36. A phase space plot of an attractor at τ=40 with D_L=6.1 is shown in Fig. 7.10. For τ=12 and τ=40 the phase space plots are closely related and both have a power spectrum consisting of sharp peaks with a broad band component (cf Fig. 7.3 (b) & Fig. 7.11). This illustrates that chaotic attractors with periodic components in their spectra can have complicated structures and large dimensions.

The study of the effect that the parameter A has on the system will proceed along similar lines. Parameter values are fixed at τ=10 and B=0.3. The dimension D_L is shown in Fig. 7 12 for A in the range 1.6-2.8 with

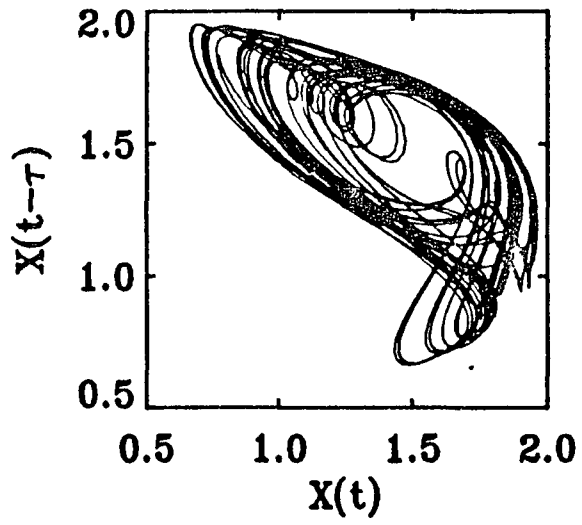

FIG. 7.10. Phase space plot for τ=40.

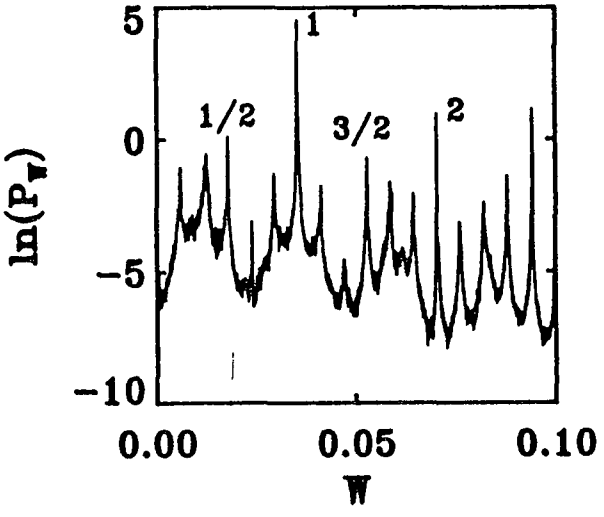

FIG. 7.11. Power spectrum for τ=40.

increments of 0.02. Windows of periodic behaviour, with attractors of dimension 1.0, exist within the chaotic regime. The four largest Lyapunov exponents are shown in Fig. 7.13. The dimension exceeds three despite the fact that there are only two positive Lyapunov exponents. A third lyapunov exponent becomes positive but the dimension never exceeds 3.8. For A greater than 2.66 there are only periodic solutions because the delay function, $f(X)=AX^2{}^4\exp(-X^2)$, tends to zero as X increases. This reduces the DDE to a linear ordinary differential equation. Although not shown, an examination of the Poincaré section

for increasing dimension shows a similar increase in the complexity of the Cantor set.

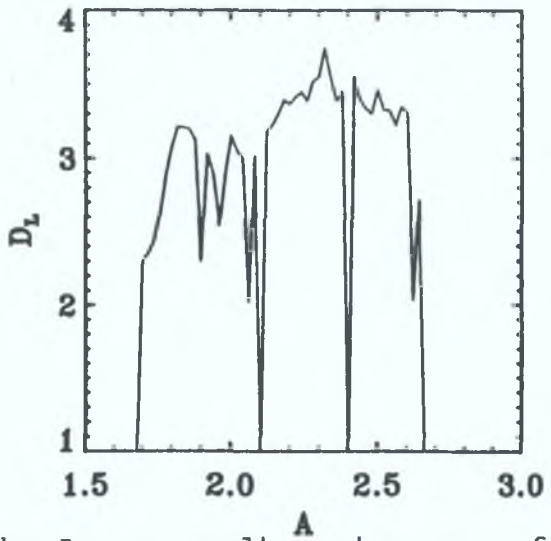

FIG. 7.12. The Lyapunov dimension as a function of A for A in the range 1.8 to 2.8 increments of 0.02.

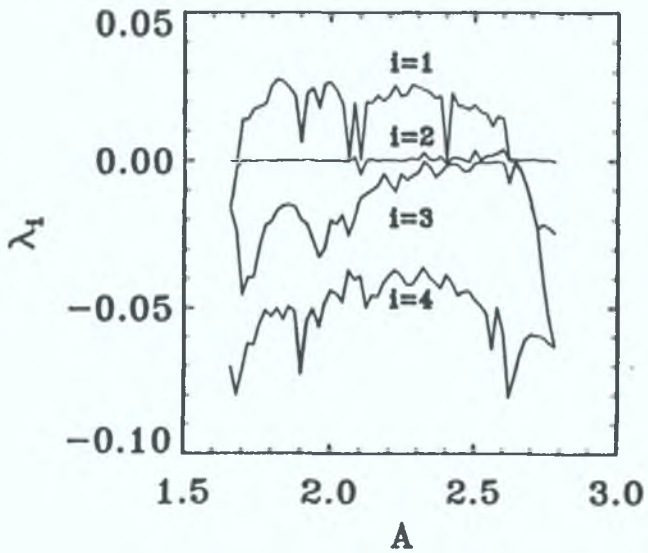

FIG. 7.13. The four largest Lyapunov exponents as a function of A for A in the range 1.8 to 2.8 increments of 0.02.

7.6 COMPARATIVE DIMENSION STUDIES

The above results were obtained by using Lyapunov exponents, as a comparison we will examine the Hausdorff dimension D_0 and the correlation dimension D_2. The calculation of these dimensions are based on the Mackey

Glass delay differential equation (Eq. (7.3)). In table 7.1 we list the dimensions D_0, D_2 and D_L for four different chaotic attractors as a function of the delay parameter τ.

For large τ the Lyapunov method is the most efficient method for computing dimensions as spatial methods and box counting methods require extremely large data sets (Sec. 2.5.2) for sufficient convergence. In all cases the following inequality is satisfied $D_0 > D_1 > D_2$. The errors quoted for D_0 and D_2 are based on a least squares fit. Attempts have been made to compute the spectrum of generalized dimensions D_q and entropies K_q for the parameter τ=23.0 (Pawelzik and Schuster (1987)). Their computed spectrum shows incomplete convergence.

Table 7.1.

A comparison of the Lyapunov dimension D_L, correlation dimension D_2 and Hausdorff dimension D_0 for four different chaotic attractors of the Mackey Glass Eq. (7.3).

	D_2		D_L		D_0
τ	Eq. 2.30	Ref. 1	Eq. 2.7	Ref. 2	Ref. 3
17	2.00±0.03	1.95±0.03	2.13±0.03	2.10±0.03	2.10±0.02
23	2.46±0.04	2.44±0.03	2.77±0.04	2.82±0.03	2.65±0.02
30	2.91±0.09	3.00±0.20	3.60±0.05	3.58±0.04	3.68±0.06
100	8.5 ±1.0	> 7.5	9.8 ±0.3	≈ 10	12.6±0.2

Ref. 1 Grassbeger[a] and Procaccia (1983).

Ref. 2 Farmer (1982).

Ref. 3 Termonia and Alexandrowicz (1984).

7.7 ASYMPTOTIC STUDIES OF CHAOTIC ATTRACTORS AS A FUNCTION OF PARAMETERS A AND τ

In Sec. 7.5 low dimensional chaos ($D_L < 4$) resulting from a variation of the parameter τ and A was examined. In this section Eq.'s (7.7) and (7.8) are examined for a range of parameters that give attractors of dimension D_L in the range 5 to 50.

The dimension D_L of Eq. (7.8) is plotted as a function of τ in Fig. 7.14 for τ in the range 20–200 with an increment of 20. The dimension increases linearly with τ. For τ=100 the dimension is of the order of D_L=18, with 10 positive Lyapunov exponents. The value of j in the Kaplan-York formula, Eq. (2.7), is 20. In comparison to this for τ=200, D_L=38 with 20 positive exponents and j=38.

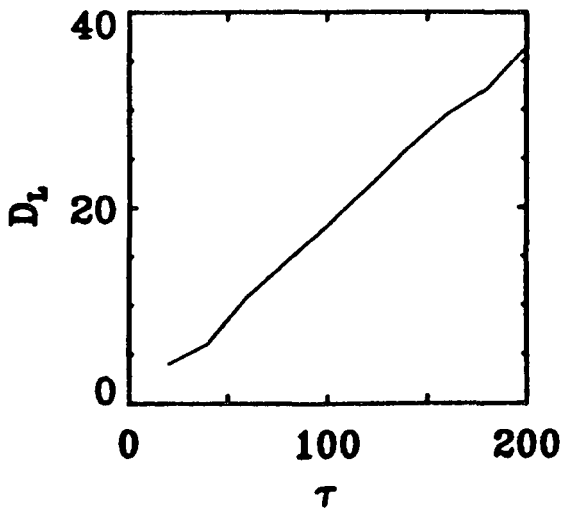

FIG. 7.14. The Lyapunov dimension D_L as a function of τ for τ in the range 20.0 to 200.0 with increments of 20.0.

Thus the dimension is approximately equal to j for large τ. Le Berre et al. (1987) relates the dimension D_L to the delay time τ divided by the correlation time of the feedback driving force for three dynamical systems. The entropy K_L is plotted in Fig. 7.15 and is approximately constant, indicating that the total number of periodic orbits in the system is constant. In order for K_L to remain approximately constant as τ increases the positive Lyapunov exponents must decline as $1/\tau$ (Farmer 1980). These attractors with large dimensions have local rates of expansion in each direction that are quite small. Error bars are shown on this plot to indicate the statistical variation in the entropy, no error bars will be shown if the fluctuation in the computed quantity is insignificant. The dimension in Fig. 7.14 depends on the ratio of the Lyapunov exponents and is not sensitive to the fluctuations

in the exponent. Increments of 20 were used to evaluate D_L and K_L, whereas a finer increment could reveal periodic windows within the chaotic regime. The deviation from the constant value of K_L in Fig. 7.15 is due to the existence of one such periodic window.

Tests have been carried out by Kaplan and Glass (1992) to determine the nature of these highly delayed attractors for τ as large as 200. These tests discriminate between the nature of a time series generated from deterministic chaotic systems and that generated from random stochastic systems. The results seem to indicate that these highly delayed attractors are deterministic in nature. This result is not surprising since no random driving force is present in these delayed equations.

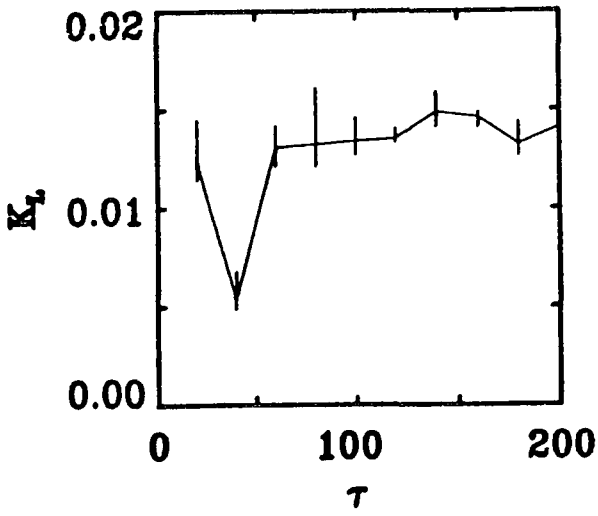

FIG. 7.15. The Lyapunov entropy K_L as a function of τ for τ in the range 20.0 to 200.0 with increments of 20.0.

To complete this chapter high dimensional attractors are examined for Eq. (7.7) which has a Sine delay term. Shown in Fig. 7.16 (a) is the Lyapunov dimension D_L as a function of τ for τ in the range 10.0 to 90.0 with increments of 20.0. The value of the parameter A being 1.0. In (b) D_L is shown as a function of A for A in the range 1.0 to 12.0 increments of 1.0. In this case τ is kept constant at 10.0. In each case there is an approximate linear increase in dimension. For the same range of

parameters the entropy K_L is plotted as a function of τ in Fig. 7.17 (a) and as a function of A in Fig. 7.17 (b). The constant entropy in (a) is consistent with the results obtained from Eq. (7.3). The entropy as a function of A is

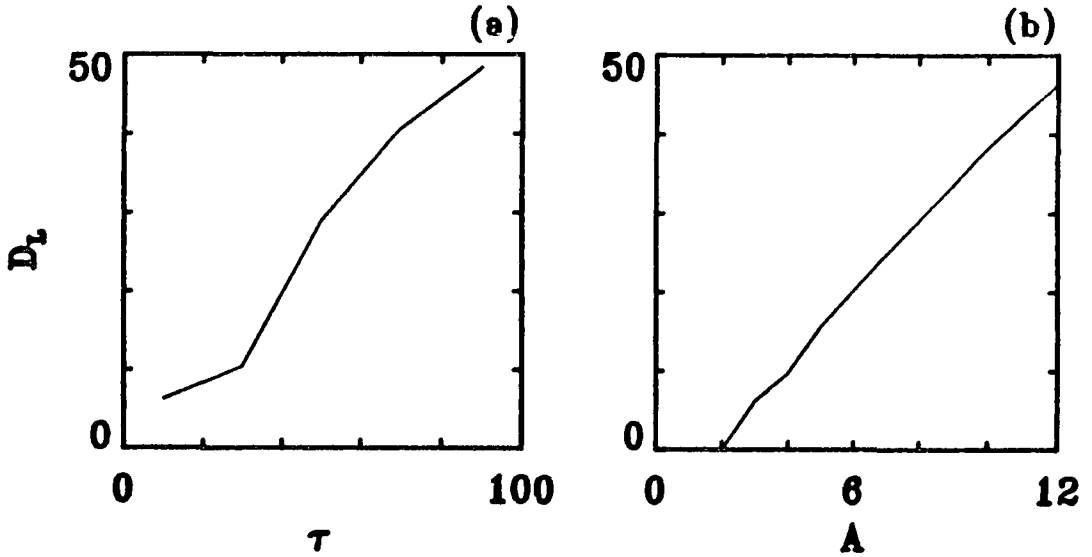

FIG. 7.16. (a) The Lyapunov dimension D_L as a function of τ for τ in the range 10.0 to 90.0 with increments of 20.0. (b) D_L as a function of A for A in the range 1.0 to 12.0 with increments of 1.0.

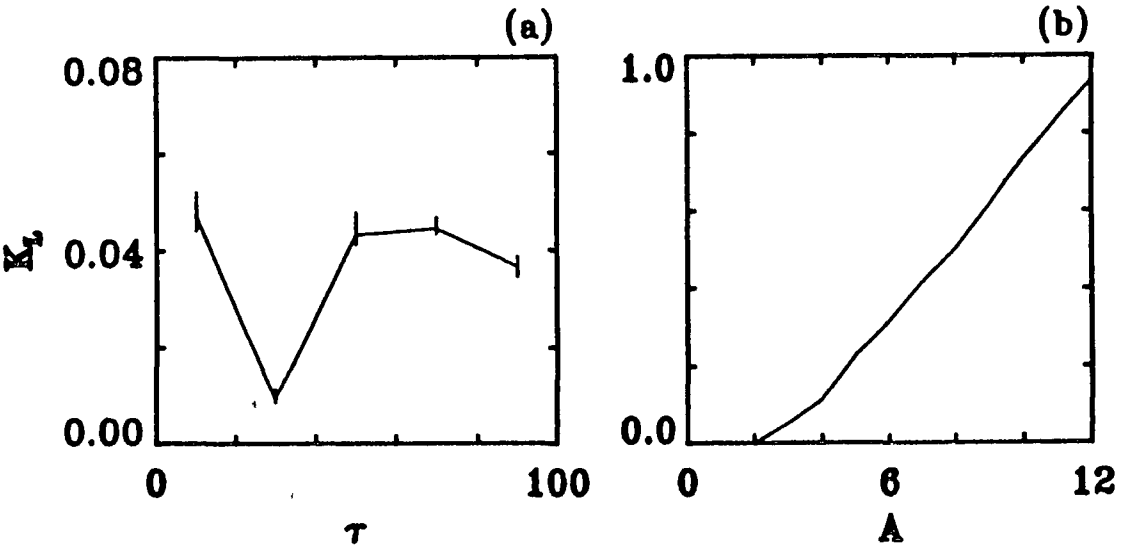

FIG. 7.17. The Lyapunov entropy K_L as a function of τ for τ in the range 20.0 to 200.0 with increments of 20.0. (b) K_L as a function of A for A in the range 1.0 to 12.0 with increments of 1.0.

linearly increasing. Note the change in scale between these

plots

Does the discrepancy between these plots indicate a difference in the nature of the chaotic behaviour? There is a difference between a variation of the parameter τ and a variation of the parameter A The maximum amplitude of X(t) is essentially independent of τ but increases with A. In both cases the local rates of expansion in each direction are small compared to this maximum amplitude of X(t). This would indicate that these highly delayed attractors obtained from a variation of τ or A have a similar nature.

7.8 CONCLUSION

This chapter has investigated the chaotic behaviour of first-order DDE's with a single delay in the parameter space A and τ. The development of the chaos as the parameter τ or A is increased proceeds with a Hopf bifurcation and a change in complexity of the structure of the attractor with an associated change in dimension. From a dimension and Poincaré section analysis evidence has been obtained to associate the changes in structure of the attractor to a Cantor set. Although it is not possible to obtain the properties of this Cantor set. The low dimension attractors are qualitatively similar to those found in systems of ordinary differential equations.

There is no limit to the dimension of the attractors in these infinite dimensional systems. The nature of these highly delayed attractors for both A and τ is such that they have local rates of expansion in many directions. The magnitude of this expansion is small compared to the amplitude of the time series X(t)

It has been shown how the frequencies in the power spectrum relates to the period of the orbit. This should prove useful in further studies connected with the extraction of the individual unstable periodic orbits.

CHAPTER 8

CONCLUSION

One of the main themes of this thesis, has been the study of the evolution of structure within the chaotic attractors of temporal chaotic systems. This evolution of structure in a two dimensional hyperbolic baker map was analyzed and quantitatively related, via its $f(\alpha)$ spectrum, to an associated Cantor set.

Most dynamical systems do not have a complete set of periodic orbits. To simulate this type of system a modified form of the baker map was analyzed. The attractors of this map were directly related to, and characterized by, a pruned Cantor set It was shown that the $f(\alpha)$ spectrum of these pruned Cantor sets have two properties different from normal Cantor sets: one, the maximum of the $f(\alpha)$ spectrum is affected by the degree of pruning and, two, the wings of the spectrum converge not to one but to a set of dimensions greater than one

Nonuniform hyperbolic systems include the toral and circle map. Using the unstable periodic orbits of the one dimensional circle map, we have illustrated the mechanism for chaotic behaviour which is independent of round off errors and numerical precision. Nonuniformities along the unstable manifold resulted in a nonconstant D_q spectrum which can not be inferred from the dimension of the periodic orbits A dissipative toral map was analyzed in detail for the first time More efficient estimates of the D_q spectrum were obtained by a rotation of the unstable manifold. This rotation had the effect of decoupling the Cantor set from the attractor New results concerning the unstable manifold show that this manifold does not wind densely around the torus but consists of an infinite number

of line segments. The evolution of structure for this system proceeds with an increase in complexity of the Cantor set and an increase in the Lyapunov dimension D_L from one to two.

Two dimensional Cantor set structures have been well documented in the literature. By analyzing a three dimensional dissipative toral map it has been shown that whenever two contracting directions compete in the formation of a strange attractor a two dimensional Cantor set is to be expected. As the structure of this set evolves there is a filling of phase space with a corresponding increase in the dimension D_L. This is the first observation of this type of Cantor set in a dynamical setting.

Nonhyperbolic systems can display intermittent crises as the system evolves. The statistical behaviour near each crisis was investigated and lead to the analysis of a new type of intermittency that is present in both dissipative and non-dissipative systems. The numerical result for the critical exponent γ are significantly less than the minimum theoretical value of $\gamma=1/2$ for both a homoclinic and a heteroclinic tangency.

The intermittent systems that were examined in this thesis have important consequences for all types of intermittency. When the colliding orbit's unstable manifold is on the attractor, the distinction between a homoclinic and heteroclinic tangency is unclear. This is because it is not possible to decompose the chaotic attractor into individual manifolds. The theoretical evaluation of the critical exponent γ is dependent on the stability of one particular orbit and this orbit may be non-dissipative even though the attractor is dissipative, which has obvious consequences for evaluating γ.

For a two dimensional chaotic attractor with positive divergence the dynamics take place on a two dimensional unstable manifold. This non-dissipative attractor can be considered as arising from a three dimensional dissipative system. When $\lambda_1+\lambda_2>0$, D_L assumes its maximum value of 2.

Surface attractor have been observed with $D_2=D_L=2$. The evolution of structure in these nonhyperbolic system is consistent with the changes in dimension and entropy for the baker map In contrast to the intermittent crisis, a process has been observed that involves the gradual merging of attractor pieces. This process was characterized in terms of the unstable periodic orbits.

The evolution of chaos in a continuous infinite dimensional delay differential system was consistent with that observed in the discrete case for both a variation of the gain A and delay τ. There is no limit to the dimension of the chaotic attractors in this system. It was found that the dimension increased, on average, linearly with A and τ, although the entropy is constant for increasing τ and linearly increasing for A. The nature of these highly delayed attractors for both A and τ is such that they have local rates of expansion in many directions.

REFERENCES

Alligood K.T. and Yorke J.A., Proc. of Sym. in Appl. Math. **39**, 41 (1989)

Amadasi L. and Casartelli M., Jour. of Stat. Phys. **65**, 363 (1991).

Arneodo A., Grasseau G. and Kostelich E.J., Phys. Lett. A **124**, 426 (1987).

Ashwin P., "Symmetric Chaos in Systems of Three and Four Forced Oscillators", Univ. of Warwick, (1990).

Atmanspacher H., Scheingraber H. and Voges W., "Global scaling properties of chaotic attractors reconstructed from experimental data", Submitted to Phy. Rev. A, May (1987).

Auerbach D., Cvitanovic P., Eckamnn J.P. and Gunaratne G., Phys. Rev. A **58**, 2387(1987).

Auerbach D., O'Shaughnessy B., and Procaccia I., Phy. Rev. A **37,** 2234 (1988).

Baake E., Baake M., Bock H.G. and Briggs K.M., Phy. Rev. A **45**, 5524 (1992).

Badii R. and Politi A., Phy. Rev. Lett. **52**, 1661, (1984).

Badii R. and Politi A., Phy. Rev. A **35,** 1288 (1987).

Baddi R., Rivista Del Nuovo Cimento, **12**, (1989).

Baier G. and Klein M., "Discrete Steps up the Dynamic Hierarchy", 11th Dynamic Days Düsseldorf (1990).

Balatoni J. and Renji A. Pub. Math. Inst. Hungarian Acad. Sci. **1,** 9 (1956).

Benedicks M. and Carleson L., Annals of Math. **133**, 73 (1991).

Bernussou J. 'Point Mapping Stability' Bergamon Press, Oxford City, (1977).

Biham O. and Wenzel W., Phy. Rev. Lett. **63**, 819 (1989); Phy. Rev. A **42**, 4639 (1990).

Block A., Bloh W. von and Schellnhuber H.J., Phys. Rev. A **42**, 1869 (1990).

Boe E. and Chang H.C., Bifurcation and Chaos **1**, 67 (1991).

Brambilla R. and Casartelli M , Il Novo Cimento, **88** B, 102 (1985).

Broggi G , "Evaluation of Dimensions and Entropies of Chaotic Systems", (1987)

Buskirk R. Van and Jeffries C., Phy. Rev. A **31**, 3332 (1985)

Buzug Th and Pfister G., Phys. Rev. A **45**, 7073 (1992).

Carroll T., Pecora L and Rachford F , Phys. Rev. A **40**, 377 (1989); Megener M. and Klingshirn C., Phys. Rev. A **35**, 4247 (1987), Caputo J and Atten P , Phys. Rev. A **35**, 1311 (1987), Gizlio M, Musazzi S. and Perini U., Phys. Rev. Lett. **53**, 2402 (1984), Brandstater A., Swift J., Swinney H , Wolf A., Farmer J , Jen E. and Crutchfield P. Phys. Rev Lett **51**, 1442 (1983), Atmanspacheret H. and Scheingaber H. Phys Rev A **34**, 253 (1986); Puccioni G., Poggi A , Gadomski W , Tredicce J and Arecchi F., Phys. Rev. Lett **55**, 339 (1985); Sato S., Sano M. and Sawada Y., Phys Rev A **37**, 1679 (1988)

Chhabra A , Jensen R and Sreenivasan K., Phys. Rev. A **40**, 4593 (1989).

Chhabra A , Meneveau C., Jensen R. and Sreenivasan K., Phys Rev A **40**, 5284 (1989)

Chrostowski J , Delisle C and Tremblay R., Can. J. Phys **61**, 188 (1983)

Cvitanovic P , Gunaratne G and Procaccia I., Phy. Rev. A **38**, 1503 (1988)

Collet P and Eckmann J., Iterated Maps on the Interval as Dynamical Systems, edited by Jaffe A. and Ruelle D. (Progress in Physics 1980)

Cohen A and Procaccia I, Phys Rev. A **31**, 1872 (1985); Termonia Y., Phys. Rev A **29**, 1612 (1984).

Cornfeld I.P., Fomain S.V. and Sini Ya. G., Erogodic Theory, translated by Sossinskii A.B., Springer-Verlag New York (1982).

Cutler C. D., Jour. of Stat Phy , **62**, 651 (1991).

Derstine M W , Gibbs H.M. Hopf F.A. and Kaplan D.L., Phy. Rev. A **27**, 3200 (1983) Derstine M.W., Gibbs H.M. Hopf F.A and Sanders L D ,IEEE J Quan Elect. **21**, 1419 (1985)

Derrida B., Gervois A and Pomeau Y., J. Phys. A **12**, 269

(1979).

Deveany R.L , An Introduction to Chaotic Dynamical Systems, Benjamin/Cummings, (1986)

Dorizzi B , Grammaticos B., Le Berre M , Pomeau Y., Ressayre E and Tallet A , Phy Rev. A **35**, 328 (1987).

Driver R.D , Ordinary and delay differential equations, Springer-Verlag, New York (1977)

Duong-van M , Nuc. Phy. B, (Proc Suppl.) **2**, 521 (1987).

Eckmann J P , Kamphorst S O., Ruelle D. and Ciliberto S., Phys. Rev A **34**, 4971 (1986) , Sano M. and Sawada Y., Phys Rev Lett. **55**, 1082 (1985).

Eckmann J P and Rulle D , Rev of Mod Phy. **57**, 617 (1985)

Eckmann J P and Procaccia I , Phy Rev. A **34**, 659 (1986).

Farmer D., Physica **4D**, 366 (1982)

Farmer J , Edward O , and York J A Physica **7**D, 153 (1983).

Farmer J D , Ott E and Yorke J A , Physica **7**D, 153 (1983); Farmer J D , Z Naturforsch **37**, 1304 (1982).

Farmer J.D. and Sidorowich J.J, Phy. Rev. Lett. **59**, 845 (1987); Jiménez J , J A. Moreno J.A. and Ruggeri G.J., Phy Rev. A **45**, 3553 (1992).

Feigenbaum M.J., J Stat Phys., **19** 25 (1978).

Feigenbaum M J , Procaccia I. and Tél T, Phy. Rev. A **39**, 5359 (1989), Jensen M H., Kadanoff L.P and Procaccia I, Phy. Rev A **36**, 1409 (1987)

Giona M., Lentini F. and Cimagalli V, Phy. Rev A **44**, 3496 (1991)

Gouesbet G., Phy. Rev. A **44**, 6264 (1991).

Grassberger P [a] and Procaccia I., Physica **9**D, 189 (1983); Phys Rev. Lett **50**, 346 (1983)

Grassberger P.[b] and Procaccia I., Phys. Rev. A **28**, 2591 (1983)

Grassbeger P and Kantz H , Phy. Lett. **113A**, 235 (1985).

Grassberger P , Z Naturforsch **43**, 671 (1988).

Grassbeger P., Kantz H. and Moening U., J. Phys. A **22**, 5217 (1989).

Graham R. and Hamm A., Phy Rev Lett. **66**, 3089 (1991).

Grebogı C., Ott E. and Yorke J A , Physıca **7D**, 181 (1983).

Grebogı[a] C., Ott E. and Yorke J.A., Phy. Rev. Lett. **56**, 1011 (1986).

Grebogı[b] C., Ott E. and Yorke J.A., Phy. Rev. Lett. **57**, 1284 (1986).

Grebogı C , Ott E. and York J.A., Phy. Rev. A **36**, 3522 (1987)

Grebogi C., Ott E., Romeıras F., and Yorke J.A , Phy. Rev. A **36**, 5365 (1987)

Grebogı C., Ott E and Yorke J., Phys. Rev. A **37**, 1711 (1988).

Gu Yan, Tung M , Yuan T M., Feng D.H. and Narducci L.M., Phy. Rev. Lett. **52**, 701 (1984).

Guckenheımer J and Holmes P., Nonlınear Oscıllatıons, Dynamıcal Systems and Bıfurcatıons of Vector Fıelds, Applıed Mathematıcal Sciences, Springer-Verlag NY, **42** (1983).

Guerrero L E and Octavıo M., Phy. Rev. A **40**, 3371 (1989).

Guevara M R., Glass L. and Shrıer A, Scıence **214**, 1350 (1981)

Gunaratne G and Procaccıa I , Phy. Rev. Lett. **59**, 1377 (1987).

Hakansson J and Russberg G , Phy Rev. A **41**, 1855 (1990).

Halsey T C , Jensen M H , Kadanoff L P , Procaccıa I. and Shraımam B I., Phys Rev A **33**, 1141 (1986).

Hamılton I., Phy. Rev. A **45**, 1259 (1992).

Hénon M, Commun Math Phys **50**, 69 (1976).

Hentschel H and Procaccıa I, Physıca **8D**, 435 (1983).

Hogg T. and Huberman B A , Phy Rev A **29**, 275 (1984); Yuan T.M., Tung M., Feng D H and Narducci L M., Phy. Rev. A **28**, 1662 (1983).

Hopf F A , Kaplan D.L., Rose M.H., Sanders L.D. and Derstıne M D , Phy. Rev. A **26**, 1394 (1986).

Hudson J.L. and Mankin J C , J of Chem. Phy. **74**, 6171 (1981).

Hsieh D.A , The Jour. of Finan **5**, 1839 (1991); Larrain M.. Finan Anal Jour. (Sept.-Oct.), 51 (1991).

Hsu C.S , 'On Nonlinear Parameter excitation problems', Advanced Applied Mechanics, **17**, 245 (1987).

Ikeda K., Daido H and Akimoto O., Phy Rev. Lett. **45**, 709 (1980).

Isola S., Europhys Lett , **11**, 523 (1990)

Jenkins P. and Heffernan D M , "Non-Fractal Chaos in Two Dimensional Discrete Systems" , 11th Dynamic Days Dusseldorf (1990)

Jenkins P., Daly M and Heffernan D.M , "F(α) spectrum of Pruned Baker Map", to be published Z Naturforsch.

Jenkins P. and Heffernan D M ,"The Formation and Evolution of Fractal Structure Within Chaotic Attractors", submitted to Inter J of Theor. Phy.

Jones H , "Fractals Before Mandelbrot", in Fractals and Chaos, edited by Crilly A J , Earnshaw R A. and Jones H., New York: Springer-Verlag (1991).

Kaplan J L. and Yorke J A , Commun. Math. Phys. **67**, 93 (1979).

Kaplan D.T. and Glass L., Phy. Rev. Lett. **68**, 427 (1992).

Kaufmann Z. and Szepfalusy P., Phy. Rev. A **40**, 2615 (1989).

Keating J P , Nonlinearity **4**, 277 (1991).

Kitano M., Yabuzaki T and Ogawa T., Phy. Rev. A **29**, 1288 (1984)

Kostelich E.J and Swinney H L , "Practial considerations in estimating dimensions from time series data", In Chaos and Related Nonlinear Phenomena edited by I Procaccia an M Shapiro, Plenum, New York, (1987).

Kovacs Z. and Tél T., Phy. Rev. A **45**, 2270 (1992).

Le Berre M Ressayre E , Tallet A.,Gibbs H.M., Kaplan D.L. and Rose M H Phy Rev A **35**, 4020 (1987).

Longtin A , Phy Rev A **44**, 4801 (1991)

Lorenz E.N , J Stat. Phys. **25**, 1 (1980).

Lowenstein J.H , Phy. Rev A **43**, 4104 (1991).

Lozi R., J. Phys. (Paris) **39** (Coll. C5): 9 (1978).

Mackey M.C. and Glass L., Science **197**, 69 (1977).

Mallet-Paret J. and Nussbaum R.D. SIAM J. Math. Anal. **20**, 249 (1989). Annali di Matematica Pura ed Appl., **145**, 33 (1986). Nussbaum R D Lecture Notes in Mathematica **730**, Springer-Verlag, Berlin, New York, 283 (1979). Nussbaum R.D. abd Peitgen H , Memoirs of the Mathematical Society, No. 310, **41** (1984)

Mandelbrot B.B, The Fractal Geometry of Nature, Freeman, New York, (1977)

Maynard Smith J , Mathematical Ideas in Biology. Cambridge University Press London, New York (1986).

Meisel L.V., Johnson M. and Cote P.J. , Phys. Rev. A **45**, 6989 (1992).

Misiurewicz M., Ann. New York Aca. of Scie. 348 (1980).

Mitschke F., Moller M and Lange W., Phys. Rev. A **37**, 4518 (1987).

Mori H., Prog. Theor. Phys. **63**,3 (1980).

Nerenberg M. and Christopher E. Phy. Rev. A, **42**, 7065 (1990).

Nomura Y., Ichikawa Y.H. and Horton W., Phy. Rev. A **45**, 1103 (1992).

O'Gorman J. PhD dissertation, Trinity College Dublin, (1989).

O'Gorman J., Hawdon B , Hegarty J , Jenkins P. and Heffernan D Journal of Mod. Optics **38** 1243 (1991).,'Coherence and Quantum Optics VI', Edited by Eberly J H., Plenum Press, New York, (1990).

Oliveira C. de and Malta C., Phy. Rev. A **36**, 3997 (1987).

Ott E., Withers W D. and York J.A., J Stat. Phys. **36**, 687 (1984), Katzen D and Procaccia I., Nuc Phy. B, (Proc. Suppl.) **2**,517 (1987)

Paoli P., Politi A., Broggi G., Ravani M. and Badii R., Phy. Rev. Lett. **62**, 2429 (1989).

Park Bae-Sig, Grebogi C , Ott E and Yorke J.A., Phy. Rev. A **40**, 1576 (1989)

Pawelizik K. and Schuster H.G., Phy. Rev. A **35**, 481 (1987).

Pawelizik K. and Schuster H G , Phy. Rev. A **43**, 1808 (1991)

Peplowski P. and Stefanski K., Phys Lett. A **132**, 408 (1988).

Pesin Ya. B., Uspekhi Mat. Nauk **32**,55 (1977).

Poincaré, Les Methods Nouvells de la Mécanique Céleste, **3** vols. Gauthier-Villars: Paris (1899).

Pomeau Y. and Manneville P., Commun. Math. Phys. **74**, 189 (1980).

Procaccia I., Nuc. Phy. B (Proc. Suppl.), **2**, 527 (1987).

Renyi A., Probability Theory (North-Holland, Amsterdam, (1970).

Ruelle D. and Takens F., Commun. Math. Phys., **20**, 167 (1971).

Sato S. and Honda K.,Phy. Rev. A **42**, 3233 (1990).

Smith L.A., Phys. Lett A **133**, 283 (1988).

Stassinopoulos D. and Alstrom P., Phy. Rev. A **45**, 675 (1992).

Stavans J., Heslot F. and Libchaber A., Phy. Rev. Lett. **55**, 596 (1985).

Stewart I., New Scientist, 4 Nov., 42 (1989).

Su Z., Rollons R.W. and Hunt E.R, Phy. Rev. A **36**, 3515 (1987).

Su Z., Rollins R.W. and Hunt E.R., Phy. Rev. A, **40**, 2689 (1989); Phy. Rev. A, **36**, 33515(1987); Gwinn E.G and Westervelt R.M., Phy. Rev. Lett. **59**, 157 (1987); Glazier J.A., Jensen M.H., Libchaber A. and Stavans J., Phy. Rev. A, **34**, 1621 (1986); Jensen M.H., Kadanoff L.P. and Libchaber A., Phy. Rev. Lett. **55**, 2798 (1985).

Tél T., Z. Naturforsch **43**, 1154 (1988).

Termonia Y. and Alexandrowicz Z., Phy. Rev. A vol **29**, 1612 (1984).

Ushiki S., Yamaguti M. and Matano H., Lect. Notes in Num. Appl. Anal., **2**, 1 (1980).

Vallee R. and Claude D., Phy. Rev. A **34**, 309 (1986).

Vallee R. and Delisle C., IEEE J. Quan. Elect. **21**, 1423 (1985). Chrostowski J., Vallee R. and Delisle C. Can. J. Prys **61**, 1143 (1983). Vallee R. and Delisle C., Phy. Rev. A **31**, 2390 (1985).

Vallee R., Delısle C. and Chrostowski J., Phy. Rev. A **30**, 336 (1984)

Vallee R and Delısle C., Phy Rev A **34**, 309 (1986).

Varosı F , Grebogı C. and Yorke J.A., Phy. Lett. A **124**, 59 (1987).

Vıvaldı F , Proc R Soc Lond A **314**, 97 (1987).

Water W. van de and Hoppenbrouwers M., Phy. Rev. A, **44**, 6388 (1991).

Wıggıns S, Global Bıfurcatons and Chaos, Springer-Verlag, Berlın, New York, (1991)

Wylıe C and Barrett L C., Advanced Engıneerıng Mathematics, Fıfth Edıtıon 1982, McGraw-Hıll.

Wısdom J., Nuc. Phy. B (Proc. Suppl.) **2**, 109 (1987).

Zeng X. Eykholt R. and Pıelke R.A., Phy. Rev. A, **66**, 3229 (1991); Bryant P., Reggıe B and Abarbanel H., Phy. Rev. Lett. **65**, 1523 (1990);Abarbanel H.,Brown R. and Kadtke J. Phy. Rev. A, **41**, 1782 (1990); Wolf A., Swift J.B., Swinney H L anh Vastano J.A , Physica **16D**, 285 (1985).

ACKNOWLEDGEMENTS

I am particularly fortunate in knowing John Scanlon and James Molloy with out who's encouragement and advice this work would not have appeared

I am very grateful to Mark Daly for his detailed constructive criticism of this thesis which led to several improvements. To my supervisor Dr Danny Heffernan for the opportunity for pursing a postgraduate degree.

I also wish to thank Siobhan Brennan and Martin Jenkins for typing corrections. I am indebted to James O'Gorman for the experimental data used in chapter 2.

To the other postgraduate students in DCU especially Collin Potter, Charles Markham, Kevin Delvin, Kevin McGuigan, Niel O'Hare, Brain Hurley, Bridget Murphy, Ruth Doyle, Simon McCabe and Kevin Mellon who made lunch time conversation both pleasant and enjoyable.

Finally my brothers and sister for support and encouragement